c. 1.

PRESSUREMETER TESTS IN SAND:
EFFECTS OF DILATION

by

TERRY LEWIS ELDRIDGE

B.A.Sc., The University of British Columbia, 1980

A THESIS SUBMITTED IN PARTIAL FULFILMENT OF

THE REQUIREMENTS FOR THE DEGREE OF

MASTER OF APPLIED SCIENCE

in

THE FACULTY OF GRADUATE STUDIES

Department of Civil Engineering

We accept this thesis as conforming

to the required standard

THE UNIVERSITY OF BRITISH COLUMBIA

February, 1983

Department of Civil Engineering

The University of British Columbia
2075 Wesbrook Place
Vancouver, Canada
V6T 1W5

Date April 19, 1983

ABSTRACT

An analysis of the response of sand to the pressuremeter is presented. An incremental linear elastic finite element program incorporating shear-volume coupling was modified such that it could efficiently handle axisymmetric plane strain stress-deformation problems. The shear-volume model was modified so that it gave a reasonable approximation to triaxial test data. A modified form of Rowe's stress dilatancy theory was used in the shear-volume coupling model.

The finite element program was used to analyze the pressuremeter test conditions. The distribution of displacements, strains and stresses around the pressuremeter were determined for soils with various volumetric responses to shear. Upon full mobilization of the soils strength, volume change characteristics have no effect on the stress distribution in the failed zone. The distribution of strain does depend upon the volume change characteristics, but beyond about three cylinder radii, such effects are small.

The assumed shape of the soil stress-strain relation significantly affects the computed response to pressuremeter type loading. An elastic-plastic material is much stiffer than a non-linear elastic material with the same initial modulus and strength. Dilation stiffens a material's response, but even a highly dilatant material is less stiff than an elastic-plastic material.

The method of determining the friction angle and dilation angle of frictional materials from pressuremeter data proposed by Hughes, Wroth and Windle was checked in the analysis. The method gives results in good agreement with the finite element results.

A method of determining the initial shear modulus and the insitu horizontal soil stress is presented. This method gives good agreement with the finite element results. When applied to actual pressuremeter test data, the shear moduli determined by this method were in better agreement with the rebound moduli than with the moduli determined from the initial portion of the pressure-expansion curve.

Table of Contents

LIST OF FIGURES

LIST OF TABLES

ACKNOWLEDGEMENT

The author would like to express his appreciation for the advice and support extended by his research supervisor, Dr. Peter M. Byrne and by Dr. Y.P. Vaid throughout this research and during the author's period of study at U.B.C.

The author would also like to acknowledge the financial support extended by the Natural Sciences and Engineering Research Council of Canada.

Chapter 1

Introduction

The self-boring pressuremeter is a relatively new soil testing device, originally being developed in the early 1970's. However, the concept of introducing a balloon-like device into the soil and inflating it was used in the 1930's. The pressuremeter in its present form was first developed in 1954 by Louis Menard, a French engineer working on a model for a final year design project in engineering. The Menard pressuremeter was further developed by a company founded by Menard and has been extensively used in France.

Few real changes were made to the pressuremeter until the early 1970's when the self-boring pressuremeter was independently developed by Hughes (1972) at Cambridge and by Jézéquel and Baguelin (1972) in France. The self-boring pressuremeter was a major step forward as it significantly reduced the amount of soil disturbance on introduction of the pressuremeter into the soil.

Soil strength and deformation characteristics can be determined from pressuremeter tests. The friction angle or cohesion and the shear modulus can be obtained from analysis of the pressure expansion curve. In addition, the dilation angle can be determined for frictional materials. Theories for the analysis of the pressuremeter assume elastic-plastic behaviour. Linear dilation can be added into the elastic-plastic model when analyzing frictional soils.

The elastic-plastic model with linear dilation incorporates some of the important features of soil behaviour. Both yield and shear volume coupling are accounted for to some extent. However, the elastic-plastic model does not account for the nonlinearity of the soil stress-strain relations, the variation of the friction angle with stress level nor the suppression of dilation with increasing stress.

A finite element analysis incorporating nonlinear stress-strain relations and shear volume coupling is required to determine the effect of this soil nonlinearity. The finite element model used in the present analysis incorporates modified hyperbolic stress-strain relations as proposed by Kondner and Zelasko (1963). An incremental approach is used, with the initial tangent modulus varying with stress. Shear volume coupling is added to the model through use of a modified form of Rowe's stress-dilatancy equation.

The pressuremeter is an axisymmetric, plane strain problem, so a plane strain finite element in polar coordinates can significantly reduce the mesh size required in the analysis. For this purpose, a finite element in polar coordinates was developed. In addition, a finite element that models triaxial conditions was developed to allow comparison of the shear-volume coupling model with triaxial test data.

Shear-volume coupling is one of the predominant features of soil behaviour that separates it from most other engineering materials. Vaid, Byrne and Hughes (1980) have proposed a method of estimating liquefaction resistance from soil

volumetric response. By empirically correlating dilation angle with relative density, an estimate of liquefaction resistance can be made. As more data becomes available, the dilation angle will be correlated directly with liquefaction resistance. However, to use this method, a realistic evaluation of the insitu dilation angle must be made.

Hughes, Wroth, and Windle (1977) have proposed a method for determining the dilation angle from pressuremeter results. This method assumes elastic-plastic behaviour and linear dilation. The finite element analysis carried out in this work checks the reasonableness of these assumptions for a nonlinear, frictional material. Determination of the shear modulus of the soil is also briefly investigated in this analysis.

Chapter 2

Pressuremeter Theories

2.1 Elastic Analysis

A useful base from which to develop an understanding of the pressuremeter is the expansion of a long cylinder in an infinite elastic medium. The solution of this problem is well known in the theory of elasticity. For a cylinder of infinite length, the problem becomes one of plane strain, and only a plane perpendicular to the long axis of the cylinder need be analyzed. The problem is axisymmetric and is conveniently analyzed in polar coordinates, r and θ, Figure 1.

For the plane problem in polar coordinates, with u and v being the displacements in the r and θ directions respectively, the strains are:

$$\varepsilon_r = -\frac{\delta u}{\delta r} \tag{2-1}$$

$$\varepsilon_\theta = -\left(\frac{u}{r} + \frac{1}{r}\frac{\delta v}{\delta \theta}\right) \tag{2-2}$$

$$\gamma_{r\theta} = -\left(\frac{1}{r}\frac{\delta u}{\delta \theta} + \frac{\delta v}{\delta r} - \frac{v}{r}\right) \tag{2-3}$$

These are Cauchy strains, and are accurate for small strains only. At large strains, second order terms become significant and cannot be neglected, as in Cauchy strains. For large strain problems, alternate definitions of strain must be used.

By the symmetry of the problem, ε_θ and $\gamma_{r\theta}$ must be constant with respect to θ. Therefore, the strains become:

$$\varepsilon_r = -\frac{du}{dr} \tag{2-1a}$$

$$\varepsilon_\theta = -\frac{u}{r} \tag{2-2a}$$

$$\gamma_{r\theta} = -\left(\frac{dv}{dr} - \frac{v}{r}\right) \tag{2-3a}$$

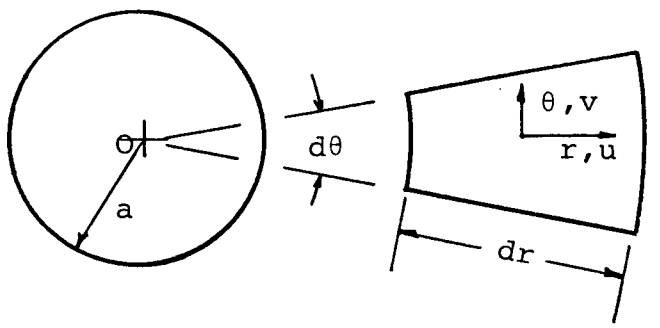

Figure 1. Coordinate System for Pressuremeter Analysis

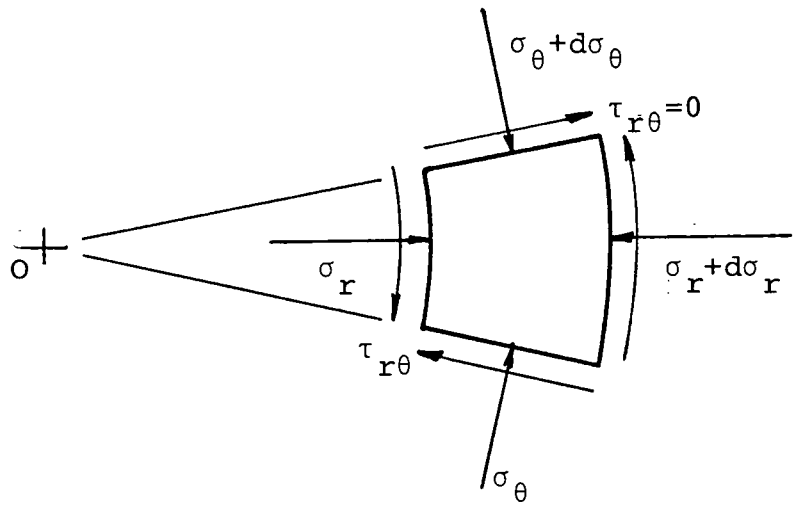

Figure 2. Stresses in Polar Coordinates

Also, it may be seen that for the axisymmetric case, no displacements can occur in the circumferential direction. Therefore, $v = 0$ and $\gamma_{r\theta} = 0$.

The radial and circumferential planes are principal planes for strain. From the strain-displacement relations, the problem is essentially one dimensional. The displacement field, u(r) in the radial direction uniquely defines the strain conditions in the material.

Figure 2 shows the state of stress within the material. For equilibrium the following equations must hold:

$$\frac{\delta\sigma_r}{\delta r} + \frac{1}{r}\frac{\delta\tau_{r\theta}}{\delta\theta} + \frac{\sigma_r - \sigma_\theta}{r} = 0 \qquad (2\text{-}4)$$

$$\frac{1}{r}\frac{\delta\sigma_\theta}{\delta\theta} + \frac{\delta\tau_{r\theta}}{\delta r} + 2\frac{\tau_{r\theta}}{r} = 0 \qquad (2\text{-}5)$$

Using the argument of symmetry again, the stresses cannot change in the θ direction, and there will be no shear stress on radial or circumferential planes. The equilibrium equations then reduce to one equation:

$$\frac{d\sigma_r}{dr} + \frac{\sigma_r - \sigma_\theta}{r} = 0 \qquad (2\text{-}4a)$$

For a homogeneous, isotropic, elastic material the stresses and strains are related by the constitutive relations:

$$\sigma_r = \frac{(1-\upsilon)E\varepsilon_r}{(1+\upsilon)(1-2\upsilon)} + \frac{\upsilon E\varepsilon_\theta}{(1+\upsilon)(1-2\upsilon)} \qquad (2\text{-}6)$$

$$\sigma_\theta = \frac{(1-\upsilon)E\varepsilon_\theta}{(1+\upsilon)(1-2\upsilon)} + \frac{\upsilon E\varepsilon_r}{(1+\upsilon)(1-2\upsilon)} \qquad (2\text{-}7)$$

Substituting equations 2-6 and 2-7 into the equilibrium equation results in the differential equation for the displacement field:

$$\frac{d^2u}{dr^2} + \frac{1}{r}\frac{du}{dr} - \frac{u}{r^2} = 0 \qquad (2\text{-}8)$$

which has general solutions:

$$u = \frac{C_1}{r} + C_2 r$$

The boundary conditions are:

$u = 0$ at $r = \infty$, yielding $C_2 = 0$,

$u = u_a$ at $r = a$, yielding $C_1 = u_a a$

Where u_a = the radial displacement at the face of the expanding cylinder.

Therefore, the displacement field is:

$$u = u_a \frac{a}{r} \tag{2-9}$$

and the strains are:

$$\varepsilon_r = u_a \frac{a}{r^2} \tag{2-10}$$

$$\varepsilon_\theta = - u_a \frac{a}{r^2} \tag{2-11}$$

Note that for the elastic case, $\varepsilon_r = -\varepsilon_\theta$ so no volumetric strain occurs.

The stresses are given by:

$$\sigma_r = \frac{E}{(1+\upsilon)} u_a \frac{a}{r^2} = 2Gu_a \frac{a}{r^2} \tag{2-12}$$

$$\sigma_\theta = \frac{-E}{(1+\upsilon)} u_a \frac{a}{r^2} = -2Gu_a \frac{a}{r^2} \tag{2-13}$$

For an initially unstressed medium undergoing a pressure increase, Δp, $\sigma_r = \Delta p$ at $r = a$. Therefore:

$$\sigma_r = 2Gu_a \frac{a}{r^2} = \Delta p$$

or

$$u_a = \frac{\Delta pa}{2G} \tag{2-14}$$

Therefore:

$$\sigma_r = \Delta p \frac{a^2}{r^2} \tag{2-15}$$

$$\sigma_\theta = -\Delta p \frac{a^2}{r^2} \tag{2-16}$$

$$\varepsilon_r = \frac{\Delta pa^2}{2Gr^2} \tag{2-17}$$

$$\varepsilon_\theta = -\frac{\Delta pa^2}{2Gr^2} \tag{2-18}$$

and,

$$u = \frac{\Delta pa^2}{2Gr} \tag{2-19}$$

For an initially stressed medium, with $\sigma_{ri} = p_i$,

$$\sigma_r = p_i + \Delta p \frac{a^2}{r^2} \tag{2-15a}$$

$$\sigma_\theta = p_i - \Delta p \frac{a^2}{r^2} \tag{2-16a}$$

and the strains and displacements are as given above. Note that $\sigma_r = -\sigma_\theta$ so the mean normal stress does not change in an elastic material. The material is subject to a pure shear as the cylinder expands.

The shear modulus may be determined from the pressure-expansion curve of the elastic material, Figure 3. By measuring the displacement of the cylinder as the pressure is increased, a linear plot of pressure versus circumferential strain u_a/a will result. As shown in the figure, the shear modulus is one half of the slope of the curve:

$$G = \frac{1}{2} \frac{\Delta p}{u_a/a} \tag{2-20}$$

2.2 Elastic-Plastic Incompressible Material

The domain remains elastic until the stresses at the inner face of the cylinder reach the yield state defined as:

$$\frac{\sigma_1}{\sigma_3} = R = \frac{1+\sin\phi}{1-\sin\phi} \tag{2-21}$$

If the pressure within the cylinder is raised beyond this level, the soil will yield and a plastic annulus will form around the cylinder. Within this annulus, the stresses will change such that they will obey the yield criterion. Beyond the plastic annulus the material will remain elastic and will obey the relations developed previously. A small strain approximation will be used to develop expressions for the stress, strain and displacements in the plastic region.

Within the plastic annulus, the equilibrium equation must

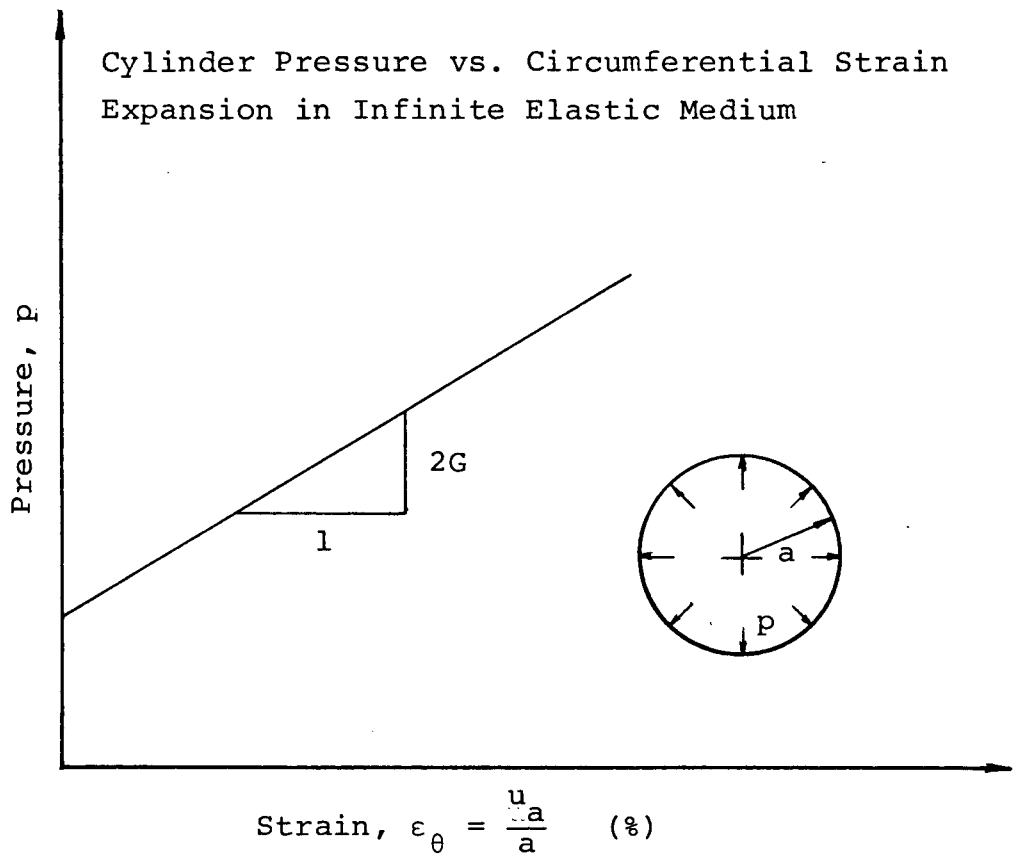

Figure 3. Pressure Expansion Curve for Elastic Material

still hold. Upon substitution of equation 2-21 into the equilibrium equation 2-4a, the following equation results:

$$\frac{d\sigma_r}{dr} + \frac{\sigma_r(1-\frac{1}{R})}{r} = 0 \qquad (2\text{-}22)$$

For an initially unstressed material, the boundary condition is:

$$\sigma_r = \Delta p \quad \text{at} \quad r = a,$$

and the solution is:

$$\ln \frac{r}{p} = -(1-\frac{1}{R}) \quad \ln\frac{r}{a} \qquad (2\text{-}23)$$

or, within the plastic zone:

$$\sigma_r = \Delta p(\frac{a}{r})^{(1-\frac{1}{R})} \quad \text{for } r < r_f \qquad (2\text{-}24)$$

where r_f = the radius of the plastic annulus

Note that the stress decays as $(\frac{1}{r})^{(1-\frac{1}{R})}$ in the plastic material while it decays as $\frac{1}{r}$ in the elastic material. The circumferential stress is:

$$\sigma_\theta = \frac{1}{R}\overset{\Delta p}{\cancel{p}}(\frac{a}{r})^{(1-\frac{1}{R})} \qquad (2\text{-}25)$$

For an initially stressed material, with free field stress, p_i:

$$\sigma_r = p_i + \Delta p(\frac{a}{r})^{(1-\frac{1}{R})} \qquad (2\text{-}24a)$$

$$\sigma_\theta = p_i + \frac{1}{R}\Delta p(\frac{a}{r})^{(1-\frac{1}{R})} \qquad (2\text{-}25a)$$

A comparison of the stresses in an elastic material and an elastic-plastic material is shown in Figure 4. The two important points are that the stress decays slower in the plastic material and that the mean normal stress increases in the plastic material while it does not increase in the elastic material.

The assumption of no volume change can be used to determine the displacement field and strains in the plastic material. For no volume change:

$$\varepsilon_v = -\frac{du}{dr} - \frac{u}{r} = 0 \qquad (2\text{-}26)$$

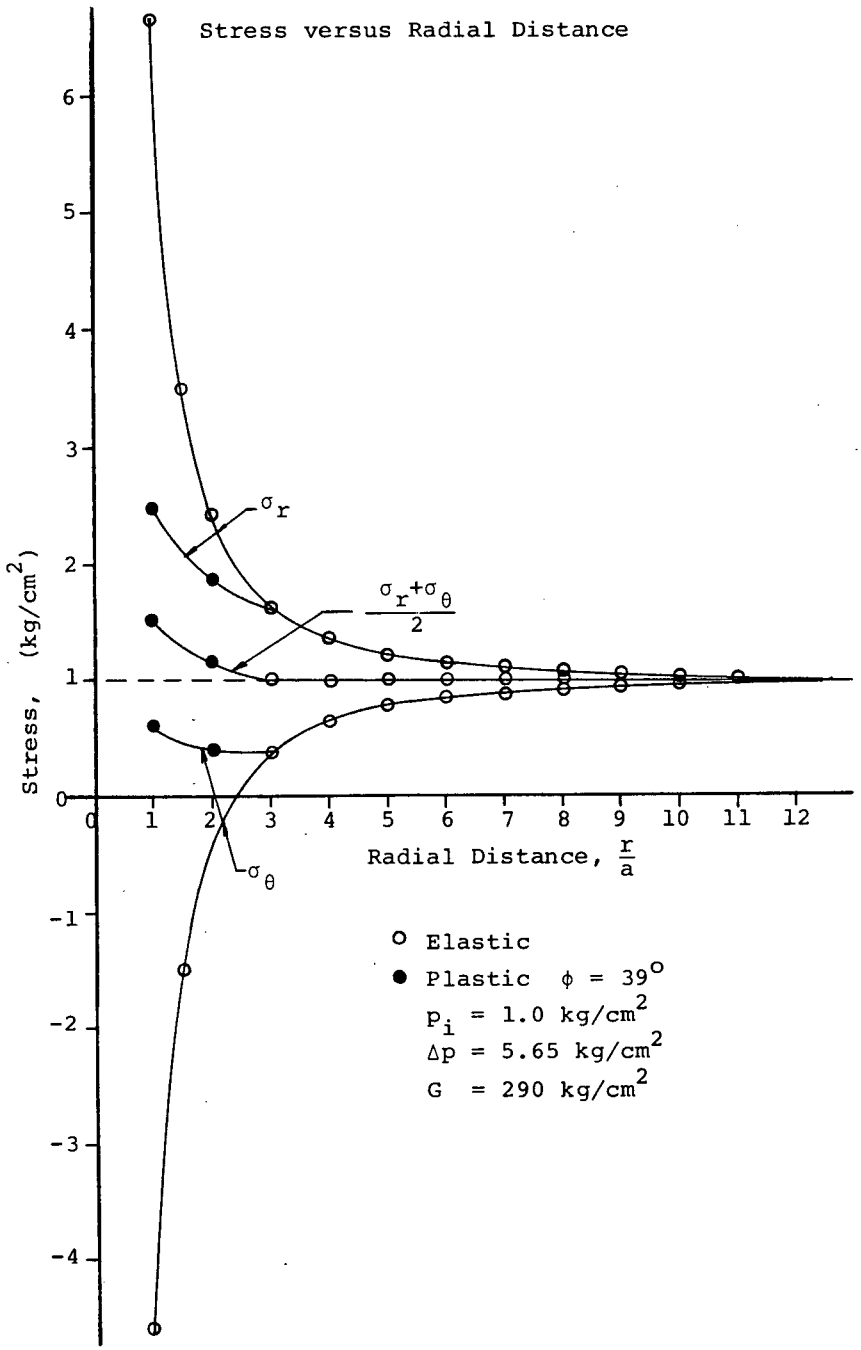

Figure 4. Comparison of Stress Distribution in Elastic and Elastic-Plastic Incompressible Materials

The boundary condition for this differential equation is:

$$u = u_a \text{ at } r = a,$$

and the solution is:

$$\ln \frac{u}{u_a} = -\ln \frac{r}{a}$$

or

$$u = u_a\left(\frac{a}{r}\right) \tag{2-27}$$

This is the same displacement field as in the elastic material. The reason that the displacement fields are the same for both the elastic and plastic cases is that no volume change occurs in either the elastic or plastic case. Also, the small strain approximation was used in the derivation of the displacement field. Not using the small strain approximation would produce a slightly different displacement field. For strains less than about ten percent the error in making the small strain approximation is small.

The pressure-expansion curve of an elastic-plastic incompressible material can be derived using the small strain approximation. Before yield the curve rises linearly at a slope of 2G. After yield, curvature begins. At the plastic-elastic interface the material is just at yield, and the strain is ε_f. The value of ε_f depends on the initial stress state and material properties G and ϕ, but not on location within the material.

For an initially stressed material, yield occurs when:

$$\frac{\sigma_r}{\sigma_\theta} = \frac{p_i + \Delta\sigma_r}{p_i - \Delta\sigma_r} = R$$

or:

$$\Delta\sigma_r = p_i\left(\frac{R-1}{R+1}\right) = p_i \sin\phi \tag{2-28}$$

The shear stress is then:

$$\tau = \frac{\sigma_r - \sigma_\theta}{2} = p_i \sin\phi \tag{2-29}$$

The corresponding shear strain, γ_f, at which yield occurs is:

$$\gamma_f = \frac{\tau}{G} = \frac{p_i \sin\phi}{G} \qquad (2\text{-}30)$$

The corresponding circumferential strain, ε_f, $= \frac{1}{2}\gamma_f$, therefore, is:

$$\varepsilon_f = \frac{p_i \sin\phi}{2G} \qquad (2\text{-}31)$$

For no volume change, this corresponds to a strain, ε_a, at the cylinder face of:

$$\varepsilon_a = \varepsilon_f \left(\frac{r_f}{a}\right)^2 = \frac{p_i \sin\phi r_f}{2G}\left(\frac{r_f}{a}\right)^2 \qquad (2\text{-}32)$$

In the plastic material:

$$\Delta\sigma_r = \Delta p \left(\frac{a}{r}\right)^{(1-\frac{1}{R})} \qquad (2\text{-}24)$$

or;

$$\Delta p = p_i \sin\phi \left(\frac{r_f}{a}\right)^{(1-\frac{1}{R})}$$

but from 2-32:

$$\left(\frac{r_f}{a}\right) = \left(\frac{2G\varepsilon_a}{p_i \sin\phi}\right)^{\frac{1}{2}} \qquad (2\text{-}33)$$

Therefore:

$$\Delta p = p_i \sin \left(\frac{2G\varepsilon_a}{p_i \sin\phi}\right)^{\left(\frac{R-1}{2R}\right)}$$

The cylinder pressure is then:

$$p = p_i (1+\sin\phi) \left(\frac{2G\varepsilon_a}{p_i \sin\phi}\right)^{\frac{(R-1)}{2R}} \qquad (2\text{-}34)$$

This curve is plotted in Figure 5. The elastic-plastic incompressible material is much softer than an elastic material.

2.2.1 Large Strains and Limit Pressure

Within the plastic zone as strains become large, the small strain approximation will not hold. In this case, Almansi strains can be used. The definition of the Almansi strain, α is:

$$\alpha = \frac{1}{2}\,\frac{dl^2 - dl_o^2}{dl} \qquad (2\text{-}35)$$

where: dl_o = the original length

dl = length after deformation

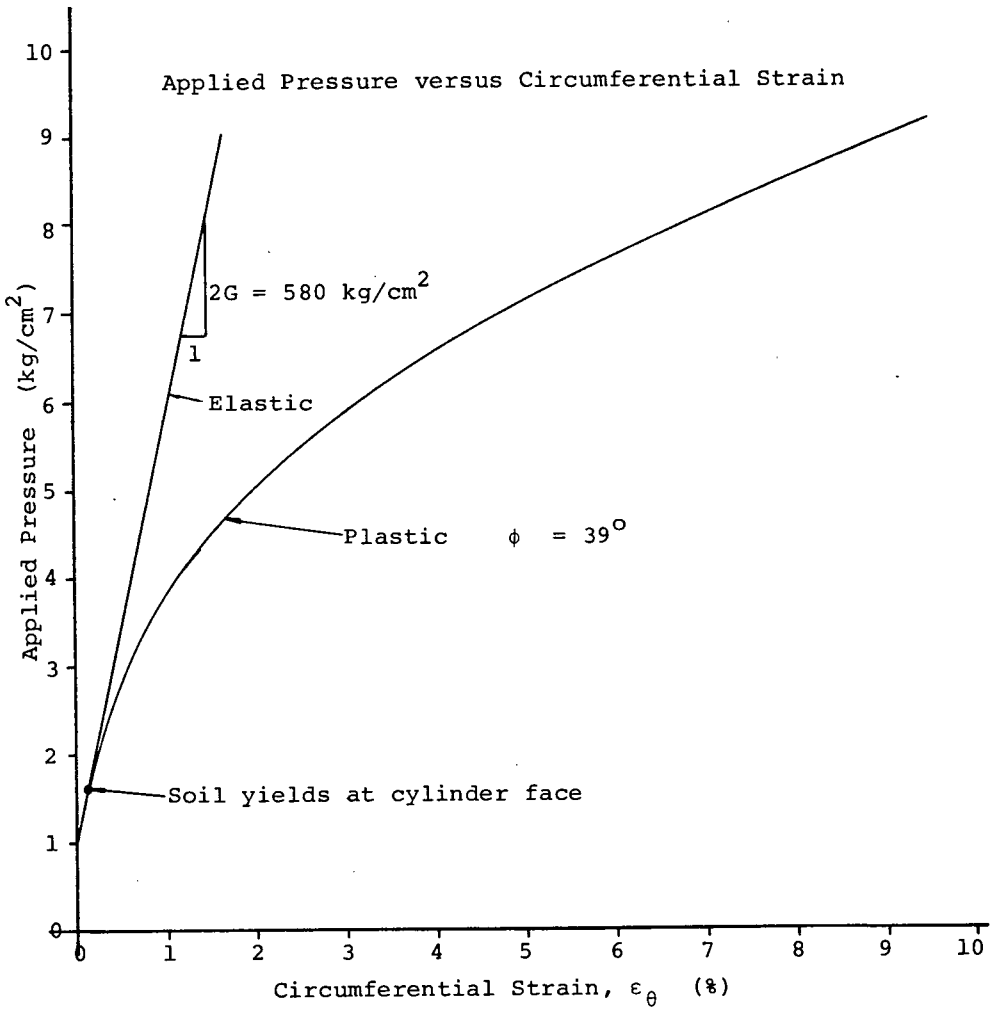

Figure 5. Pressure-Expansion Curve for Elastic-Plastic Material

The Almansi strain and Cauchy strain are related by:

$$(1 + \varepsilon)^2 = \frac{1}{1-2\alpha} \qquad (2\text{-}36)$$

Even at high strains the equilibrium equation must hold. For large strain conditions, the equilibrium equation is written for the material in the deformed state:

$$\frac{d\sigma_r}{d\rho} + \frac{\sigma_r - \sigma_\theta}{\rho} = 0 \qquad (2\text{-}37)$$

where: ρ = radius after deformation

The stresses must remain on the yield surface, therefore the equilibrium equation becomes:

$$\frac{d\sigma_r}{d\rho} + \frac{\sigma_r - (1-\frac{1}{R})}{\rho} = 0 \qquad (2\text{-}38)$$

This differential equation may be solved for the stress distribution within the plastic material. The boundary conditions are:

$\rho = \rho_o$ and $\sigma_r = p_o$ at the face of the cylinder, and:

$\rho = \rho_f$ and $\sigma_r = p_f$ at the limit of the plastic zone

where: p_f = pressure at which material yields.

The solution of this differential equation with the above boundary conditions is:

$$(\frac{p_f}{p_o} = (\frac{\rho_o}{\rho_f})^{(1-\frac{1}{R})} \qquad (2\text{-}39)$$

or in terms of σ_r at any radius ρ in the plastic zone:

$$\frac{\sigma_r}{p} = (\frac{\rho_o}{\rho})^{(1-\frac{1}{R})} \qquad (2\text{-}40)$$

The circumferential stress is then:

$$\sigma_\theta = \frac{p}{R}(\frac{\rho_o}{\rho})^{(1-\frac{1}{R})} \qquad (2\text{-}41)$$

This is the same expression as developed using the small strain approximation, except ρ replaces r.

When the plastic region expands from r_f to ρ_f, the condition of no volume change implies:

$$\pi(\rho_f^2 - \rho_o^2) = \pi(r_f^2 - r_o^2)$$

where; r_o = radius of cylinder

ρ_o = deformed radius of cylinder

or:

$$\rho_f^2 - r_f^2 = \rho_o^2 - r_o^2 \qquad (2\text{-}42)$$

This may be transformed to:

$$\frac{(\rho_f^2 - r_f^2)\rho_f^2}{\rho_f^2} = \frac{(\rho_o^2 - r_o^2)\rho_0^2}{\rho_o^2}$$

or:

$$\frac{\alpha_f}{\alpha_o} = \left(\frac{\rho_o}{\rho_f}\right)^2 \qquad (2\text{-}43)$$

where: α_f = Almansi strain to yield

α_o = Almansi strain at cylinder

Substituting equation 2-43 into equation 2-40 results in the equation:

$$p_o = p_f\left(\frac{\rho_f}{\rho_o}\right)^{(1-\frac{1}{R})} = \rho_o\left(\frac{\alpha_o}{\alpha_f}\right)^{\left(\frac{R-1}{2R}\right)} \qquad (2\text{-}44)$$

This equation allows prediction of a limit pressure. The strain at the face of the cylinder, α_o, is related to the volume of the cylinder by:

$$\alpha_o = \frac{1}{2}\left(\frac{V-V_o}{V}\right) = \frac{1}{2}\,\frac{\Delta V}{V} \qquad (2\text{-}45)$$

where: V = current volume

V_o = initial volume

In the limit, as the volume becomes large, V_o becomes negligible with respect to V, so $\alpha_o = \frac{1}{2}$. The strain, α_f, at which yield

occurs is equal to the Cauchy strain to failure, ε_f:

$$\varepsilon_f = \frac{p_i \sin\phi}{2G} = \alpha_f$$

The limit pressure for a frictional material then becomes:

$$p_L = p_f \left(\frac{G}{p_i \sin\phi}\right)^{\left(\frac{R-1}{2R}\right)} \qquad (2\text{-}46)$$

where: $p_f = p_i(1+\sin\phi)$

For a linear elastic-plastic incompressible frictional material, the friction angle and the shear modulus may be obtained from the pressure expansion curve. The shear modulus is obtained from the initial linear portion of the line and the friction angle is obtained from the curved portion of the line.

2.3 Limitations of Elastic-Plastic Analysis

The simple elastic-plastic model presented allows an analytic solution for the pressuremeter conditions and yields characteristic pressure-expansion curves. The linear portion occurs before yield, when the material is subject to pure shear, and the curved portion occurs at the onset of plastic behaviour. The model also shows that the limit pressure is related to the soil strength ϕ and the shear modulus G or the strain to failure ε_f.

This type of analysis does have several major limitations. It can only handle compressive volumetric strains due to changes in the mean normal stress in the elastic phase, although no volume change occurs along the stress path followed in this case. Also, the soil is incompressible in the plastic phase, which is valid only for undrained tests. The theory also neglects stress level dependency of the soil properties, which has

a major effect on the response of soil. Linear dilation can be added into the closed form solution, but stress level dependency requires numerical analysis.

2.4 Linear Dilatant Analysis

The effect of dilation on the response of soil to the pressuremeter was examined by Baguelin, Jézéquel and Shields (1978) using the small strain case and assuming linear dilation. For the small strain case, Cauchy strains are used. Volume changes due to dilation are added into the analysis by:

$$\varepsilon_v = \frac{\Delta\sigma_m}{B} - \frac{\Delta\tau_{max}}{D_t} \qquad (2\text{-}47)$$

where: D_t = dilatant parameter (positive for volume increase)

For plane strain conditions:

$$\varepsilon_v = \varepsilon_\theta + \varepsilon_r = -\frac{u}{r} - \frac{du}{dr} \qquad (2\text{-}48)$$

or:

$$-\left(\frac{u}{r} + \frac{du}{dr}\right) = \frac{\Delta\sigma_m}{B} - \frac{\Delta\tau_{max}}{D_t} \qquad (2\text{-}49)$$

The shear strain, γ, is given by:

$$\gamma = \varepsilon_r - \varepsilon_\theta = -\frac{du}{dr} + \frac{u}{r} \qquad (2\text{-}50)$$

But:

$$\gamma = \frac{\Delta\tau_{max}}{G} = \frac{\Delta\sigma_r - \Delta\sigma_\theta}{2G} \qquad (2\text{-}51)$$

Therefore:

$$\frac{u}{r} - \frac{du}{dr} = \frac{\Delta\sigma_r - \Delta\sigma_\theta}{2G} \qquad (2\text{-}52)$$

Equations 2-49 and 2-52 allow determination of $\Delta\sigma_r$ and $\Delta\sigma_r - \Delta\sigma_\theta$ in terms of $\frac{u}{r}$ and $\frac{du}{dr}$:

$$\Delta\sigma_r - \Delta\sigma_\theta = 2G\left(\frac{u}{r} - \frac{du}{dr}\right) \qquad (2\text{-}53)$$

$$\Delta\sigma_r = \frac{u}{r}\left(\frac{3BG}{2(1+\upsilon)D_t} - \frac{3B}{2(1+\upsilon)} + G\right) - \frac{du}{dr}\left(\frac{3BG}{2(1+\upsilon)D_t} + \frac{3B}{2(1+\upsilon)} + G\right) \qquad (2\text{-}54)$$

The term $\frac{3B}{2(1+\upsilon)}$ can be simplified to $\frac{G}{(1-2\upsilon)}$, in which case:

$$\Delta\sigma_r = \frac{u}{r}\left(\frac{G^2}{(1-2\upsilon)D_t} - \frac{2\upsilon G}{1-2\upsilon}\right) - \frac{du}{dr}\left(\frac{G^2}{(1-2\upsilon)D_t} + \frac{2G(1-\upsilon)}{1-2\upsilon}\right) \tag{2-55}$$

or:

$$\Delta\sigma_r = \xi\frac{u}{r} - \eta\frac{du}{dr} \tag{2-55a}$$

On substitution of equation 2-55a into the equilibrium equation, the following differential equation results:

$$r^2\frac{d^2u}{dr^2} + \frac{(2G-\xi)}{\eta}\left(r\frac{du}{dr} - u\right) = 0 \tag{2-56}$$

where:

$$\frac{2G - \xi}{\eta} = \frac{2D_t(1-\upsilon) - G}{2D_t(1-\upsilon) + G} = n$$

The differential equation has solutions of the form:

$$u = Ar + Br^{-n}$$

The boundary condition of $u = 0$ at $r = \infty$, yields $A = 0$ and $n > 0$. The condition that $n > 0$ yields:

$$D_t > \frac{G}{2(1-\upsilon)} \quad \text{for volume increase}$$

$$D_t < \frac{G}{2(1-\upsilon)} \quad \text{for volume decrease}$$

which can be combined as:

$$\frac{-2(1-\upsilon)}{D_t} < \frac{1}{G} < \frac{2(1-\upsilon)}{D_t} \tag{2-57}$$

The boundary condition at the face of the cylinder, $r = a$, is $u = u_a$ and $\sigma_r = \Delta p + p_i$. This gives the solution for displacements:

$$u = u_a\left(\frac{a}{r}\right)^n \tag{2-58}$$

$$\text{where:} \quad u_a = \frac{\Delta pa}{2G}$$

As developed previously, in elastic material with no dilation:

$$u = u_o\left(\frac{a}{r}\right) \tag{2-9}$$

For a given value of u_o, dilation causes the displacement to propagate further from the cylinder.

In the dilatant material:

$$\Delta\sigma_r = \frac{u}{r}(\xi + n\eta)$$

which on simplification becomes:

$$\Delta\sigma_r = 2G\frac{u}{r} = 2G\varepsilon_\theta = \Delta p\left(\frac{a}{r}\right)^{n+1} \qquad (2\text{-}59)$$

Note that linear dilation does not affect the initial straight line portion of the pressuremeter curve, it still rises at a slope of 2G.

The stresses are given by:

$$\Delta\sigma_r - \Delta\sigma_\theta = 2\tau_m = 2G\left(\frac{u}{r}\right)(1+n) = (1+n)\Delta\sigma_r \qquad (2\text{-}60)$$

$$\Delta\sigma_\theta = -n\Delta\sigma_r = -n\Delta p\left(\frac{a}{r}\right)^{n+1} \qquad (2\text{-}61)$$

and:

$$\Delta\sigma_m = (\Delta\sigma_r + \Delta\sigma_\theta)\frac{(1+\upsilon)}{3} = \Delta\sigma_r\frac{(1-n)}{3}(1+\upsilon)$$

or:

$$\Delta\sigma_m = \frac{2Ga}{3r}(1+\upsilon)(1-n) = \frac{\Delta p}{3}\left(\frac{a}{r}\right)^{(n+1)}(1+\upsilon)(1-n) \qquad (2\text{-}62)$$

The strains are given by:

$$\varepsilon_r = \frac{n\Delta p}{2G}\left(\frac{a}{r}\right)^{(n+1)} \qquad (2\text{-}63)$$

and:

$$\varepsilon_\theta = -\frac{\Delta p}{2G}\left(\frac{a}{r}\right)^{(n+1)} \qquad (2\text{-}64)$$

Figures 6, 7 and 8 show a comparison of the displacements, strains and stresses, respectively, in a dilatant material and an elastic material. In Figure 8 note that higher shear stresses exist at the face of the cylinder in the elastic material but the shear stresses propagate further into the material in the dilatant material. Also note that dilation increases the mean normal stress in the material.

Yield of the dilatant material will occur when $\frac{\sigma_r}{\sigma_\theta} = R$.

But:

$$\Delta\sigma_r = p_i + 2G\left(\frac{u}{r}\right) \qquad (2\text{-}65)$$

and:

$$\Delta\sigma_\theta = p_i - n\Delta\sigma_r = p_i - 2Gn\left(\frac{u}{r}\right) \qquad (2\text{-}66)$$

For yield just occurring at the cylinder:

$$\frac{\sigma_r}{\sigma_\theta} = R = \frac{p_i + 2G\varepsilon_f}{p_i - 2G\varepsilon_f} \qquad (2\text{-}67)$$

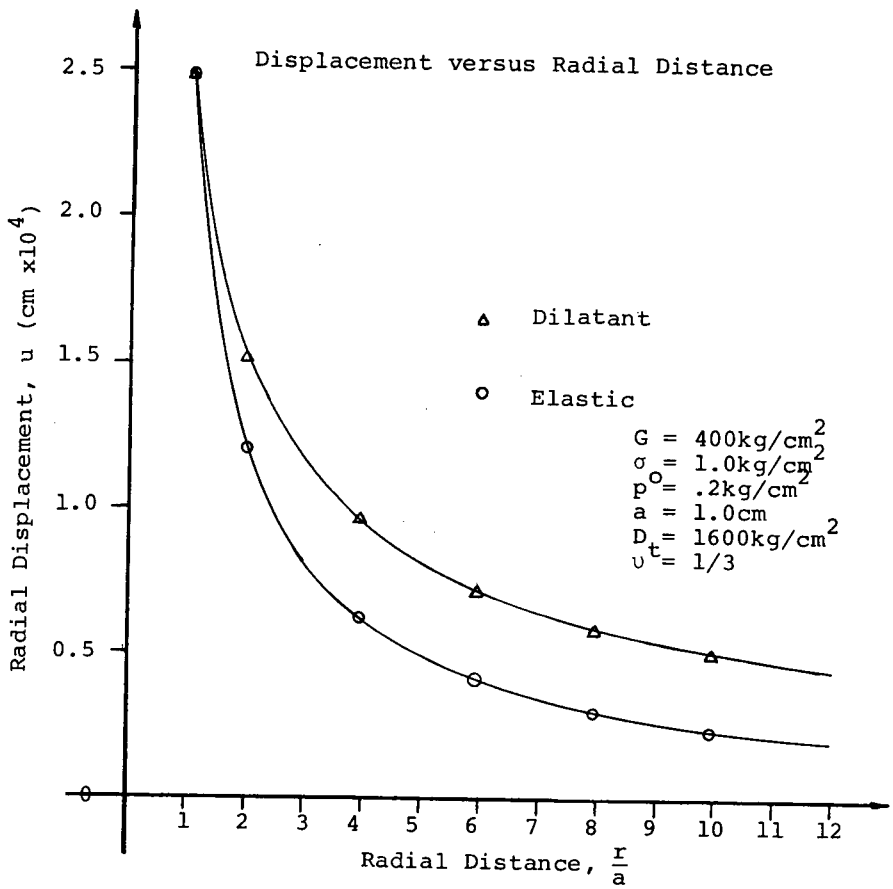

Figure 6. Comparison of Displacements in Dilatant and Elastic Material

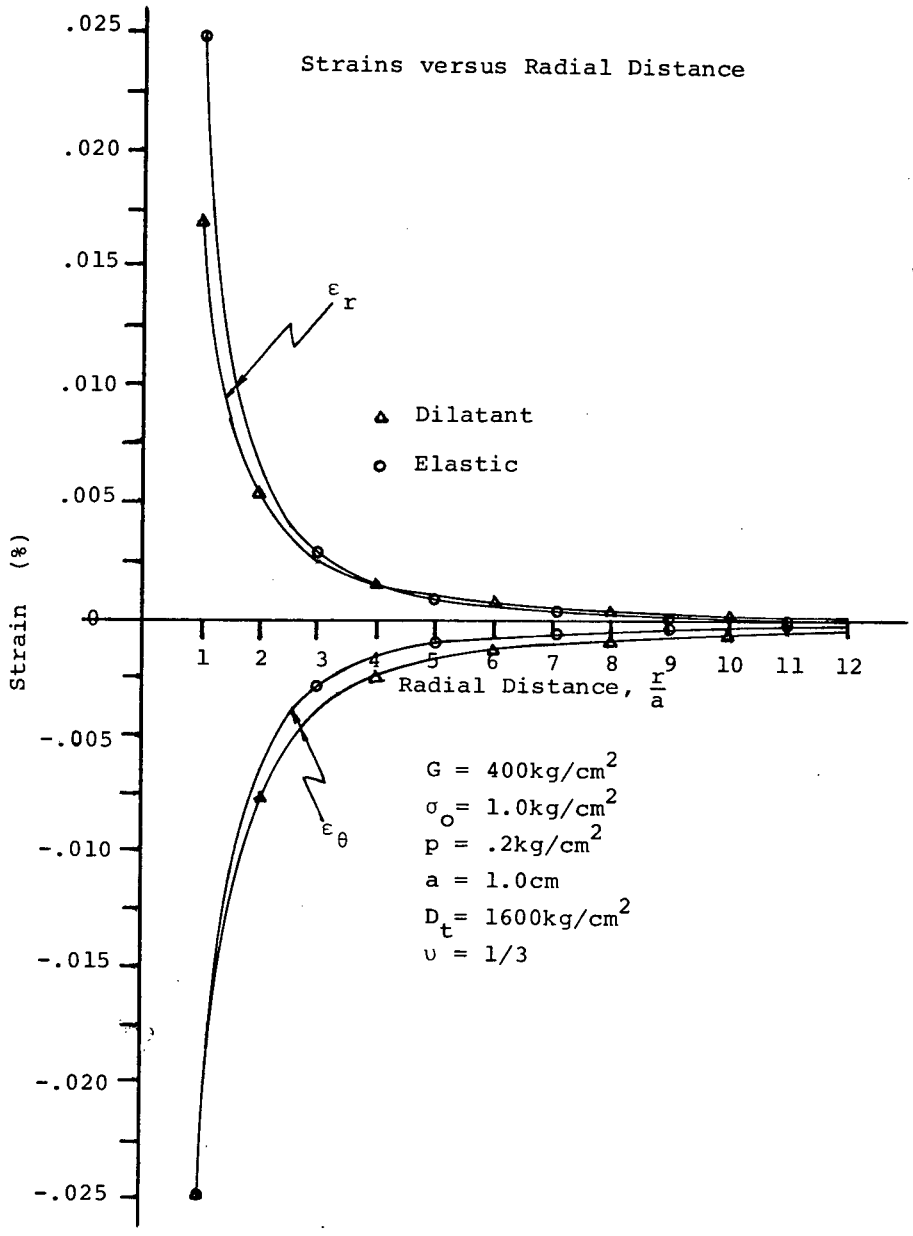

Figure 7. Comparison of Strains in Dilatant and Elastic Material

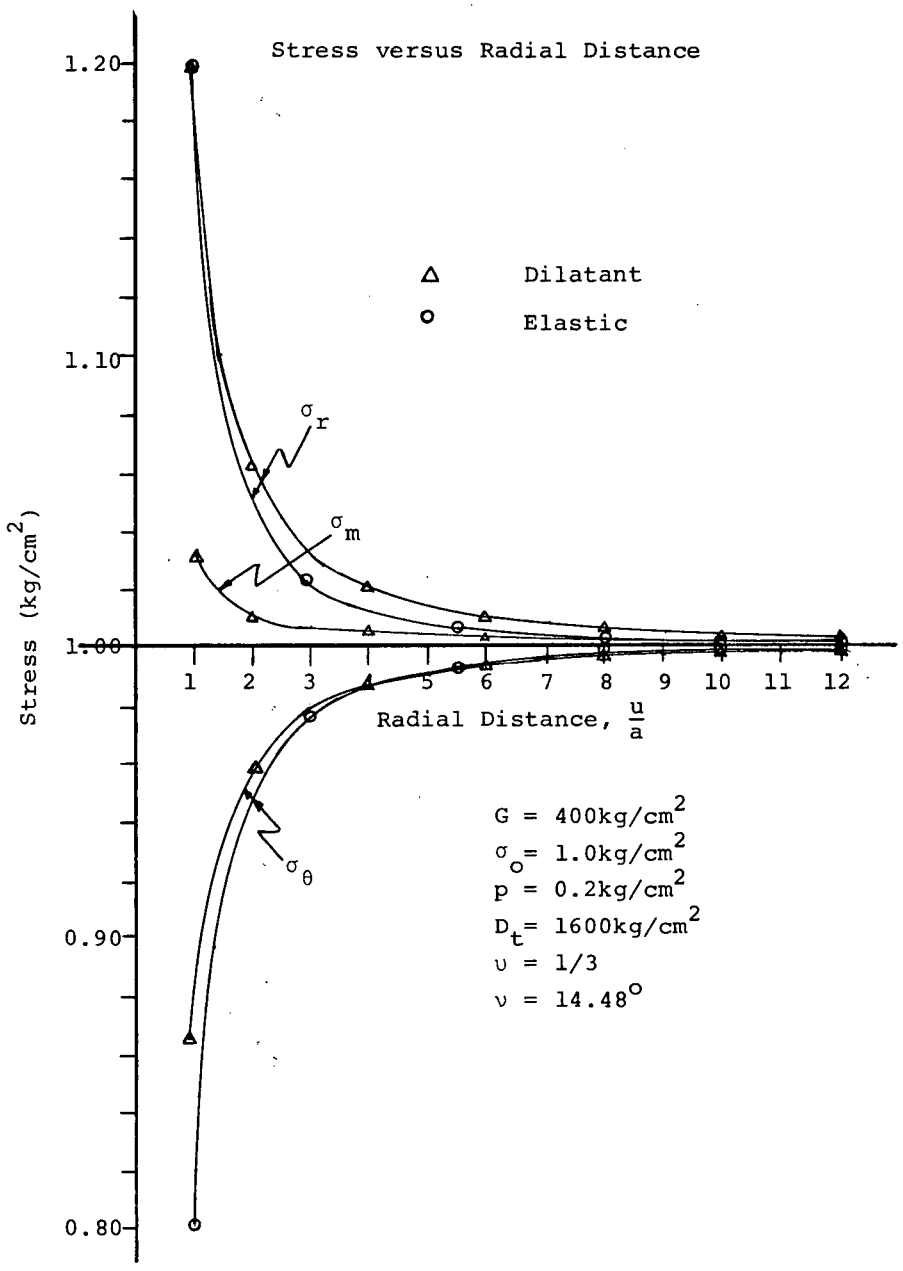

Figure 8. Comparison of Stresses in Dilatant and Elastic Material

which simplifies to:

$$\varepsilon_f = \frac{p_i \ (R-1)}{2G(Rn+1)} \qquad (2\text{-}68)$$

For an elastic material with no dilation $D_t = \infty$ so $n = 1$ and:

$$\varepsilon_{fe} = \frac{p_i(R-1)}{2G(R+1)} = \frac{p_i}{2G}\sin\phi \qquad (2\text{-}69)$$

but in a dilatant material with, for example, $D_t = \frac{1}{2}G$ and $n=0$

$$\varepsilon_{fd} = p_i\frac{(R-1)}{2-G} > \varepsilon_{fe} \qquad (2\text{-}70)$$

Dilation makes a soil have a higher strain to yield. Since the pressure-expansion curve still rises at a slope of 2G before yield, the dilatant soil appears stronger but not stiffer than the nondilatant elastic soil. On a modified Mohr diagram, the stress path for the dilatant material is inclined to the right, so the soil fails at a higher stress and appears stronger.

Hughes, Wroth and Windle (1977) handle dilation in basically the same manner. By assuming that volumetric strain due to increases in mean normal stress are negligible, Hughes et al give an equation for strain distribution within the plastic zone:

$$(\varepsilon_\theta + \frac{\kappa}{2}) = (\varepsilon_r + \frac{\kappa}{2})\left(\frac{p_i}{\sigma_R}\right)^{\left(\frac{n+1}{1-N}\right)} \qquad (2\text{-}71)$$

where: κ = the intercept of the ε_v vs. γ plot Figure 9.

p_i = initial soil stress

σ_R = radial stress at elastic-plastic boundary

The reasoning behind this equation can be applied to the elastic behaviour before any material yields. By assuming $\kappa = 0$, which Hughes et al do, the displacement field is the same as developed by Baguelin et al. For this case, the dilatant parameter D_t is related to the shear modulus and dilation angle:

$$D_t = \frac{G}{\sin\nu} \qquad (2\text{-}72)$$

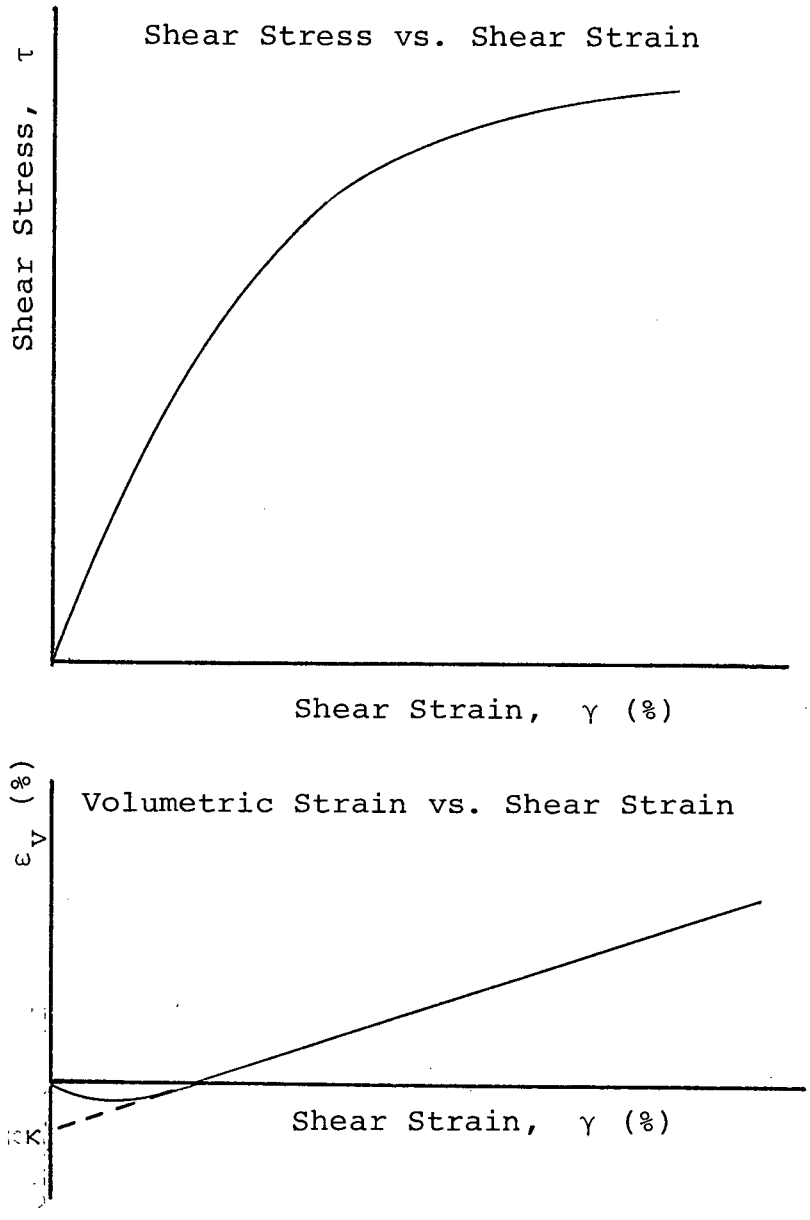

Figure 9. Volume Change Response used in Pressuremeter Analysis

which, for the pre-yield behaviour, results in:

$$u = u_a\left(\frac{a}{r}\right)^n$$

$$\text{where: } n = \frac{1-\sin\nu}{1+\sin\nu},\ 0 < n < 1$$

Going back to the case where a plastic annulus has formed, at radius r_f, the soil is just at yield. The displacement field is given by:

$$ur^n = -\frac{\kappa}{2}\, r^{(n+1)} + C_1 \qquad (2\text{-}73)$$

$$\text{where: } C_1 = \text{constant}$$

The boundary condition at the elastic-plastic interface is:

$$r = r_f,\quad \frac{u_{rf}}{r_f} = \varepsilon_f$$

which, when combined with 2-73 produces:

$$C_1 = \left(\varepsilon_f + \frac{\kappa}{2}\right) r_f^{(n+1)}$$

The displacement field within the plastic zone is, therefore:

$$\frac{u}{r} = -\frac{\kappa}{2} + \left(\varepsilon_f + \frac{\kappa}{2}\right)\left(\frac{r_f}{r}\right)^{(n+1)} \qquad (2\text{-}74)$$

$$\text{where: } a < r < r_f$$

As developed previously, the stress distribution within the plastic zone is:

$$\frac{\sigma_r}{\sigma_R} = \left(\frac{r_f}{r}\right)^{\left(1-\frac{1}{R}\right)} \qquad (2\text{-}24)$$

Upon substitution into 2-74, a relation between stress and strain is produced:

$$\frac{u}{r} = -\frac{\kappa}{2} + \left(\varepsilon_f + \frac{\kappa}{2}\right)\left(\frac{\sigma_r}{\sigma_R}\right)^{\left(\frac{R(n+1)}{R-1}\right.} \qquad (2\text{-}75)$$

At the cylinder face, $r = a$, and $\sigma_r = p$, therefore:

$$\varepsilon_a = \frac{u_a}{a} = -\frac{\kappa}{2} + \left(\varepsilon_f + \frac{\kappa}{2}\right)\left(\frac{p}{\sigma_R}\right)^{\left(\frac{R(n+1)}{R-1}\right.} \qquad (2\text{-}76)$$

Taking logarithms:

$$\log\left(\varepsilon_a + \frac{\kappa}{2}\right) = \log\left(\varepsilon_f + \frac{\kappa}{2}\right) + \frac{R(n+1)}{R-1}\log\frac{p}{\sigma_R} \qquad (2\text{-}77)$$

This reduces to:

$$\log p = \frac{R-1}{R(n+1)}\log(\varepsilon + \frac{\kappa}{2}) + \text{constant} \qquad (2\text{-}78)$$

where: $\varepsilon = \varepsilon_a$

By neglecting κ and plotting the applied pressure (in terms of effective stress) against the strain $\frac{u_a}{a}$ on log-log paper the slope of the straight line portion of the curve will be:

$$s = \frac{R-1}{R(n+1)} = \frac{\sin\phi\ (1+\sin\nu)}{1+\sin\phi} \qquad (2\text{-}79)$$

But, as will be developed in Chapter 3,

$$\frac{1+\sin\nu}{1-\sin\nu} = (\frac{1+\sin\phi}{1-\sin\phi})(\frac{1-\sin\phi_{cv}}{1+\sin\phi_{cv}}) \qquad (2\text{-}80)$$

or: $D = \frac{R}{K}$

where: ϕ_{cv} = constant volume friction angle

Equations 2-79 and 2-80 may be solved for the dilation angle, ν, and the friction angle, ϕ:

$$\sin\phi = \frac{(K+1)s}{(K-1)s+2} \qquad (2\text{-}81)$$

$$\sin\nu = \frac{2Ks-(K-1)}{K+1} \qquad (2\text{-}82)$$

A pressuremeter curve for fine sand in Sea Island is shown in Figure 10. This data is plotted on the log-log plot in Figure 10 . The slope of the linear portion of the curve is $s = 0.429$. In order to solve for the friction angle and dilation angle, the value of ϕ_{cv} is required. Figure 11 shows a graphical method of solution for ϕ and ν for various values of ϕ_{cv}. As can be seen in the figure, the value of ϕ_{cv} markedly affects the calculated values of ϕ and ν. Changing ϕ_{cv} from 30° to 36° changes the friction angle from 37° to 40° and changes the dilation angle from 8.3^o to 5.3^o. In order to accurately determine the soil properties, the constant volume friction angle must be determined accurately.

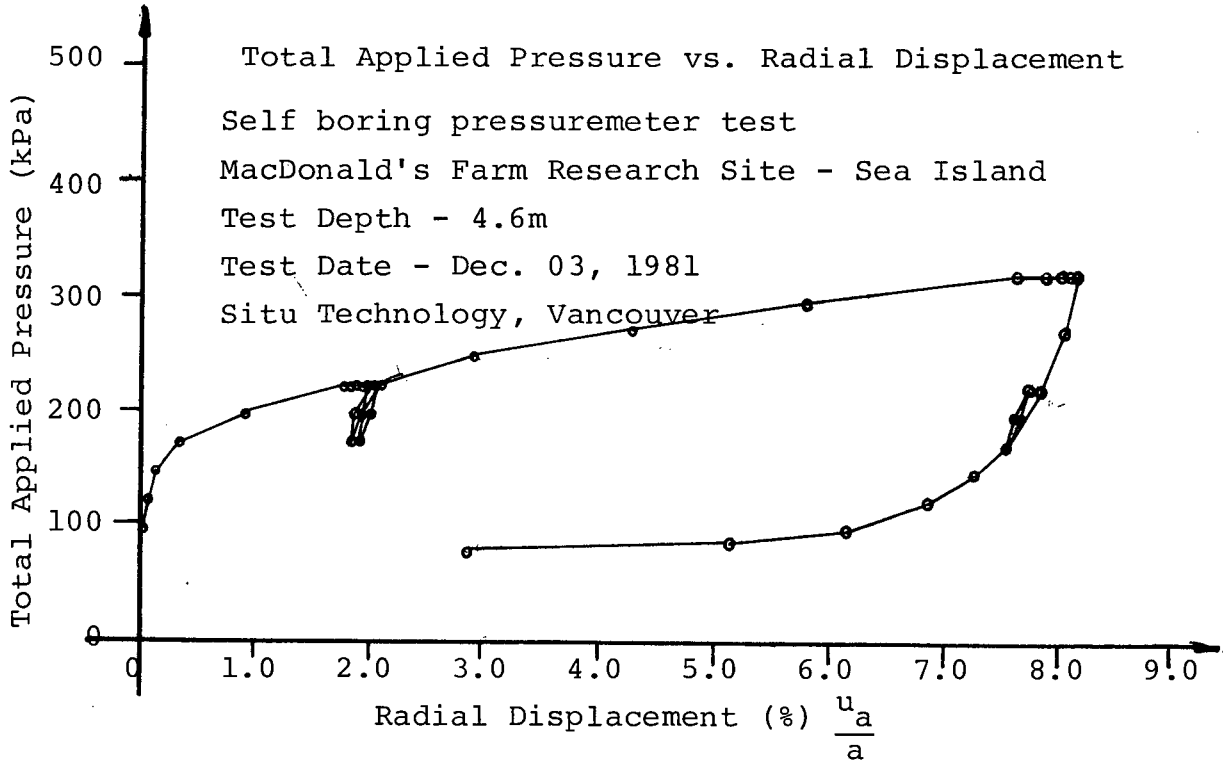

Pressure Expansion Curve for Fine Sand

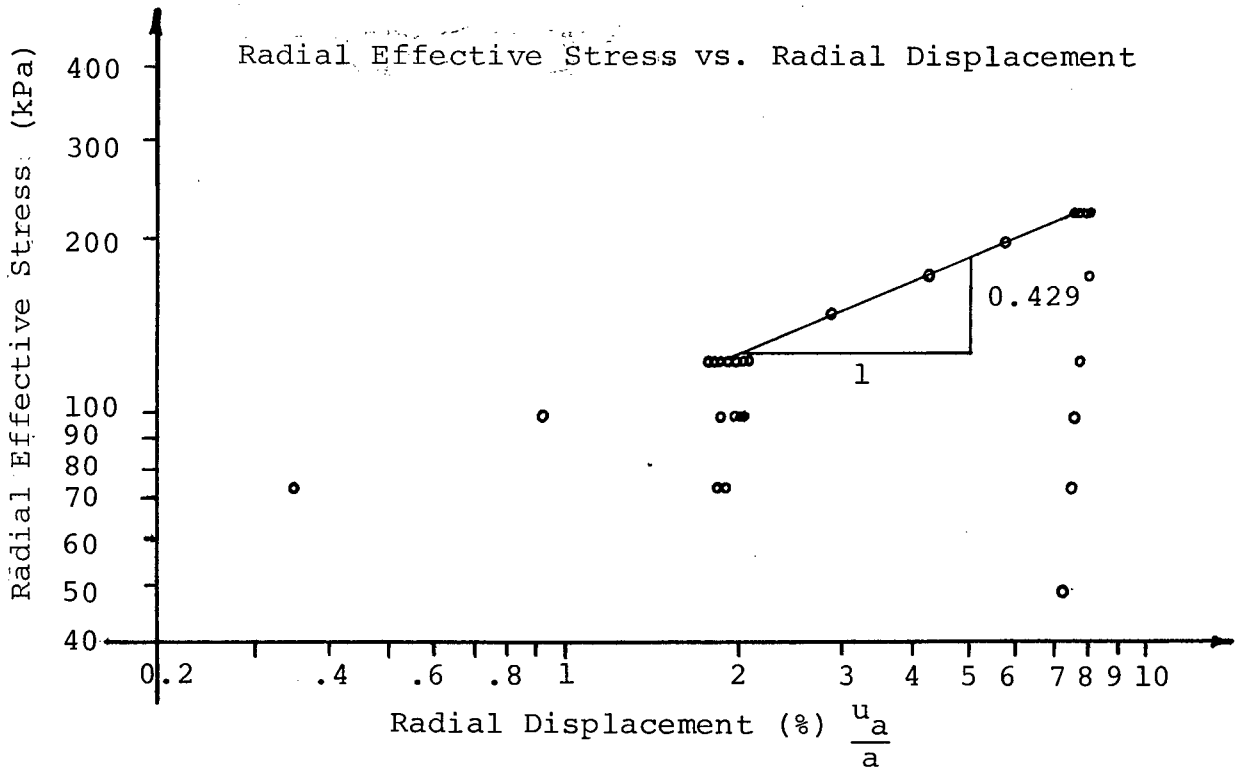

Figure 10 Log-Log Pressure Expansion Curve for Fine Sand

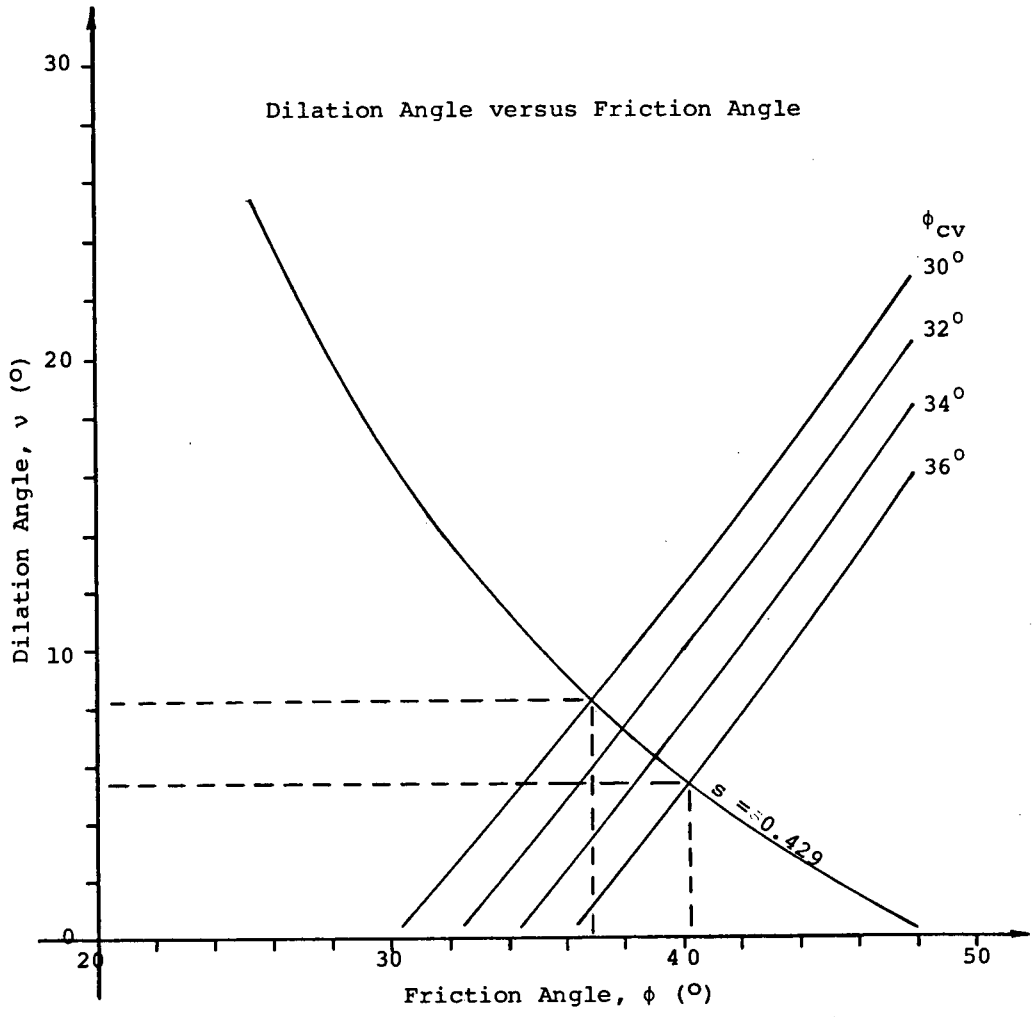

Figure 11. Graphical Method of Solution for values of ϕ' and ν.

Hughes et al show that the value of κ is small and can be neglected, however, examination of the simple shear data on loose sands by Vaid et al (1980), Stroud (1971) and the constant mean normal stress triaxial test data by Kokusho (1978), Figures 12 and 13, shows that for loose sands the value of κ may be in the range of one to two percent. The pressuremeter data from Sea Island is replotted in Figure 14, assuming various values of κ from 0.1% to 2.0%. The friction angle and dilation angle are graphically determined for $\phi_{cv} = 32^{o}$ in Figure 15. A value of κ = 0.1% changes the calculated values of ϕ and ν only slightly, but a value of κ= 2.0% changes the friction angle from 38° to 44° and changes the dilation angle from 7.2^{o} to 15.6^{o}. This is a significant difference. Neglecting the value of κ produces low estimates of ϕ , which may or may not be conservative, depending on the problem at hand.

The calculated values of the dilation angle and friction angle are also sensitive to the calculation of the slope of the log-log plot. Minor errors in plotting or determining the slope of the linear portion of the curve can easily change the value of the slope by ten percent. Figure 16 shows the variation of the friction angle and dilation angle for a $\pm$10% change in the slope of the log-log plot of the Sea Island sand using a $\phi_{cv} = 32^{o}$. The 10% change in the slope changes the friction angle by about 4° and changes the dilation angle by about 4°.

The method of analyzing the pressuremeter curve developed by Hughes et al is theoretically sound, however, it is sensitive

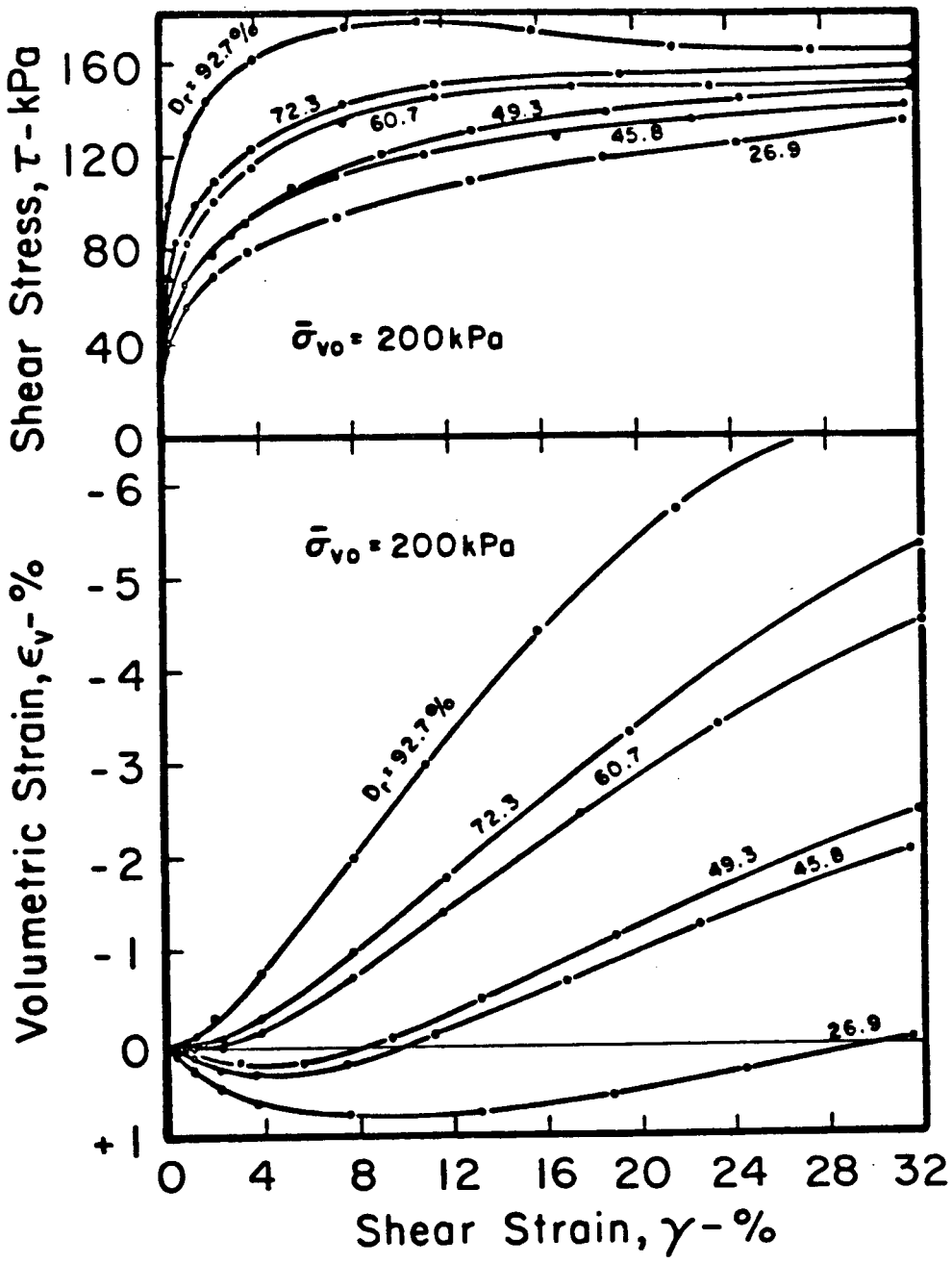

Figure 12. Stress-Strain behaviour of Ottawa Sand in drained simple Shear.(After Vaid,Byrne & Hughes).

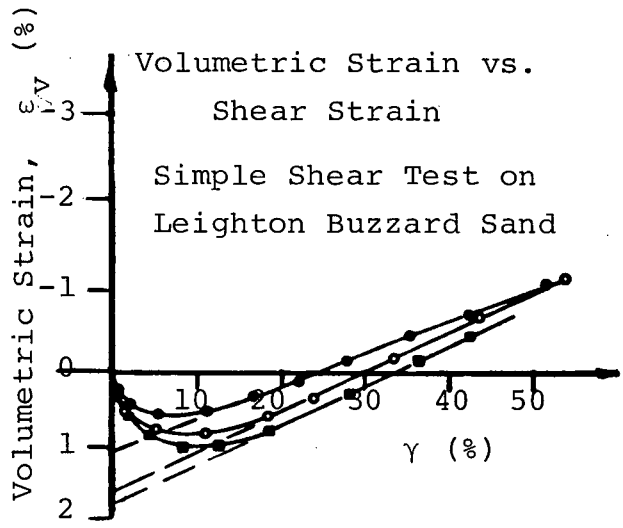

(After Stroud, 1971)

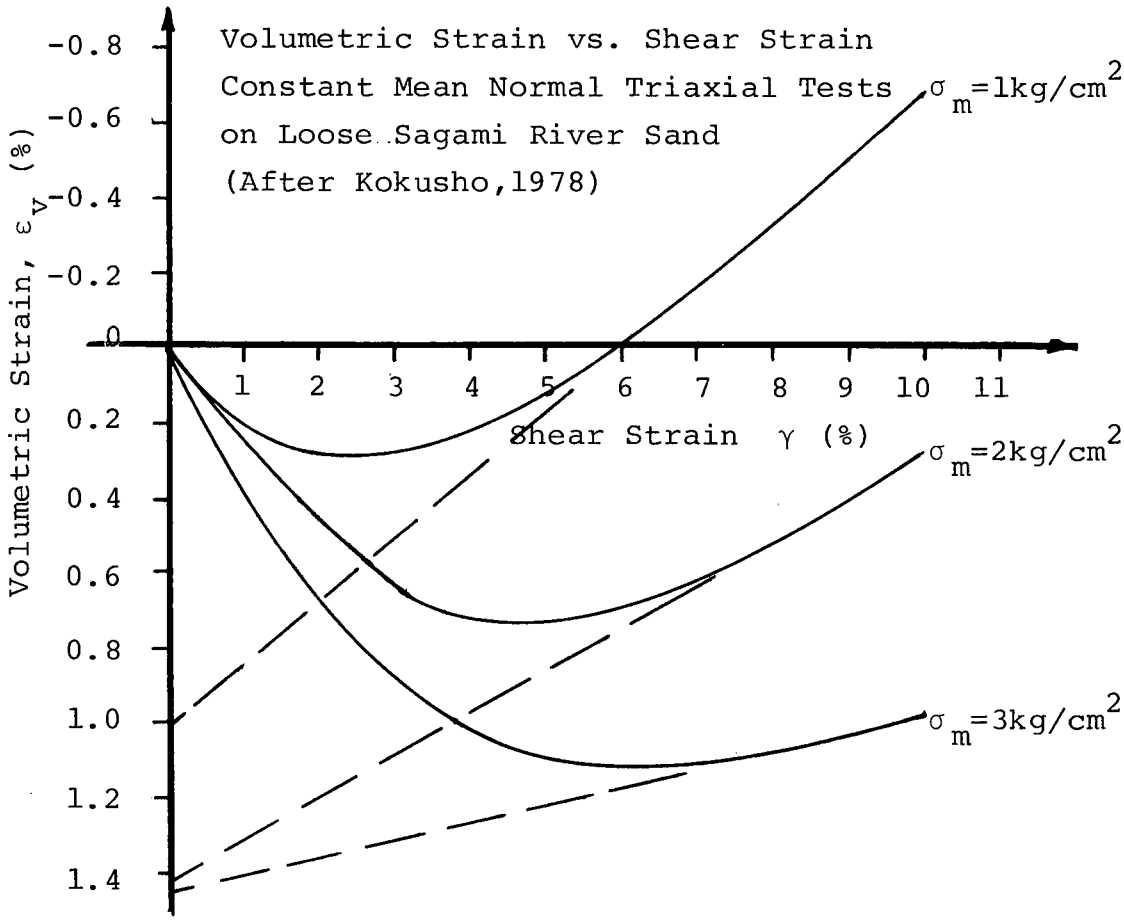

Figure 13. Volume Change Data for Loose Sand

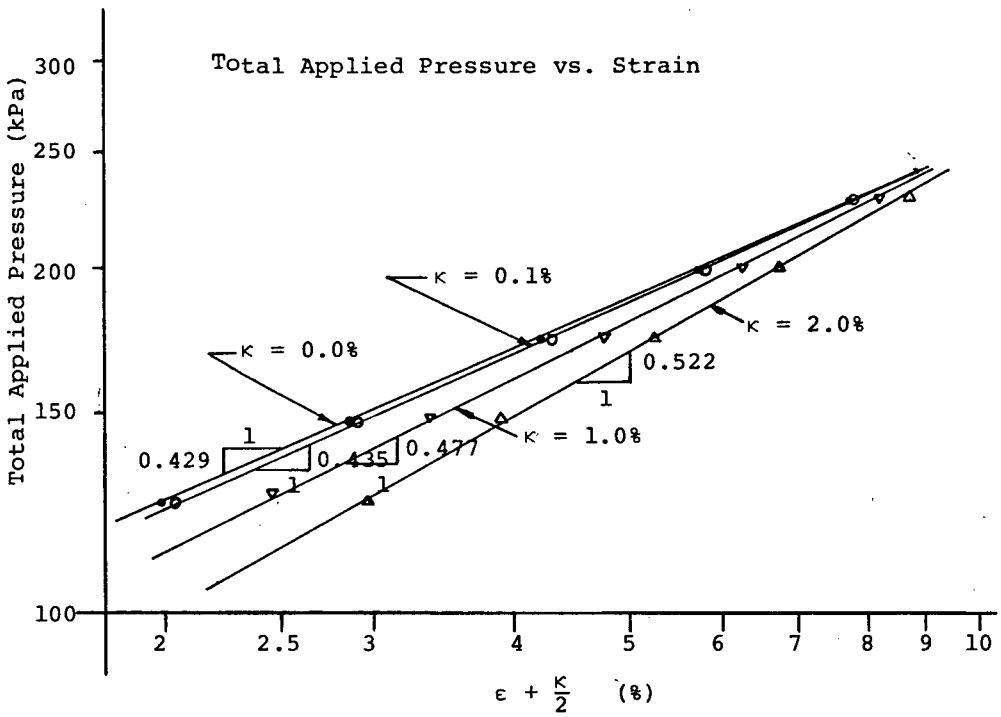

Figure 14. Log-Log Pressure Expansion Curve for Fine Sand With Non-zero 'κ'

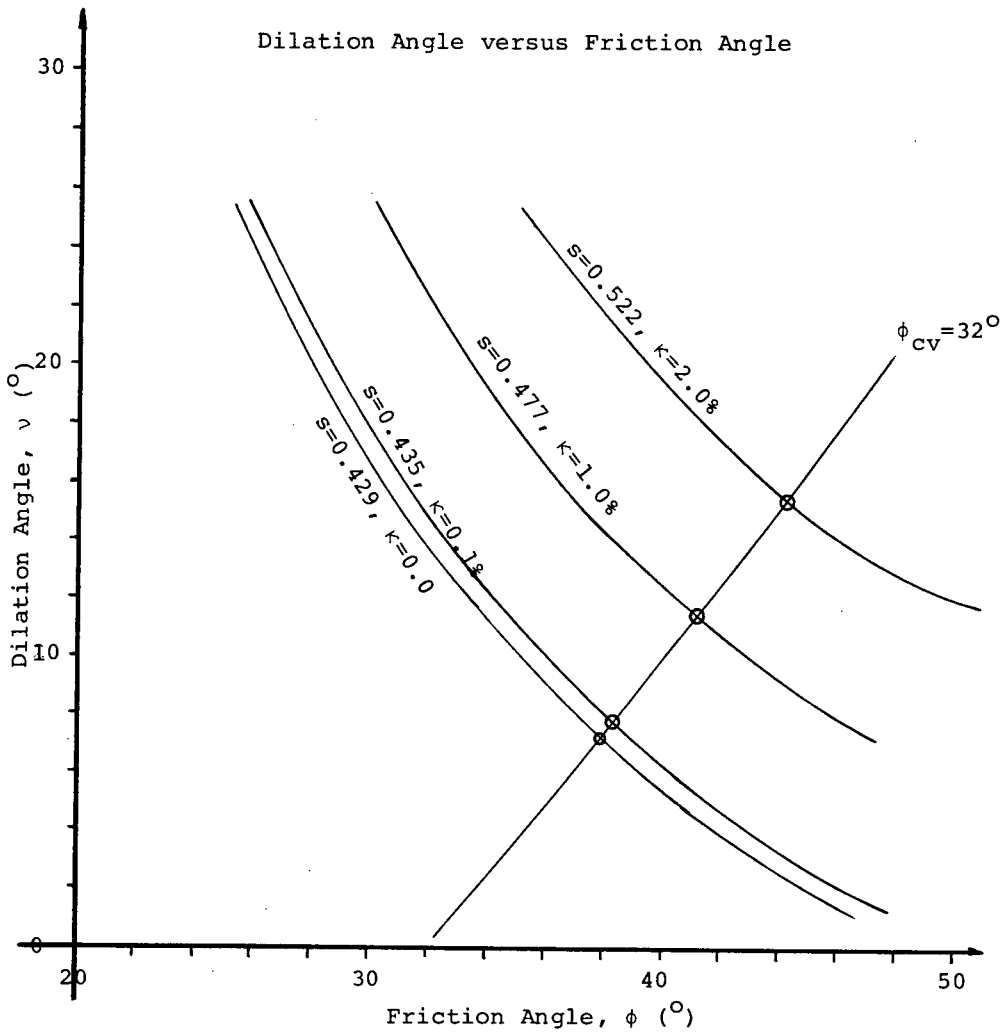

Figure 15. Variation of Calculated Values of ϕ and ν with Changes in the Value of 'κ'

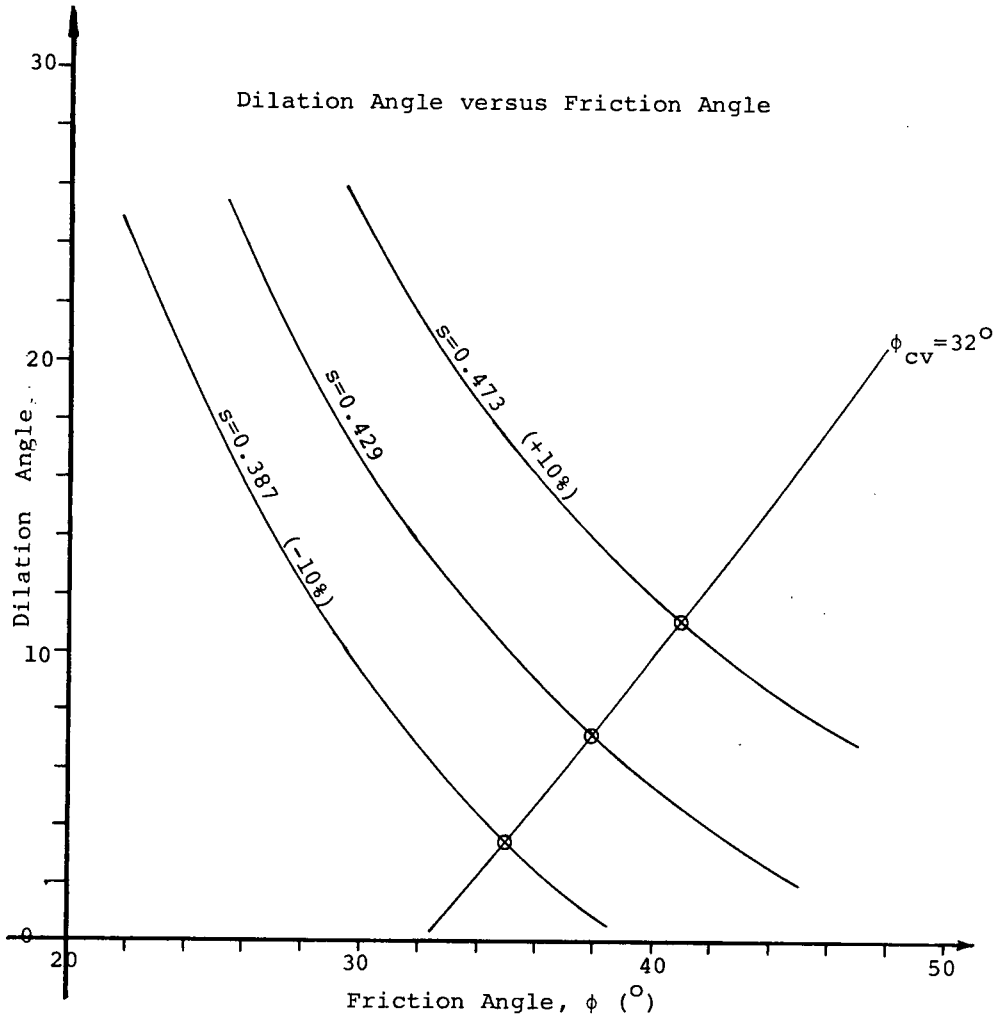

Figure 16. Variation of Calculated Values of ϕ and ν with Changes in the Value of 's'

to the value of ϕ_{cv} and calculation of the slope of the log-log plot of radial effective stress and strain. Combining the three uncertainties discussed above, the friction angle and dilation angle will probably only be accurate to about $\pm 2^{o}$. The error may be greater if κ is large or the estimated value of ϕ_{cv} is grossly in error.

Dilation significantly affects the manner in which the soil responds to the pressuremeter. Accurate strength and deformation characteristics cannot be determined unless the effect of dilation can be correctly incorporated in the analysis. The linear dilatant model shows qualitatively the effect of dilation, but a numerical analysis with shear-volume coupling and stress level dependent soil properties is required to determine the full effect of dilation on the pressuremeter.

Chapter 3

Soil Model

3.1 Definition of Stress and Strain

The soil is modelled as a homogeneous, isotropic, incremental linear elastic continuum. From a microscopic view, soil is far from being a homogeneous continuum, but from a macroscopic view, when the geometrical dimensions defining the form of the body are large in comparison with the dimension of individual soil grains, the assumption of homogeneity and continuity can be made with sufficient accuracy.

The strength and deformation of soil is controlled by the effective stress. This was defined by Terzaghi as:

$$\sigma' = \sigma - \mu \qquad (3\text{-}1)$$

where: σ = the total stress

μ = the pore pressure

σ' = the effective stress

Other relations have been proposed for the effective stress that take account of the intergranular contact area, but for most engineering problems at low pressures, Terzaghi's definition is sufficiently accurate. The soil model will be derived in terms of effective stress parameters, but the computer program is able to handle either effective stress or total stress. In further work, all references to stress will mean effective stress.

The model will be presented for the general case of a three dimensional rectangular Cartesian coordinate system. Within the computer program, the model is used for two dimensional problems in either rectangular or polar coordinates or three dimensional problems under triaxial conditions ($\sigma_1, \sigma_2 = \sigma_3$

or $\sigma_1 = \sigma_2, \sigma_3$).

In a three dimensional space, with a rectangular coordinate system using x, y and z, the following stresses may occur in a body:

$$\begin{array}{lll} \sigma_x, & \sigma_y, & \sigma_z, \\ \tau_{xy}, & \tau_{yz}, & \tau_{zx}, \\ \tau_{xz}, & \tau_{yx}, & \tau_{zy}, \end{array}$$

These stresses are shown in Figure 17. In order to satisfy equilibrium of the body:

$$\begin{aligned} \tau_{xy} &= \tau_{yx} \\ \tau_{zy} &= \tau_{yz} \\ \tau_{zx} &= \tau_{xz} \end{aligned}$$

Therefore six quantities are required to uniquely define the state of stress of a body in a three dimensional space.

A body undergoing a change of its stress state will also undergo deformations. In the three dimensional rectangular coordinate system the displacements u, v and w are the displacements in the x, y and z directions, respectively. A compatible set of strains may be determined from the displacement field. For the three dimensional case:

$$\begin{aligned} \varepsilon_x &= -\frac{du}{dx}, \\ \varepsilon_y &= -\frac{dv}{dy}, \\ \varepsilon_z &= -\frac{dw}{dz}, \\ \gamma_{xy} &= -(\frac{dv}{dx} + \frac{du}{dy}) \\ \gamma_{yz} &= -(\frac{dw}{dy} + \frac{dv}{dz}) \\ \gamma_{zx} &= -(\frac{du}{dz} + \frac{dw}{dx}) \\ \gamma_{yx} &= -(\frac{du}{dy} + \frac{dv}{dx}) \\ \gamma_{zy} &= -(\frac{dv}{dz} + \frac{dw}{dy}) \\ \gamma_{xz} &= -(\frac{dw}{dx} + \frac{du}{dz}) \end{aligned} \qquad (3\text{-}2)$$

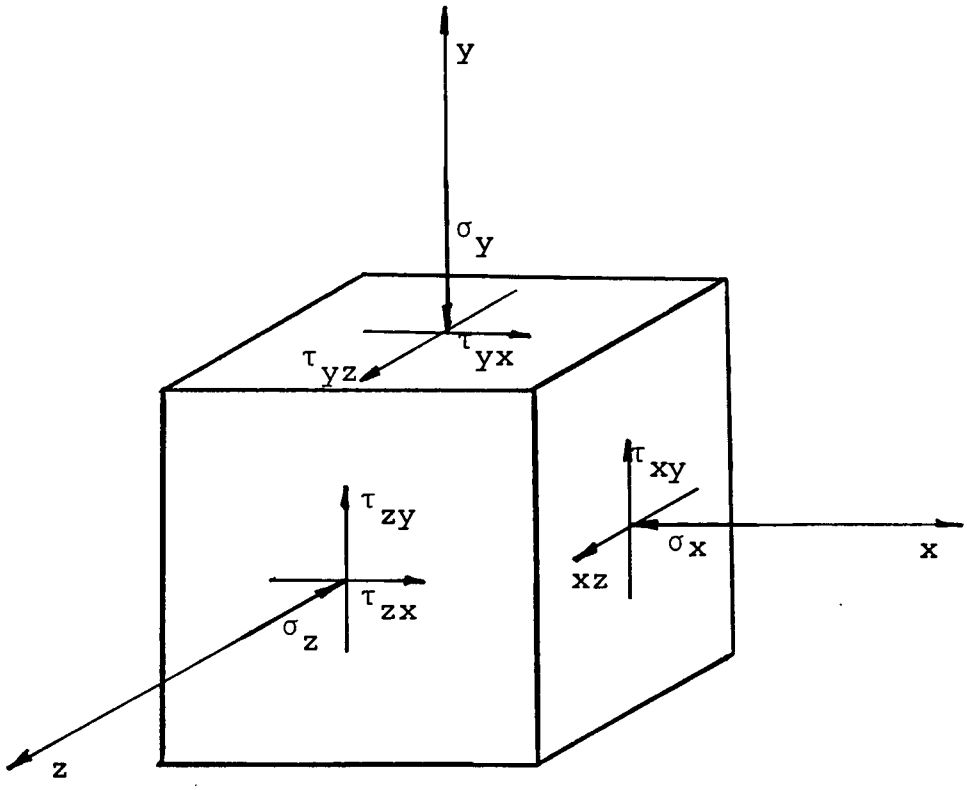

Figure 17 Stresses in Cartesian Coordinates

It may be seen that:

$$\gamma_{xy} = \gamma_{yx}, \quad \gamma_{yz}, \quad \gamma_{zy}, \quad \gamma_{zx} = \gamma_{xz}.$$

Therefore, only six strains define the state of deformation of the body. This definition may be used only when strains are small and second order effects may be neglected. When second order effects must be included, an alternate definition of strain must be used. Almansi strains were used in Chapter 2 to determine the pressuremeter limit pressure.

Six strains are derived from three independent displacements. Three equations of compatibility must exist to uniquely determine the six strains from the three displacements. By deriving the strains from the displacement field, the compatibility conditions are automatically satisfied.

3.2 Constitutive Relation

In order to be of any use in solving stress-deformation problems, stresses and strains must be related in some fashion. The constitutive relations define the stress-strain relation. The constitutive relations for soil are highly complex. Soil is anisotropic, nonhomogeneous, nonlinear and inelastic. Under these conditions 36 coefficients are required to relate stress to strain. In addition, these 36 coefficients are stress level dependent and will also depend on the stress path followed during deformation. Specifying such a relation would be a formidable task, at best, and in many cases, impossible.

In order to reduce the complexity of the problem a number of simplifying assumptions must be made. By assuming that the material is linear elastic, homogeneous and isotropic, the number of coefficients is reduced from thirty-six to two. The

assumption of linearity means that strains due to a set of stresses may be obtained through superposition of the strains due to each stress. Elastic means that stress and strain are uniquely related, regardless of stress path. Isotropy means that the material constants are the same in all directions. Homogeneity means that the material is the same at all points in the body and no shear volume coupling means that no volumetric strains occur on application of a pure shear stress. For a linear elastic isotropic medium, the stress-strain relation is defined by the matrix (D):

$$(D) = \frac{E}{(1-2\upsilon)(1+\upsilon)} \begin{bmatrix} 1-\upsilon & \upsilon & \upsilon & 0 & 0 & 0 \\ \upsilon & 1-\upsilon & \upsilon & 0 & 0 & 0 \\ \upsilon & \upsilon & 1-\upsilon & 0 & 0 & 0 \\ 0 & 0 & 0 & \frac{1-2\upsilon}{2} & \upsilon & \upsilon \\ 0 & 0 & 0 & \upsilon & \frac{1-2\upsilon}{2} & \upsilon \\ 0 & 0 & 0 & \upsilon & \upsilon & \frac{1-2\upsilon}{2} \end{bmatrix}$$

where: $\{\sigma\} = (D) \quad \{\varepsilon\}$ (3-3)

and: $\{\sigma\}$ = stress vector

$\{\varepsilon\}$ = strain vector

Four elastic constants are defined, with any two being independent and sufficient to uniquely specify the constitutive relation. The four constants are:

Young's modulus, E

Bulk modulus, B

Shear modulus, G

Poisson's ratio, υ

The four constants are related by:

$$G = \frac{E}{2(1+\upsilon)} \tag{3-4}$$

$$B = \frac{E}{3(1-2\upsilon)} \tag{3-5}$$

The computer finite element program has been developed using the Young's modulus and Bulk modulus as input parameters.

A linear elastic isotropic material would not model soil behaviour very well. Nonlinearity, plastic strains and shear volume coupling are three characteristics of soil behaviour that must be incorporated in a soil model.

3.3 Nonlinearity

Nonlinearity of the stress-strain relation is accounted for by using stress level dependent moduli. Typical deviator stress versus axial strain behaviour for sand in drained triaxial tests is shown in Figure 18. Kondner and Zelasko (1963) and Duncan and Chang (1970) have shown that these curves may be approximated by modified hyperbolas of the form:

$$(\sigma_1 - \sigma_3) = \frac{\varepsilon}{\left(\frac{1}{E_i} + \frac{\varepsilon}{(\sigma_1 - \sigma_3)_{ult}}\right)} \tag{3-6}$$

When an incremental elastic approach is used, the tangent Young's modulus is given by:

$$E_t = E_i\left(1 - \frac{R_f(1-\sin\phi)(\sigma_1 - \sigma_3)}{2c\cos\phi + 2\sigma_3\sin\phi}\right)^2 \tag{3-7}$$

where: E_i = initial tangent Young's Modulus

σ_1 = major principal effective stress

σ_3 = minor principal effective stress

ϕ = friction angle

R_f = the failure ratio, the ratio of maximum deviator stress from triaxial test to the asymptotic deviator stress defined by the hyberbola.

Figure 19 shows a typical hyperbolic stress-strain relation.

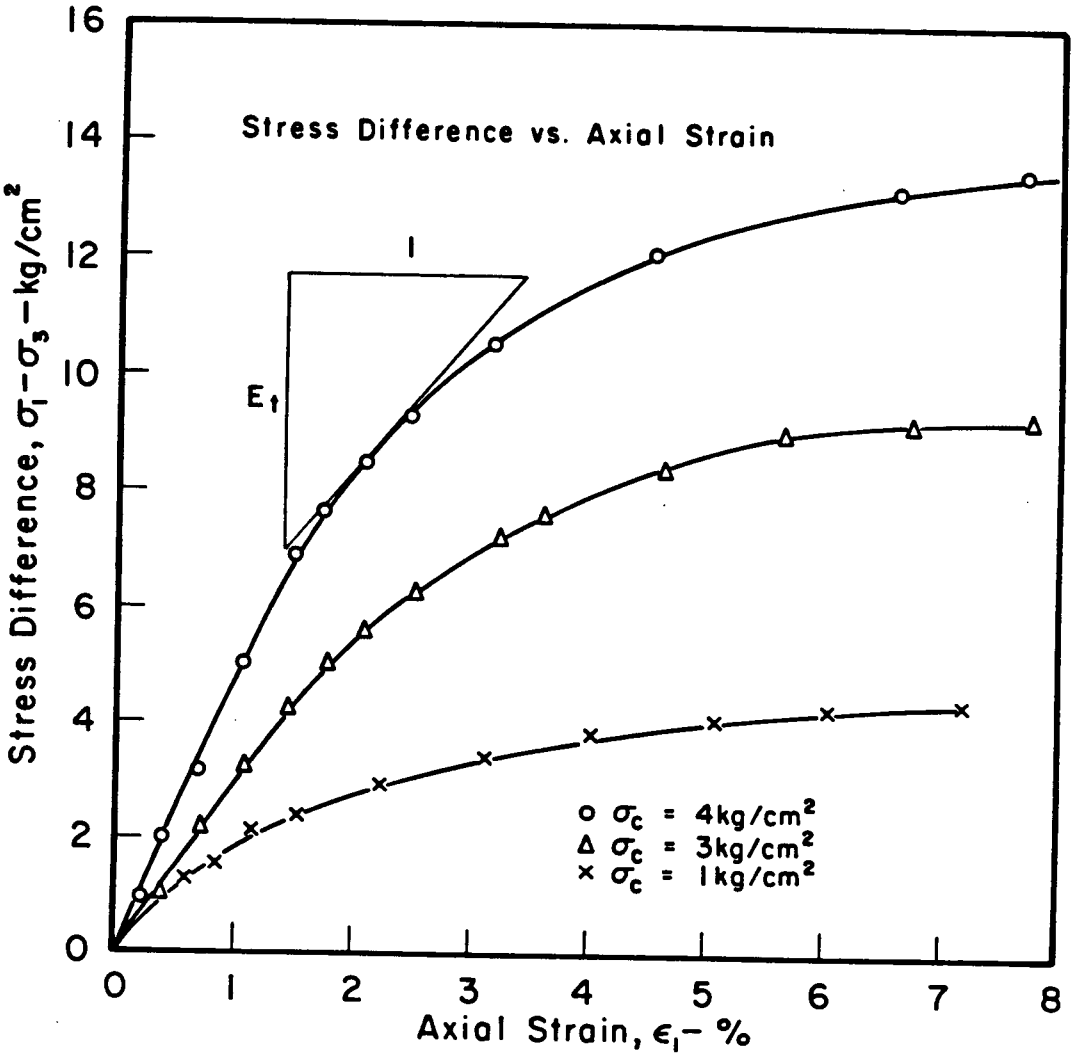

Figure 18 Stress Strain Curves for Drained Triaxial Tests on Sand. (After Varadarajan and Mishra).

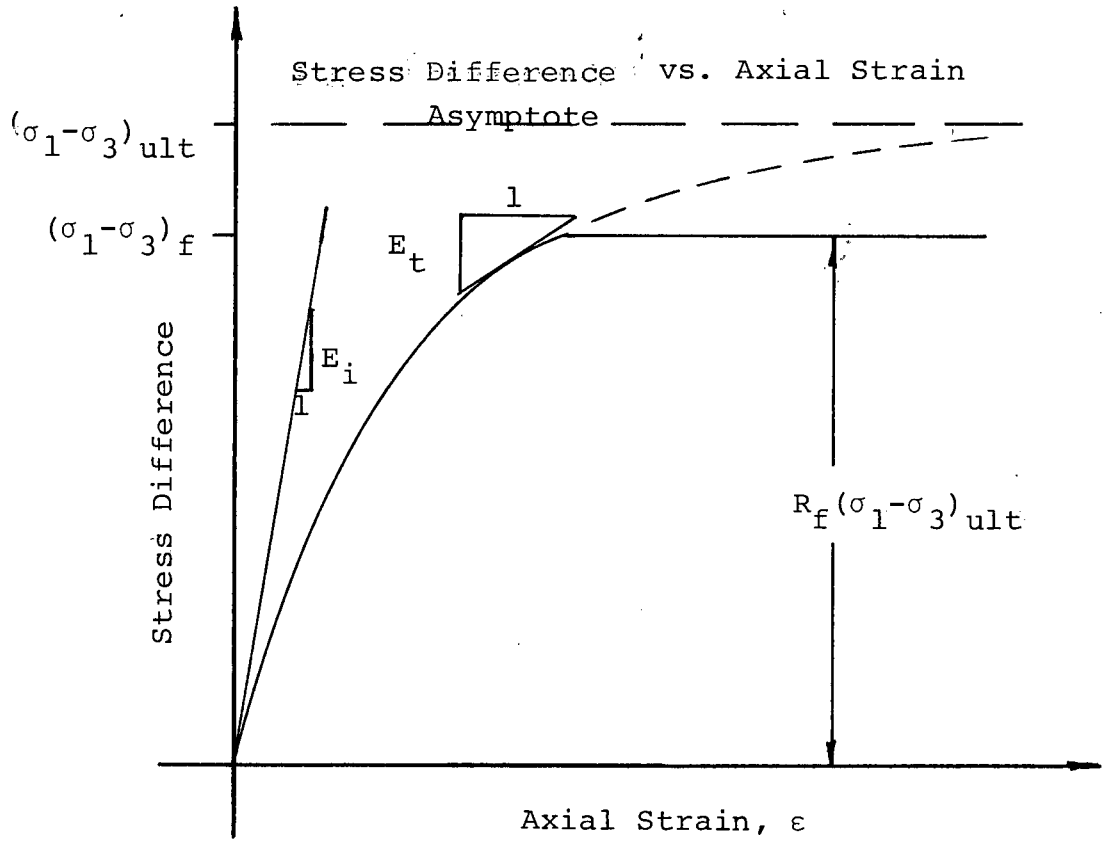

Figure 19. Modified Hyperbolic Stress-Strain Relation

The initial tangent Young's modulus is also stress level dependent. Janbu (1963) presented an empirical relation for E_i:

$$E_i = k_e p_a \left(\frac{\sigma_3}{p_a}\right)^n \qquad (3\text{-}8)$$

where: k_E = Young's modulus number

n = modulus exponent

p_a = atmospheric pressure

Triaxial tests are generally conducted with a constant confining pressure, σ_3. For this reason σ_3 is used in the relation for the initial modulus. However, the soil stiffness is related to the level of the mean normal stress, in which case:

$$E_i = k_E p_a \left(\frac{\sigma_m}{p_a}\right)^n \qquad (3\text{-}9)$$

In order to use this relation, triaxial tests must be conducted at constant mean normal stress. The pressure control system is complex, so tests of this nature are not usually conducted. The finite element program is set up to use either σ_3 or σ_m in the calculation of E_i, at the user's discretion.

The method of obtaining the hyperbolic parameters from triaxial tests is discussed in detail by Duncan and Chang and by Duncan et al (1978) and will not be presented here.

The friction angle, ϕ, is also stress level dependent. Work by Vesic and Clough (1968) has shown that the variation of ϕ with the logarithm of the mean normal stress is nearly linear, as shown in Figure 20. The friction angle at any stress level is given by:

$$\phi = \phi_1 - \Delta\phi \log\left(\frac{\sigma_m}{p_a}\right) \qquad (3\text{-}10)$$

where: ϕ_1 = the friction angle at one Atm.

$\Delta\phi$ = the change in friction angle over one log cycle increase in pressure

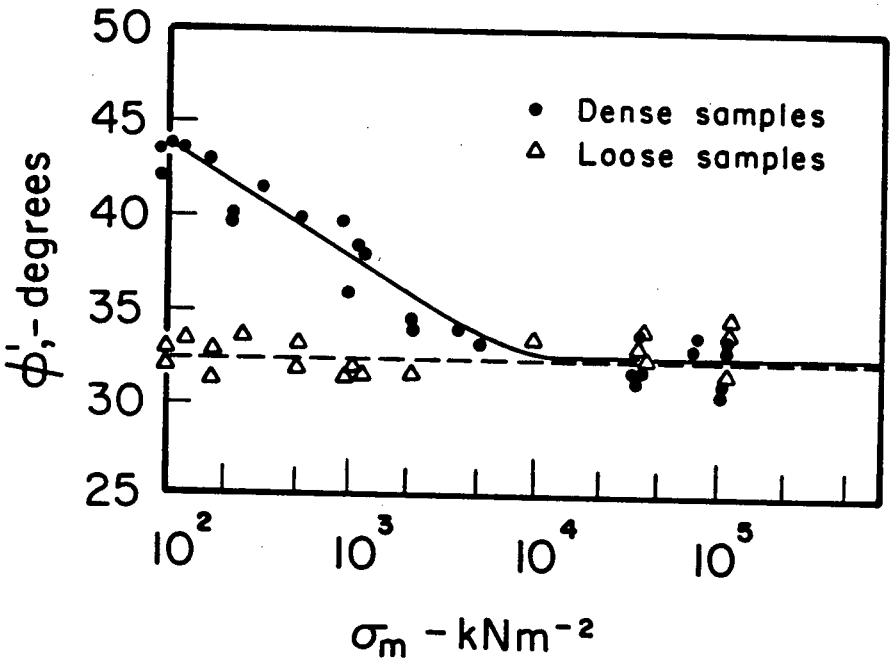

Figure 20.
Angle of Internal Friction for Chattahoochee River Sand tested at different Stress levels in the Triaxial Apparatus.
(After Vesic and Clough, 1968).

The volumetric response of the soil to increases in the mean normal stress is also nonlinear. Characteristic mean normal stress versus volumetric strain behaviour for loose Calais sand as tested by El-Sohby and Andrawes (1972) is shown in Figure 21. The tangent modulus at any stress level is given by:

$$B_t = k_B p_a \left(\frac{\sigma_m}{p_a}\right)^m \qquad (3\text{-}11)$$

where: k_B = modulus number

m = modulus exponent

The modulus number and exponent may be determined from isotropic consolidation data. The volumetric strain may be related to the mean normal stress by:

$$\varepsilon_v = a(\sigma_m)^{(1-m)} \qquad (3\text{-}12)$$

Differentiating yields:

$$\frac{d\varepsilon_v}{d\sigma_m} = a(1-m)(\sigma_m)^{-m} \qquad (3\text{-}13)$$

or:

$$B_t = \frac{d\sigma_m}{d\varepsilon_v} = \frac{(\sigma_m)^m}{a(1-m)} \qquad (3\text{-}14)$$

By equating 3-11 and 3-14 the modulus number and exponent can be determined:

$$k_B = \frac{1}{a(1-m)(p_a)^{(1-m)}} \qquad (3\text{-}15)$$

The values of 'a' and 'm' can be determined by plotting ε_v and σ_m on log-log paper. Taking logarithms results in:

$$\log\varepsilon_v = \log(a) + (1-m)\log(\sigma_m) \qquad (3\text{-}16)$$

So, as shown in Figure 22, the intercept on the log-log plot gives the value 'a' and the slope is (1-m). This method can be used with any ε_v versus σ_m data to obtain 'm', however, isotropic consolidation test data starting from the unstrained

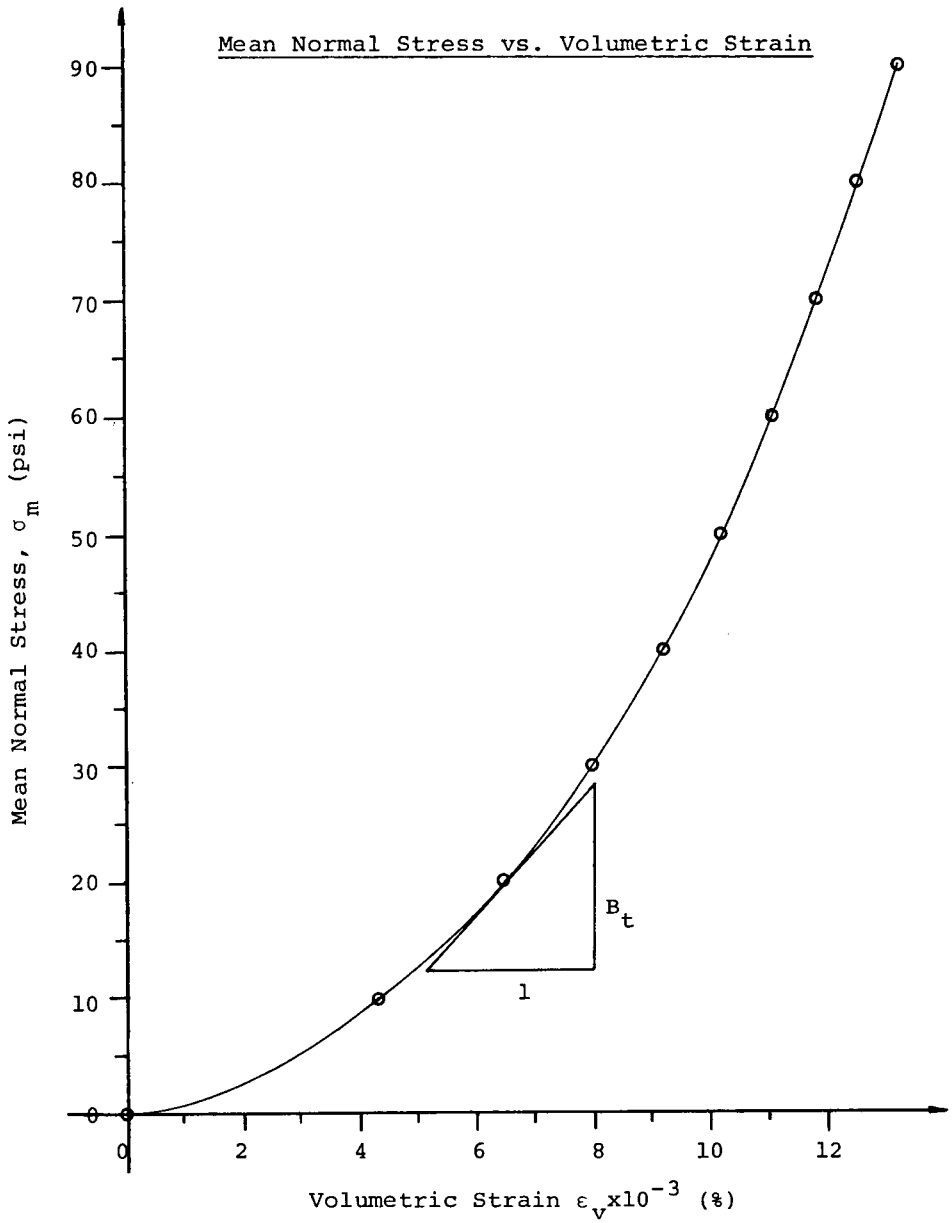

Figure 21. Isotropic Consolidation Data (After El-Sohby&Andrawes)

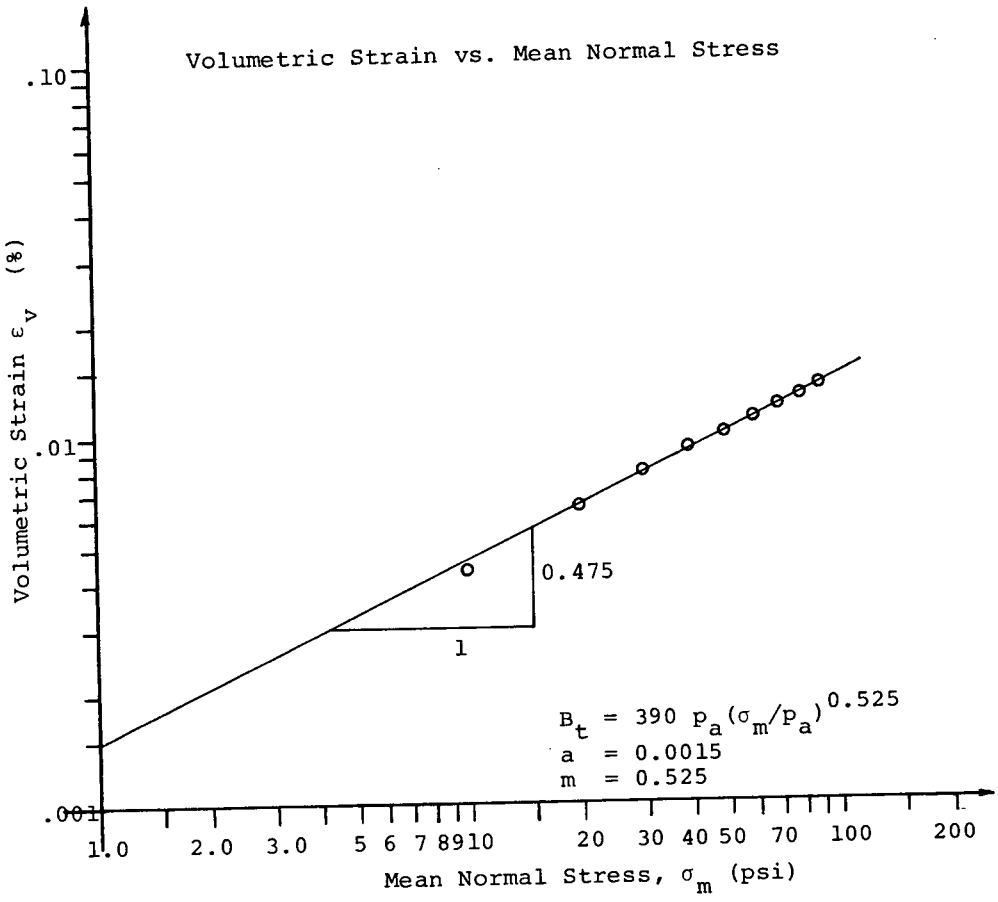

Figure 22 . Log-Log Volumetric Strain vs. Mean Normal Stress

condition is required to correctly determine 'a'.

3.4 Plastic Strains

On application of stress, soil undergoes both elastic (recoverable) and plastic (irrecoverable) strains. Under the loading conditions found in the pressuremeter test, in which the stresses and strains continually increase, the ability to differentiate between the plastic strain and the elastic strain is not crucial. However, for those cases in which the load cycles and the strain increment reverses, the separation of the elastic and plastic strain accumulated during the loading is important. Both plastic shear strain and plastic volumetric strain occur. Plastic shear strain may be taken into account with reasonable accuracy by the use of a rebound shear modulus, as shown in Figure 23. The program is not as yet set up to correctly handle the plastic strain on stress reversal.

Plastic volume changes occur both from changes in the mean normal stress and changes in the shear stress. Most of the shear induced volume change is plastic, while a portion of the consolidation volume change is elastic, even for virgin loading. The proportion of elastic volumetric strain from consolidation increases with the number of load cycles.

3.5 Shear Volume Coupling

The phenomenon of shear volume coupling is one of the predominant differences between soil and other engineering materials. Upon application of a pure shear stress, materials such as steel will undergo no volume changes. Soil, on the other hand, may undergo significant volume changes depending on the level of the stress. This shear volume coupling is

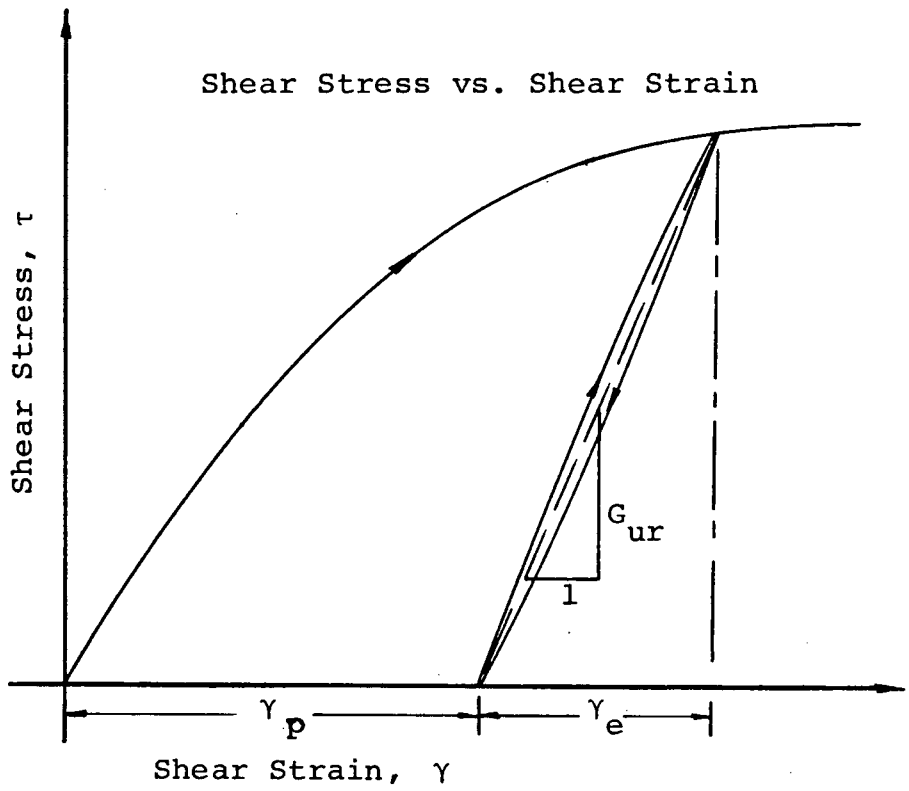

Figure 23. Definition of Rebound Modulus

shown in the simple shear test data in Figure 12. The simple shear test is not one of pure shear. Changes in the mean normal stress do occur, so some of the volumetric strain is due to consolidation. However, as can be seen in the figure, even the loose samples undergo dilation after the initial contraction, so all sands have some shear volume coupling.

The phenomenom of shear volume coupling has been studied by Rowe (1962,1971). He has proposed a stress dilatancy theory that has been used by other researchers. His theory is for the separation of plastic and elastic volume changes and cannot be directly used in the present model. A simple modification is proposed so that the theory can be incorporated in the model.

3.5.1 Rowe's Stress Dilatancy Theory

Rowe developed his theory from a study of particulate mechanics. The stress dilatancy equation is based upon the conditions of equilibrium, limiting friction and minimization of absorbed energy for rigid particles in sliding contact. Rowe looked at both the plastic strains and the elastic strains. In Rowe's theory, plastic strains are due to two components. One component is rigid particle slip and is related to the principal stress ratio. The other component is particle crushing and is related to the level of the mean normal stress. The model derived by Rowe is limited to cases in which the major principal strain direction does not reverse.

Only Rowe's theory developed for slip strains will be discussed. The slip strains so calculated will be used to model shear induced volume changes. The stress dilatancy equation has been discussed by Rowe and by Gunaratne (1981), so only the

major points and the modification will be discussed in this work.

A number of assumptions underlie the theory. These are:

1) Particles are rigid. This means that elastic deformation of the particles does not occur.

2) Deformations occur as a result of relative motion between groups of particles. The number of rolling contacts within the soil mass is negligible compared to the number of sliding contacts.

The stress dilatancy equation as developed by Rowe is:

$$\frac{d\sigma_{1s}}{(\sigma_2 d\varepsilon_{2s} + \sigma_3 d\varepsilon_{3s})} = \tan^2\left(45 + \frac{\phi_f}{2}\right) \qquad (3\text{-}17)$$

where: σ_1, σ_2 and σ_3 = principal effective stresses

$d\varepsilon_{1s}$, $d\varepsilon_{2s}$ and $d\varepsilon_{3s}$ = principal slip strain increments

ϕ_f = a friction angle which lies between ϕ_u and ϕ_{cv}

where: ϕ_u = angle of friction of particles in sliding

ϕ_{cv} = constant volume friction angle

Under ideal conditions, if all sliding takes place at the critical angle, β_c, and no rolling contacts occur, ϕ_f will be equal to ϕ_u. Since not all sliding takes place at β_c, more energy is absorbed and ϕ_f approaches ϕ_{cv}. Rowe has experimentally determined that for:

Triaxial compression $\sigma_2 = \sigma_3$ and extension $\sigma_1 = \sigma_2$

Dense sand, pre-peak	$\phi_f = \phi_u$
Dense sand, large strains	$\phi_f = \phi_{cv}$
Loose sand, all strains	$\phi_f = \phi_{cv}$
Plane strain, all strains	$\phi_f = \phi_{cv}$

Under plane strain conditions, and assuming small strains:

$$d\varepsilon_2 = 0 = d\varepsilon_{2s} + d\varepsilon_{2e} \qquad (3\text{-}18)$$

Slip strains can occur in the 2 direction, but are balanced by elastic strains such that the total strain is zero. It will be assumed that $d\varepsilon_{2s} = d\varepsilon_{2e} = 0$. For this case:

$$d\varepsilon_{vs} = d\varepsilon_{1s} + d\varepsilon_{3s} \tag{3-19}$$

and the stress dilatancy equation can be written as:

$$\frac{\sigma_1}{\sigma_3} = (1-\frac{d\varepsilon_{vs}}{d\varepsilon_{1s}})\tan^2(45 + \frac{\phi_f}{2}) \tag{3-20}$$

This is often written as:

$$R = DK \tag{3-21}$$

where: $R = \frac{\sigma_1}{\sigma_3}$ = principal stress ratio

$D = (1-\frac{d\varepsilon_{vs}}{d\varepsilon_{1s}})$ = dilatancy factor

$K = \tan^2(45 + \frac{\phi_f}{2})$

and for plane strain conditons: $\phi_f = \phi_{cv}$

Brinch Hansen (1958) proposed the introduction of the dilation angle, which defines the relationship between the volumetric strain increment and the shear strain increment, Figure 24:

$$\sin\nu = -\frac{d\varepsilon_v}{d\gamma} \tag{3-22}$$

where: ν = the dilation angle

In terms of the shear-induced volume change:

$$\sin\nu = -\frac{d\varepsilon_{vs}}{d\gamma_s} \tag{3-23}$$

$$\text{where:} \quad d\gamma_s = d\varepsilon_{1s} - d\varepsilon_{3s} \tag{3-24}$$

The dilatancy factor is related to the dilation angle:

$$D = 1- \frac{d\varepsilon_{vs}}{d\gamma_s} = \tan^2(45 + \frac{\nu}{2}) \tag{3-25}$$

Then, as proposed by Hughes (1977) the stress dilatancy equation for plane strain becomes:

$$\tan^2(45 + \frac{\nu}{2}) = \frac{\tan^2(45 + \frac{\phi_d}{2})}{\tan^2(45 + \frac{\phi cv}{2})} \tag{3-26}$$

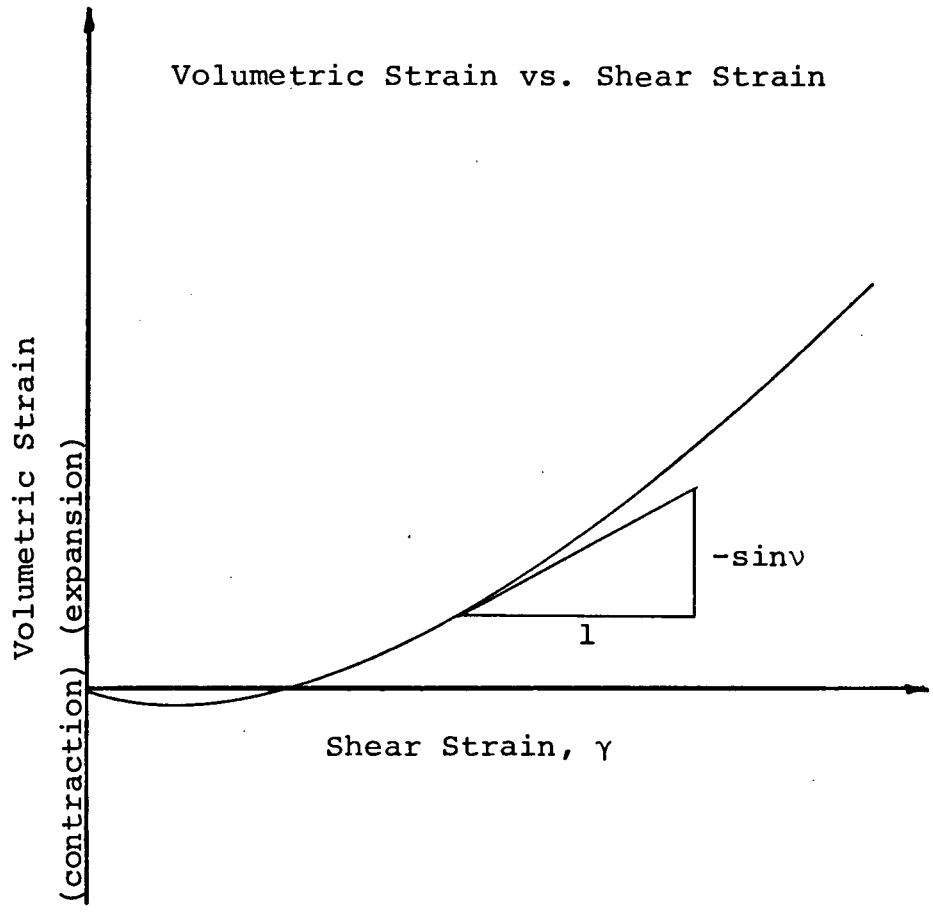

Figure 24 Definition of Dilation Angle

This is a convenient form of the stress dilatancy equation. For developed friction angles below ϕ_{cv} equation 3-26 predicts contraction. For $\phi_d = \phi_{cv}$ equation 3-26 predicts $\nu = 0$, or no shear induced volume change. The maximum dilation rate depends on the values of ϕ_{dmax} and ϕ_{cv}. As the stress level is increased, ϕ_{dmax} is reduced and, hence, dilation is suppressed. When $\phi_d = 0$, the isotropic consolidation case, 3-26 predicts that the dilation angle, $\nu = -\phi_{cv}$. When considering shear induced volume changes, this is obviously wrong, as no shear induced volume changes occur during isotropic consolidation.

In order to use Rowe's theory to model shear volume coupling, a simple modification is proposed. The stress dilatancy equation will be used to model volume strains due to changes in shear stress. The bulk modulus term will be used to model volume changes due to changes in the mean normal stress.

Various researchers (Varadarajan and Mishra (1980), Krishnamurthy, Nagaraj and Sridrahan (1981), Tobita and Yanagisawa (1980), Lindenberg and Konig (1981) and Kokusho (1978)) have published data for constant mean normal stress triaxial tests. Tests of this nature separate volume changes due to shear stress from volume changes due to mean normal stress. This data, Figure 25, shows that the shear induced contractions are small when compared to the shear induced expansions, and that the contractions may be neglected without introducing appreciable errors into the model. The proposed modification is to assume no shear induced volume change for $\phi_d < \phi_{cv}$ and to use Rowe's stress dilatancy equation to determine the shear induced volume change for $\phi_d > \phi_{cv}$.

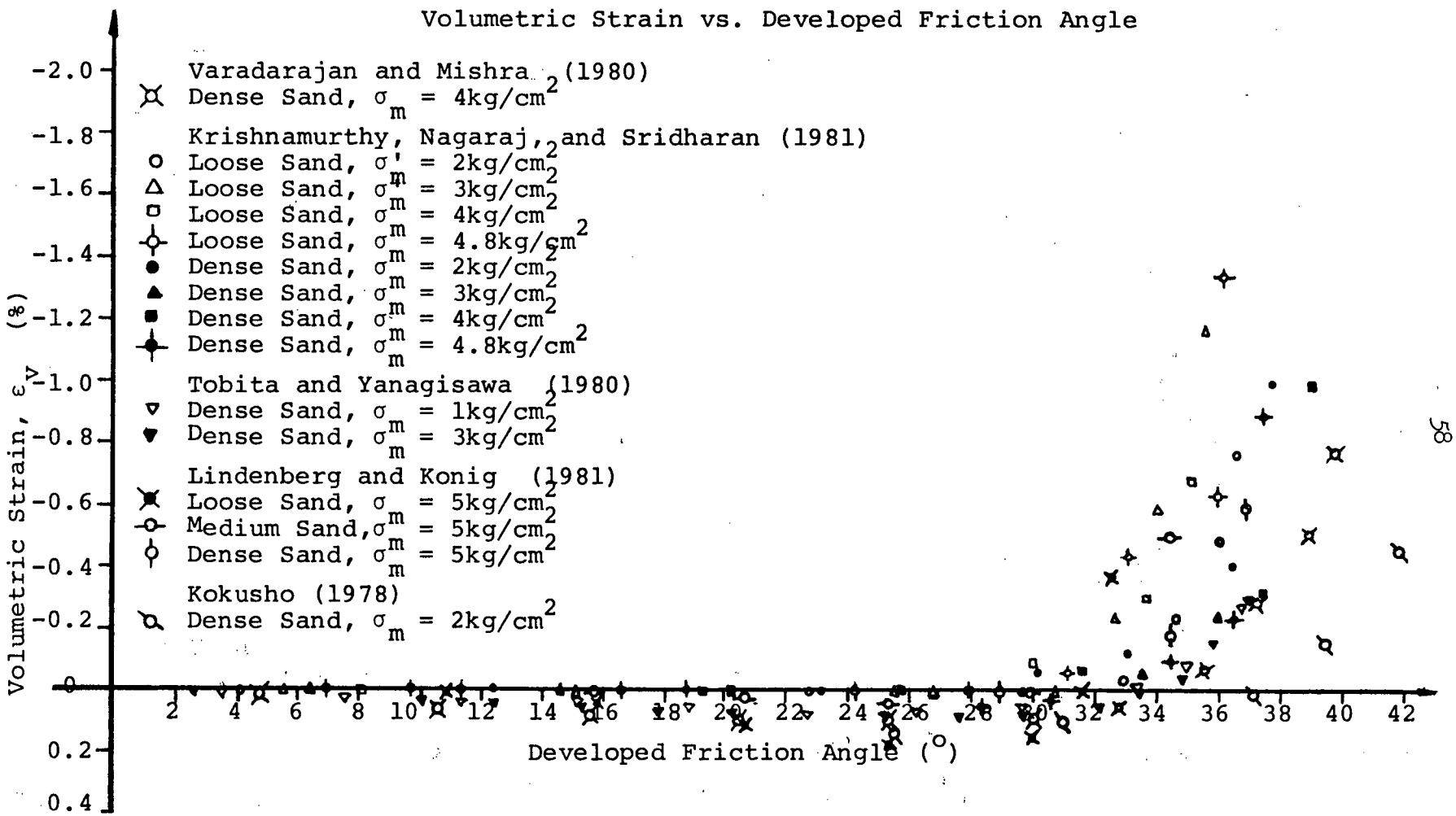

Figure 25 . Volume Change in Constant Mean Normal Stress Triaxial Tests

3.5.2 Variation of Dilation Angle with Stress Level

Vaid et al (1980) use simple shear test data from Cole (1967) to determine a linear variation of the dilation angle with vertical confining stress, Figure 26. Rowe's stress dilatancy equation can also be used to determine a relationship between dilation angle and stress. The maximum dilation angle for a given stress occurs when the peak friction angle is mobilized. The peak friction angle, ϕ, varies with stress as:

$$\phi = \phi_1 - \Delta\phi \log\left(\frac{\sigma_m}{p_a}\right) \qquad (3\text{-}10)$$

Substituting 3-10 into the stress dilatancy equation 3-26 yields:

$$\tan\left(45 + \frac{\nu}{2}\right) = \frac{\tan\left(45 + \dfrac{\phi_1 - \Delta\phi \log\left(\frac{\sigma m}{pa}\right)}{2}\right)}{\tan\left(45 + \frac{\phi cv}{2}\right)} \qquad (3\text{-}34)$$

This equation is plotted in Figure 27 for various values of ϕ_{cv}, ϕ and $\Delta\phi$. As can be seen in the figure, for the stress range of interest, a nearly linear variation of the dilation angle with the stress occurs. The greater the value of $\Delta\phi$, the faster the decrease in the dilation angle, and the more curvature in the relation. For a given value of $\Delta\phi$ and ϕ, the value of ϕ_{cv} shifts the curve vertically, but does not change the slope of the relation.

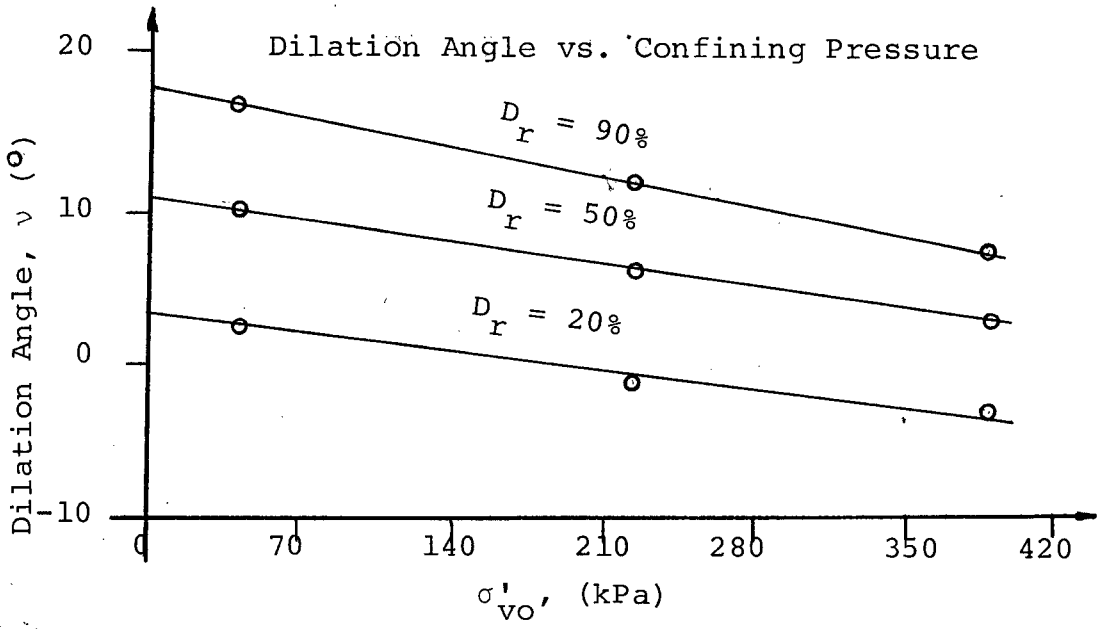

Figure 26. Dependence of Dilation Angle on Relative Density and Confining Pressure (Data from Cole, 1967)

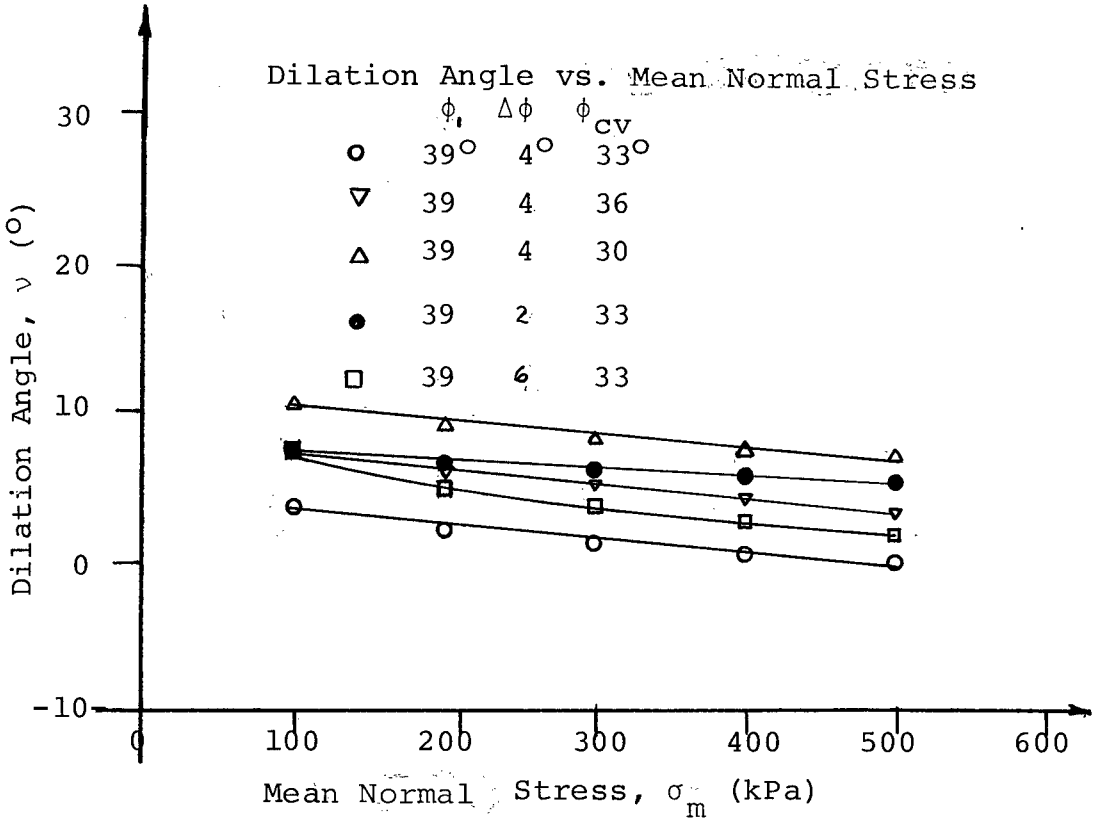

Figure 27. Dependence of Dilation Angle on Mean Normal Stress Based on Rowe's Stress-Dilatancy Equation

Chapter 4 Finite Element Program

4.1 Incremental Programs

The numerical analysis of the pressuremeter is based on the finite element computer Nonlinear Soil Structure Interaction Program (NLSSIP) developed by Byrne and Duncan (1979) to analyze long span flexible culverts. NLSSIP is a revised version of the Berkeley computer program ISBILD. The program NLSSIP was revised by Gunaratne (1981) to allow the determination of shear induced volume changes and stress redistribution from elements that violate the Mohr-Coulomb failure criteria. The thrust of the present work was to refine the changes made by Gunaratne so that the program could handle general plane strain problems involving soil dilatancy, and more specifically, to modify the program so that it could efficiently handle plane strain axisymmetric problems.

The NLSSIP has been well documented by Byrne and Duncan and by Gunaratne. In order to minimize repetition of this previous work, the program will only be discussed briefly, however the new changes will be discussed in more detail. A derivation of the finite element formulation of the new triaxial element is in Appendix A and a derivation of the new polar coordinate element is in Appendix B.

The program uses an incremental dilatant linear elastic approach. An increment of load may be the addition of a construction soil layer, the addition of a structure, the application of an external load, or an increment of pore pressure. The basic logic of the program is shown in the simplified flowchart, Figure 28. The functions of the various subroutines are

Figure 28 Simplified Flowchart of Mainline Program

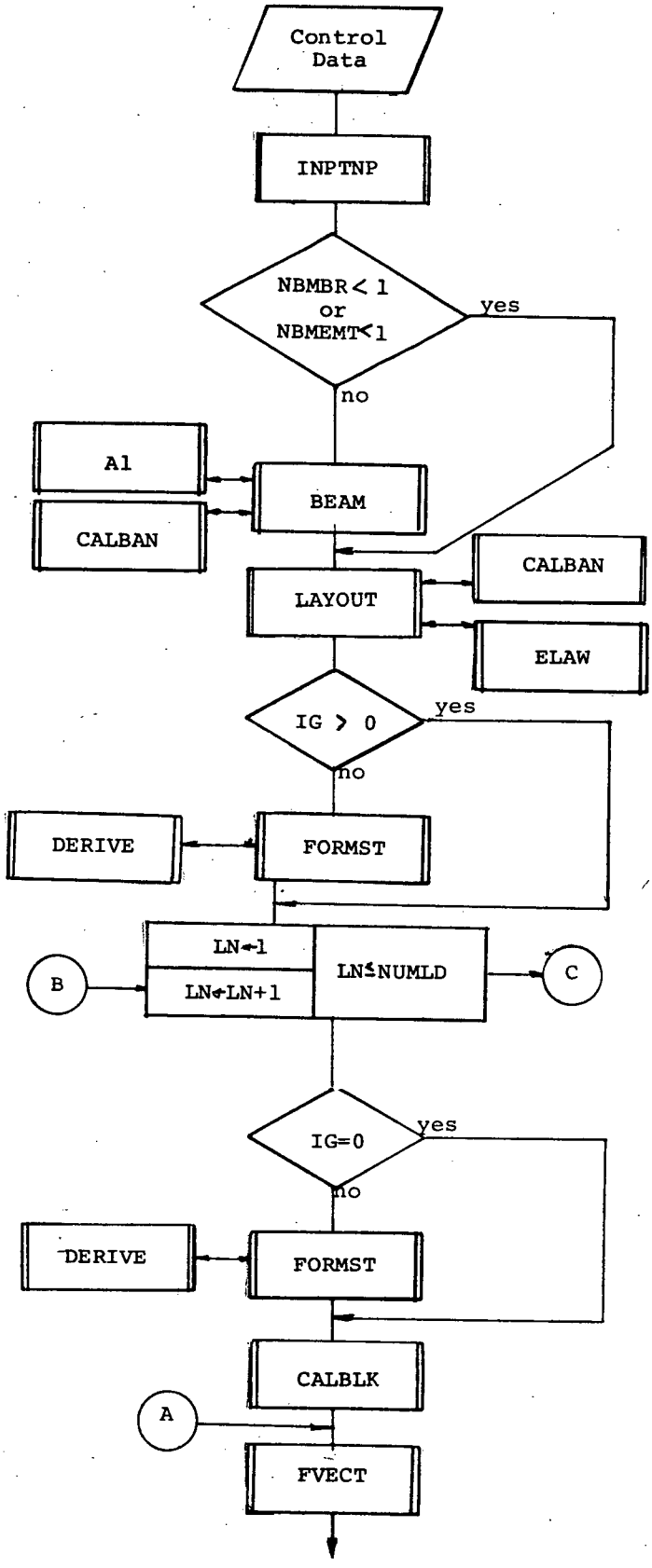

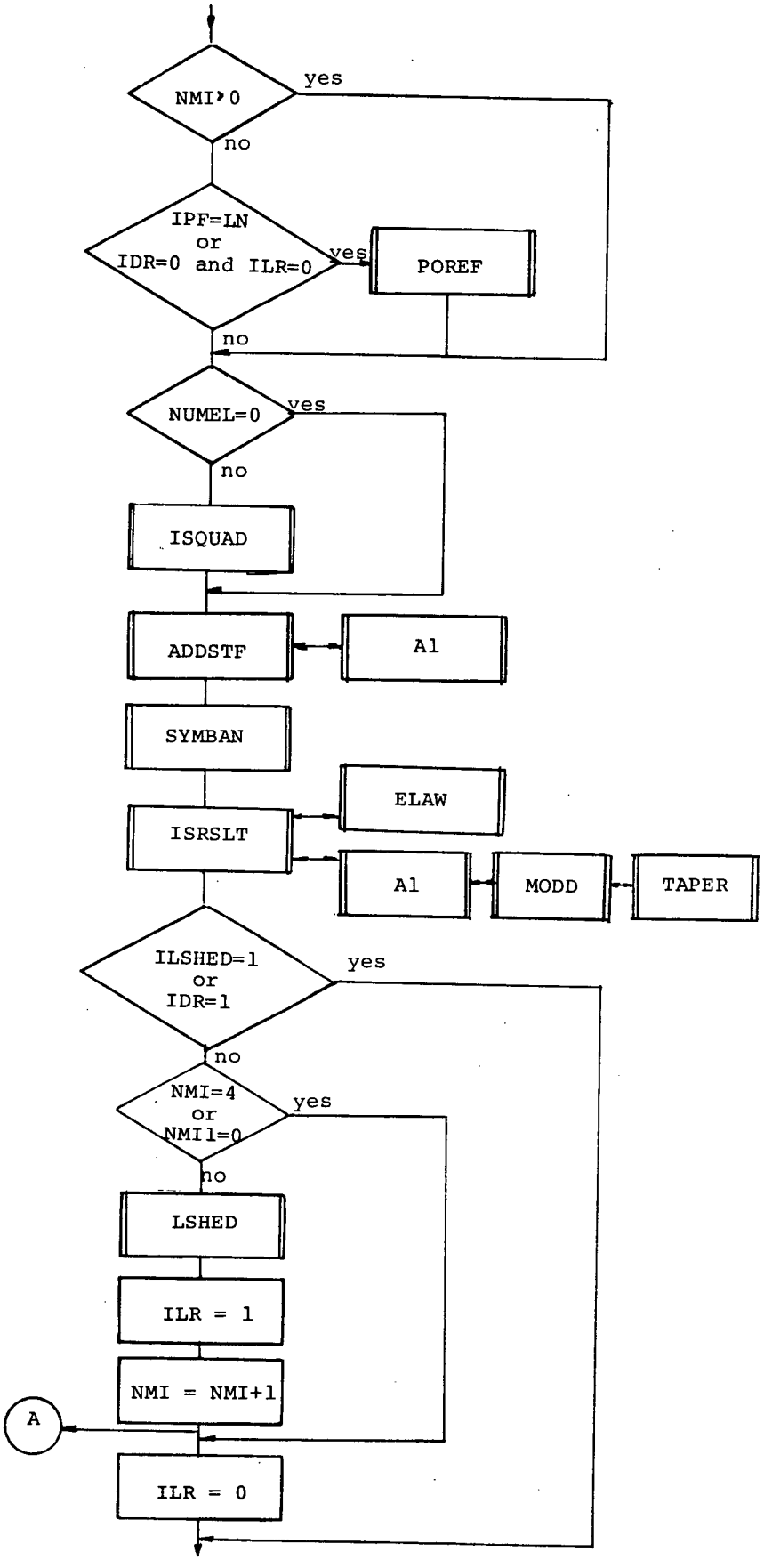
NMI>0
yes
no
IPF=LN
or
IDR=0 and ILR=0
yes
POREF
no
NUMEL=0
yes
no
ISQUAD
ADDSTF
A1
SYMBAN
ELAW
ISRSLT
A1
MODD
TAPER
ILSHED=1
or
IDR=1
yes
no
NMI=4
or
NMI1=0
yes
no
LSHED
ILR = 1
NMI = NMI+1
A
ILR = 0

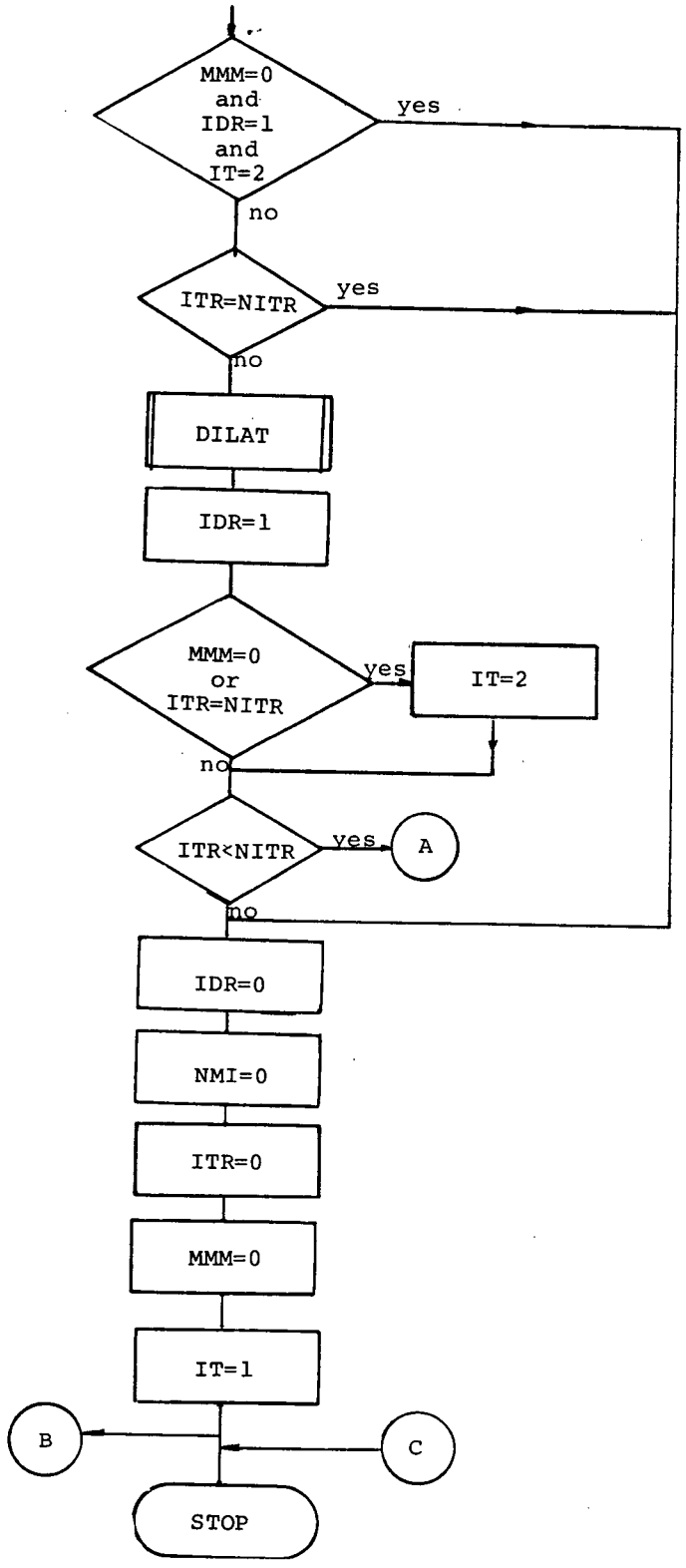
MMM=0
and
IDR=1
and
IT=2
yes
no
ITR=NITR
yes
no
DILAT
IDR=1
MMM=0
or
ITR=NITR
yes
IT=2
no
ITR<NITR
yes
A
no
IDR=0
NMI=0
ITR=0
MMM=0
IT=1
B
C
STOP

given in Table I.

In an incremental program, soil properties (moduli, friction angle, and Poisson's ratio), stresses and strains are evaluated before the load is applied. The load is applied and the element deformations and stress changes are determined using the soil properties at the beginning of the stress interval. The soil properties are reevaluated for the stress conditions at the midpoint of the predicted stress interval. The global stiffness matrix is evaluated using these soil properties and the load is applied again. The new deformations, stresses and strains are then computed. For programs without shear volume coupling or stress redistribution usually only two iterations are made. For a load step, in NLSSIP, soil properties are printed for the midpoint of the stress interval, while displacements, strains and stresses are printed for the end of the interval.

When shear volume coupling and stress redistribution are added to an incremental program, additional iterations within each load step must be made to achieve the correct shear induced volume change and the stress redistribution. Within the new program, stress redistribution from the elements that violate the Mohr-Coulomb failure criterion is performed first. The program will iterate to a maximum of four times to achieve stress redistribution. Soil properties at the end of the stress interval are used in stress redistribution.

After elements are brought back onto the failure surface, shear volume coupling is introduced. The program will iterate twice, or to a maximum number specified by the user, to achieve the correct shear induced volume change. If convergence of

TABLE I

SUBROUTINE	DESCRIPTION
INPTNP	Reads and prints nodal point data, establishes a relationship between each nodal point degree of freedom and the corresponding equation number and sets the equation number to zero for constrained boundary conditions.
BEAM	Reads and prints beam element data and calculates the internal force-displacement matrix and the element stiffness matrix.
CALBAN	Calculates the band width of a group of elements
LAYOUT	Reads and prints the soil input data and computes and prints the initial stresses and the initial moduli values for the soil elements.
ELAW	Calculates moduli values for the soil elements in accordance with the magnitudes of the stresses.
FORMST	Calls subroutine DERIVE to establish strain-displacement matrices for the three types of soil elements.
DERIVE	Forms the soil strain-displacement matrix for the three element types.
CALBLK	Determines the number of elements and nodal points for the entire mesh, the number of elements and nodal points in the pre-existing part and the newly added

TABLE I (continued)

	layers, the number of equations, the number of equations in each block, and the number of blocks for each construction layer increment or load increment.
FVECT	Calculates nodal point forces due to weights of added elements, reads concentrated load data and/or boundary pressure data, prints nodal point forces and sets up the force vector-
POREF	Reads element incremental porewater pressures and computes equivalent nodal forces.
ISQUAD	Formulates the constitutive equations, forms the element stiffness matrix for each element, and forms the strain-displacement matrix used in stress calculations.
ADDSTF	The total stiffness matrix for each increment is formed two blocks at a time by making a pass through the element stiffness matrices and adding the appropriate coefficients.
SYMBAN	Solves the simultaneous equations representing the stiffness matrix and the load vector for nodal point displacements using the Gaussian elemination technique.
ISRSLT	Calculates stress increments and average stresses and evaluates the modulus of each soil element after the first iteration. For the subsequent iterations ISRSLT calculates the incremental and cumulative

TABLE I (continued)

	stresses and strains for each soil element to be used in the next iteration, and internal forces in structural elements.
A1	Calculates the element stiffness matrix and generalized force-displacement matrix for beam elements.
MODD	Calculates the flexural stiffness of beam elements.
TAPER	Calculates the generalized force-displacement matrix for a section with linearly varying flexural stiffness.
LSHED	Calculates the element force vector to redistribute stress from a soil element that violates the Mohr-Coulomb failure criteria.
DILAT	Calculates the element force vector to produce shear-volume coupling in soil elements.

the volume change is achieved within the specified number of iterations, the program will print out data as in NLSSIP. If convergence is not achieved, the convergence of those elements violating the convergence criterion for the volume change will be printed along with the other results. The program will then go on to the next load case. The number of iterations to achieve stress redistribution and shear volume coupling can be minimized by using small load steps, especially near failure when dense sand dilates rapidly.

It should be noted that since shear volume coupling follows stress redistribution, some elements may be forced to violate the failure criterion when the shear volume coupling is performed. These elements will be brought back onto the failure surface on the next load step. Since shear volume coupling is the primary feature of the program, it was thought better to achieve the correct volume change and to possibly have a few elements marginally violating the failure criterion than to have all elements within the failure surface, but to have the wrong volume change.

The stress redistribution technique is not required in the present work, and since it is covered by Gunaratne, it will not be discussed in this work. However, care should be taken when using stress redistribution as it can cause elements to violate stress boundary conditions.

4.2 Shear Induced Volume Change

Shear induced volume changes are handled in an analogous manner to thermal volume changes in thermoelasticity. The sand is considered to be isotropic with its incremental linear elas-

tic response modelled by two stress level dependent elastic parameters, the Youngs's modulus and the bulk modulus. The shear induced volume change is modelled by an additional dilatant parameter, forming a three parameter model.

The volumetric response of the soil is divided into two components, one due to changes in the mean normal stress and the other due to changes in the shear stress. Volume change due to changes in the mean normal stress are modelled by the bulk modulus term. This volumetric strain will have both elastic and plastic components, the plastic component being mainly due to grain crushing and clip. Cyclic hydrostatic loading will significantly reduce the amount of plastic volume change occurring on loading. Within the program it does not matter if the problem is for virgin loading or for loading after cyclic loading. Provided that the bulk modulus term has been determined from tests that reasonably model the field conditions, the program will give reasonable results.

Shear induced volume changes are handled by a dilatant parameter, D_t. The exact form of D_t does not affect the program logic. The dilatant parameter may be input in any fashion that fits the test data or theory used to model the shear volume coupling by making some minor changes to subroutine DILAT in the program.

The incremental shear induced volume change, $\Delta\varepsilon_{vs}$, is obtained from:

$$\Delta\varepsilon_{vs} = D_t \Delta\gamma \qquad (4\text{-}1)$$

Rowe developed his theory using the plastic shear strain increment, however, as discussed below, using the total shear

strain increment in the determination of the shear induced volume change introduces little error.

A convenient method of specifying the dilatant parameter is with the dilation angle:

$$D_t = -\sin\nu \qquad (4\text{-}2)$$

Within the program, two options are available for calculation of the dilatant parameter, Figure 29. Option 1 uses a constant dilation angle after a certain shear strain. This specification of the shear induced volume change has been used by Hughes et al (1977) and by Byrne et al (1980). Hughes specified the constant dilation angle as the maximum dilation angle that occurs at the peak stress ratio, and the starting strain, γ_o, as the strain at which yield first occurs. Byrne specified the starting strain as twice the strain at which the constant volume friction angle is first reached.

The second option of specifying D_t uses Rowe's stress dilatancy theory as modified in Chapter 3. The program uses Rowe's theory above a developed friction angle equal to the constant volume friction angle. At developed friction angles below ϕ_{cv}, no shear induced volume change is assumed to occur. This assumption models the volume change behaviour well, as shown in Figure 30. The figure compares the volume change predicted by Option 1, by Option 2 using either the total shear strain increment or the plastic shear strain increment and Rowe's theory from $\phi_d = 0$. It may be seen that Option 1 and Option 2 model the test data equally well. Rowe's theory from $\phi_d = 0$ overpredicts volumetric compression, as expected. The figure also shows that using the total shear strain increment instead of the plastic shear strain increment changes the

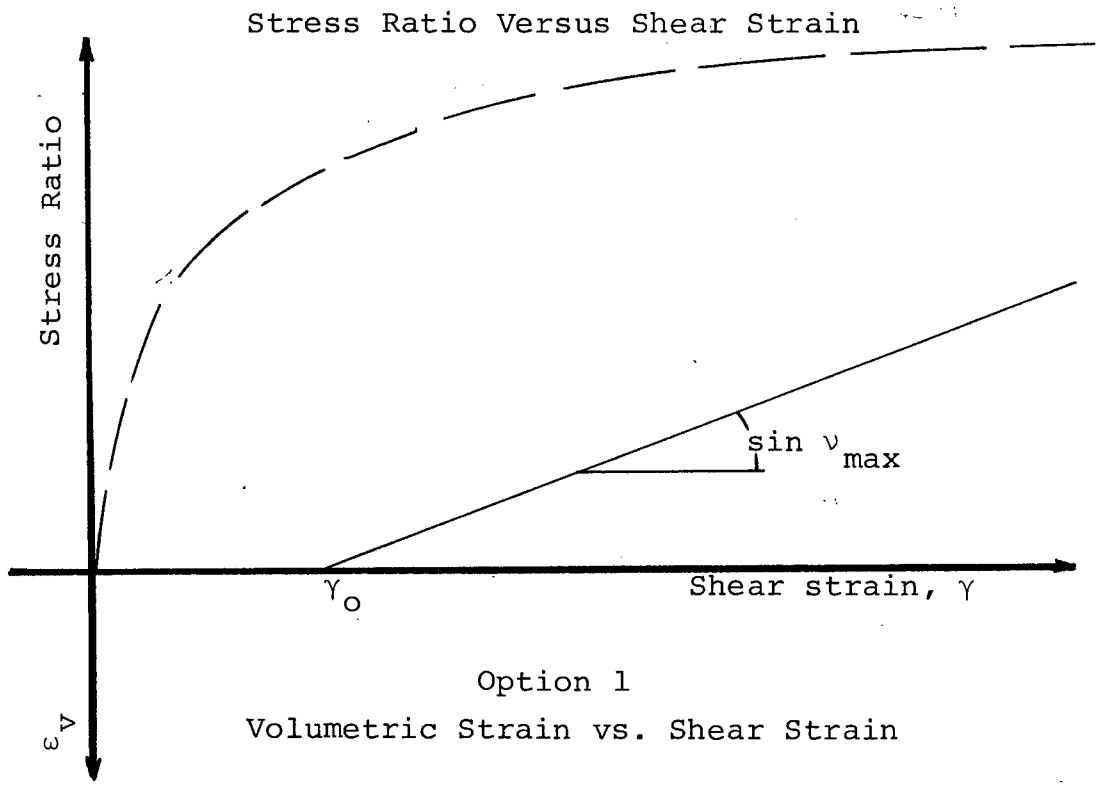

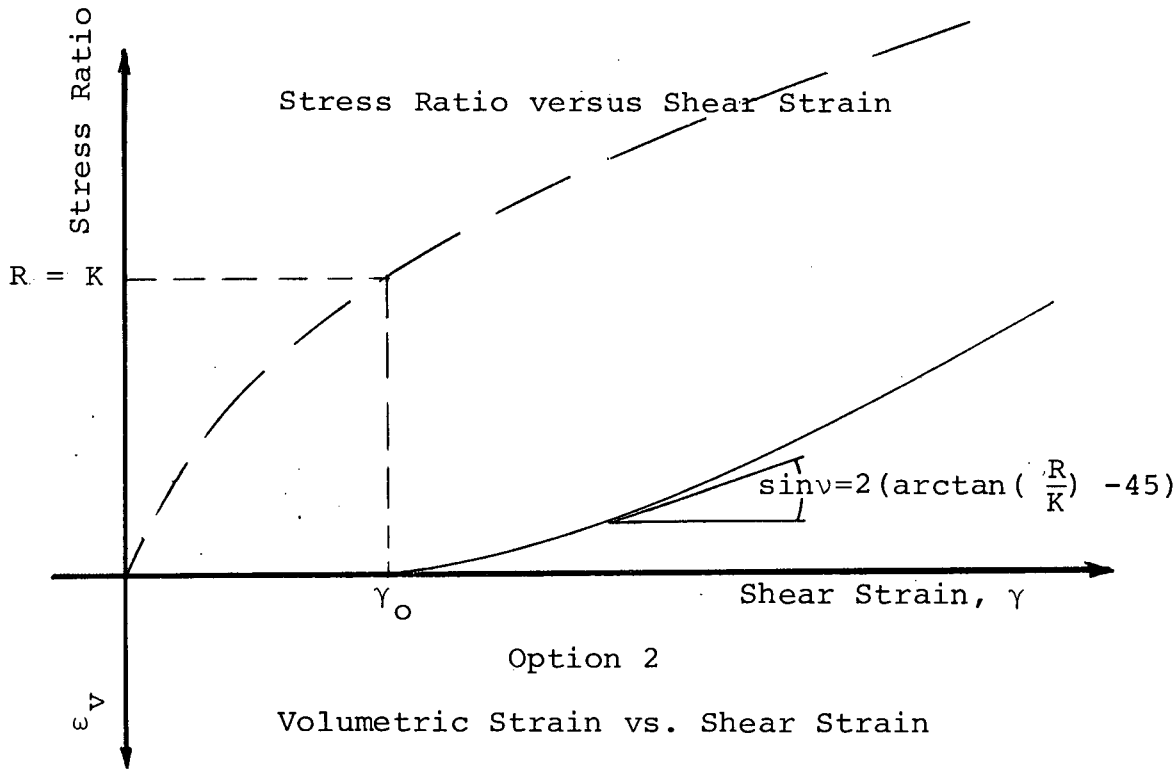

Figure 29. Specification of Shear Induced Volume Change

29

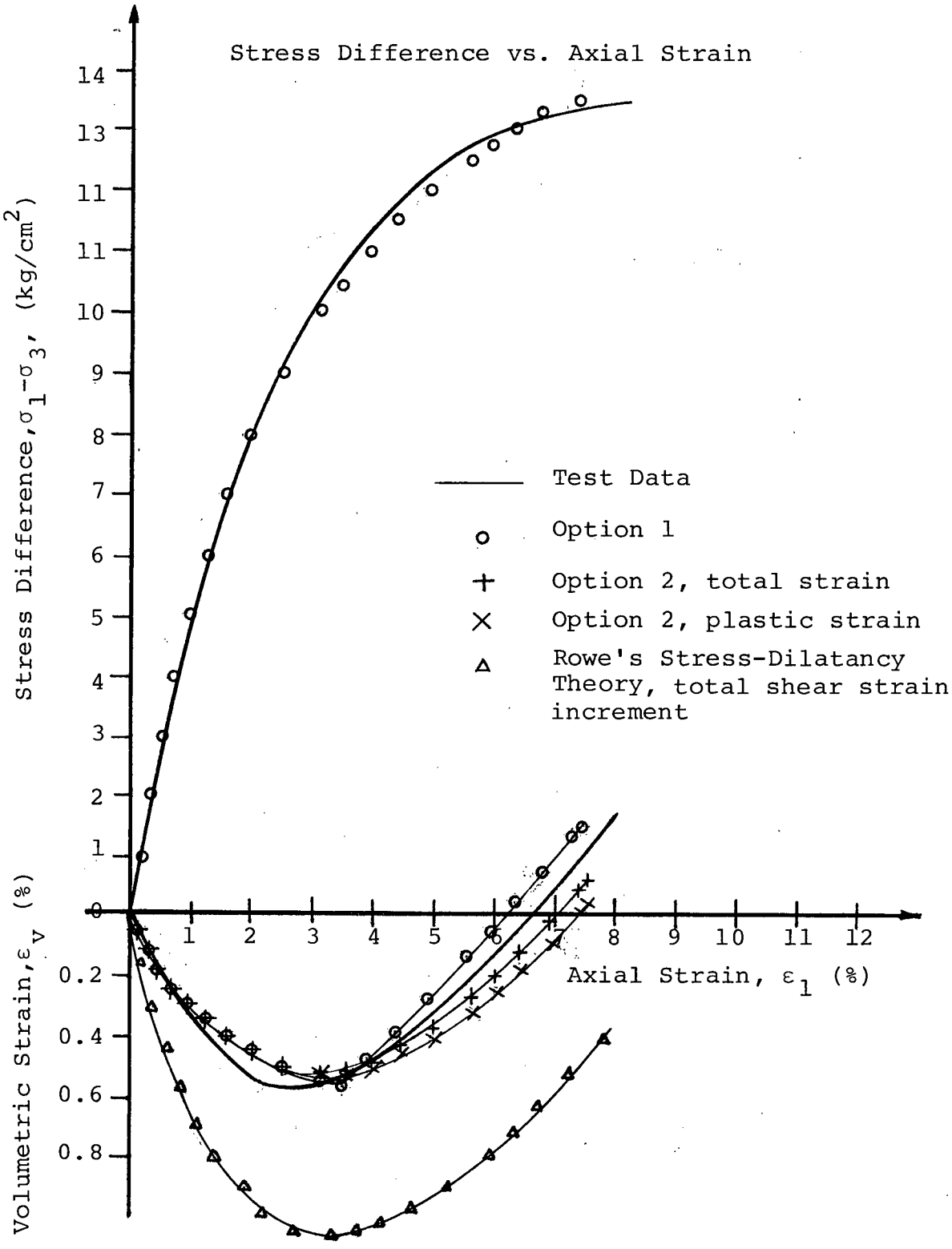

Figure 30 . Comparison of Shear Induced Volume Change Models

Analysis of σ_3 Constant Triaxial Test

prediction of volume changes very little. Once dilation begins the elastic strains are small compared to the plastic strains, so little error is introduced in Option 2 by using the total shear strain increment. The advantage of Option 2 over Option 1 is that Option 2 suppresses dilation as the stress level increases and the friction angle decreases.

4.3 Finite Element Formulation of the Shear Induced Volume Change

In thermoelasticity, the force system to prevent deformations due to temperature change is calculated for each element. The domain is then subjected to a force system equal but opposite to the system just calculated, allowing the deformation and stresses in the domain due to the temperature change to be calculated.

Within the present program, the force required to produce the required volume change is calculated for each element. The forces are applied to the domain and the stresses and deformations are determined. An iterative procedure is required because application of forces to all elements will cause redistribution of the stress and strain in the finite element domain. Figure 31 gives a simplified flowchart for subroutine DILAT, which calculates the forces for shear volume coupling.

The method of calculating the forces for an element will be presented for the three element types. The plane strain polar coordinate element will be discussed in detail, while the other two elements will be discussed briefly.

Assuming that Option 2 is used, the dilation angle is determined by:

$$\nu = 2(\arctan(\sqrt{\frac{R}{K}} - \frac{\pi}{4})), \quad R > K \qquad (4\text{-}3)$$

Figure 31. Flowchart for Subroutine DILAT

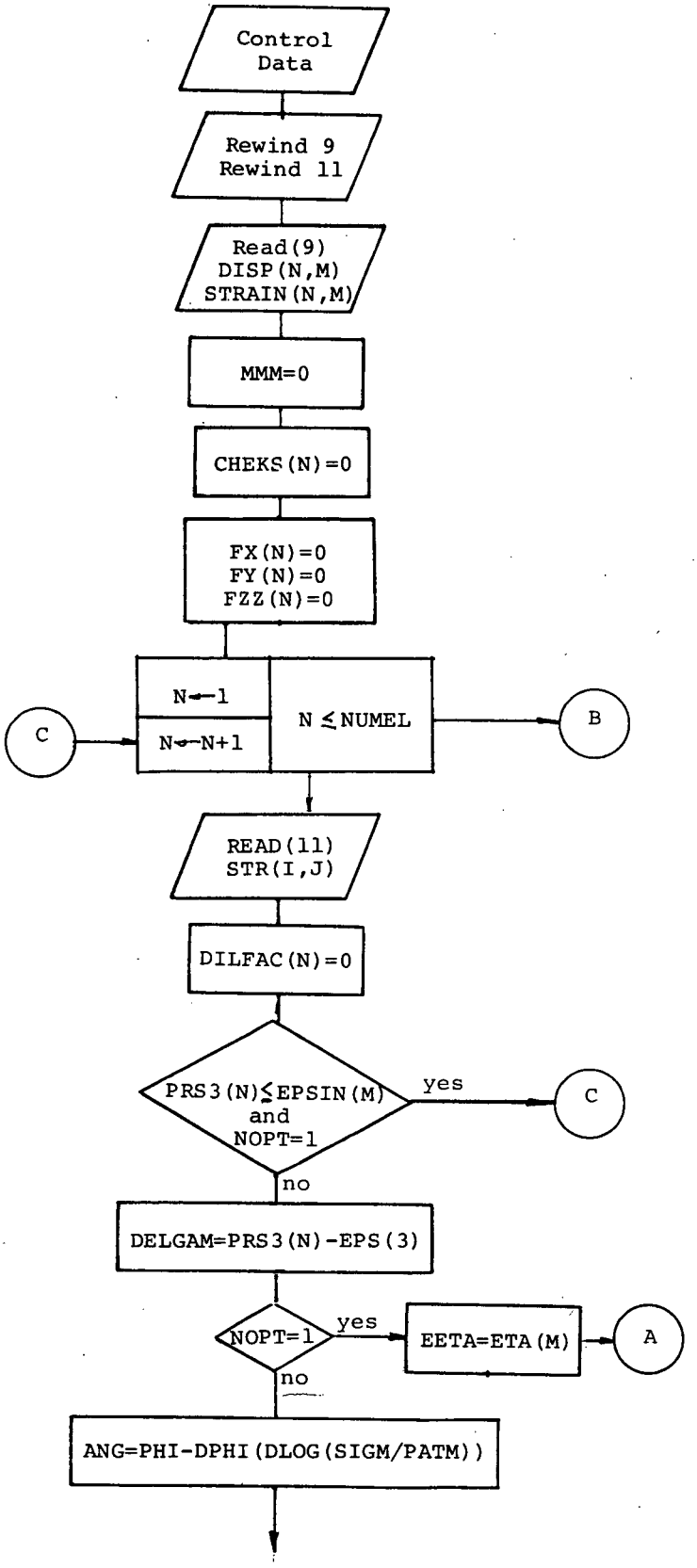

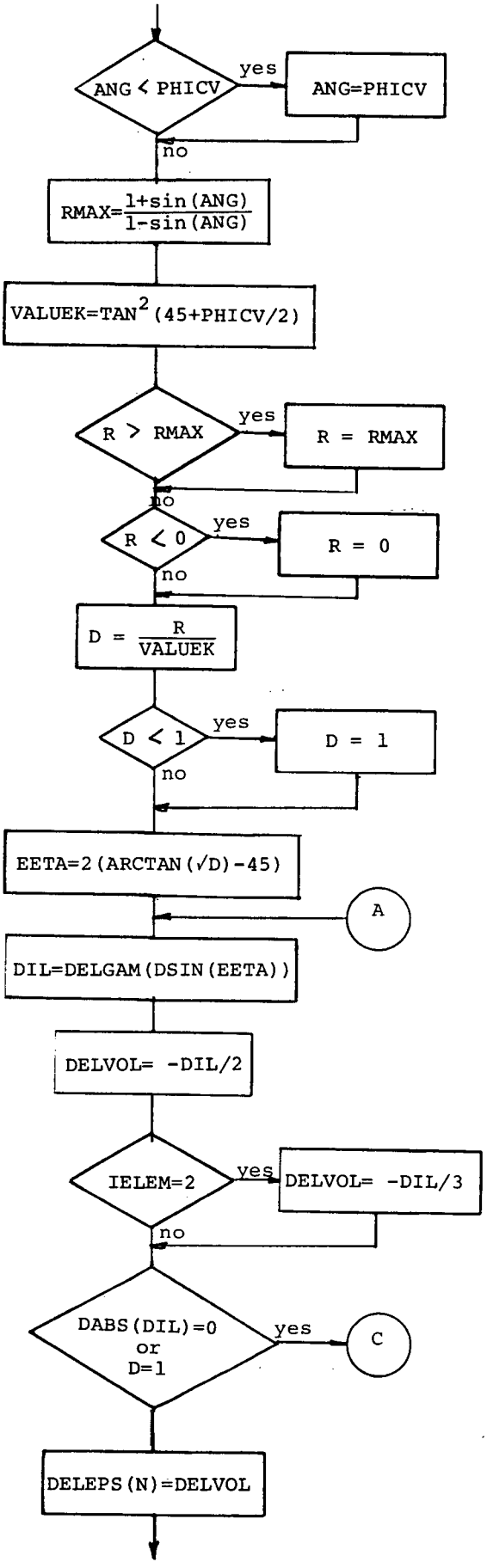
ANG < PHICV
yes
ANG=PHICV
no
RMAX=(1+sin(ANG))/(1-sin(ANG))
VALUEK=TAN2(45+PHICV/2)
R > RMAX
yes
R = RMAX
no
R < 0
yes
R = 0
no
D = R/VALUEK
D < 1
yes
D = 1
no
EETA=2(ARCTAN(√D)-45)
A
DIL=DELGAM(DSIN(EETA))
DELVOL= -DIL/2
IELEM=2
yes
DELVOL= -DIL/3
no
DABS(DIL)=0
or
D=1
yes
C
DELEPS(N)=DELVOL

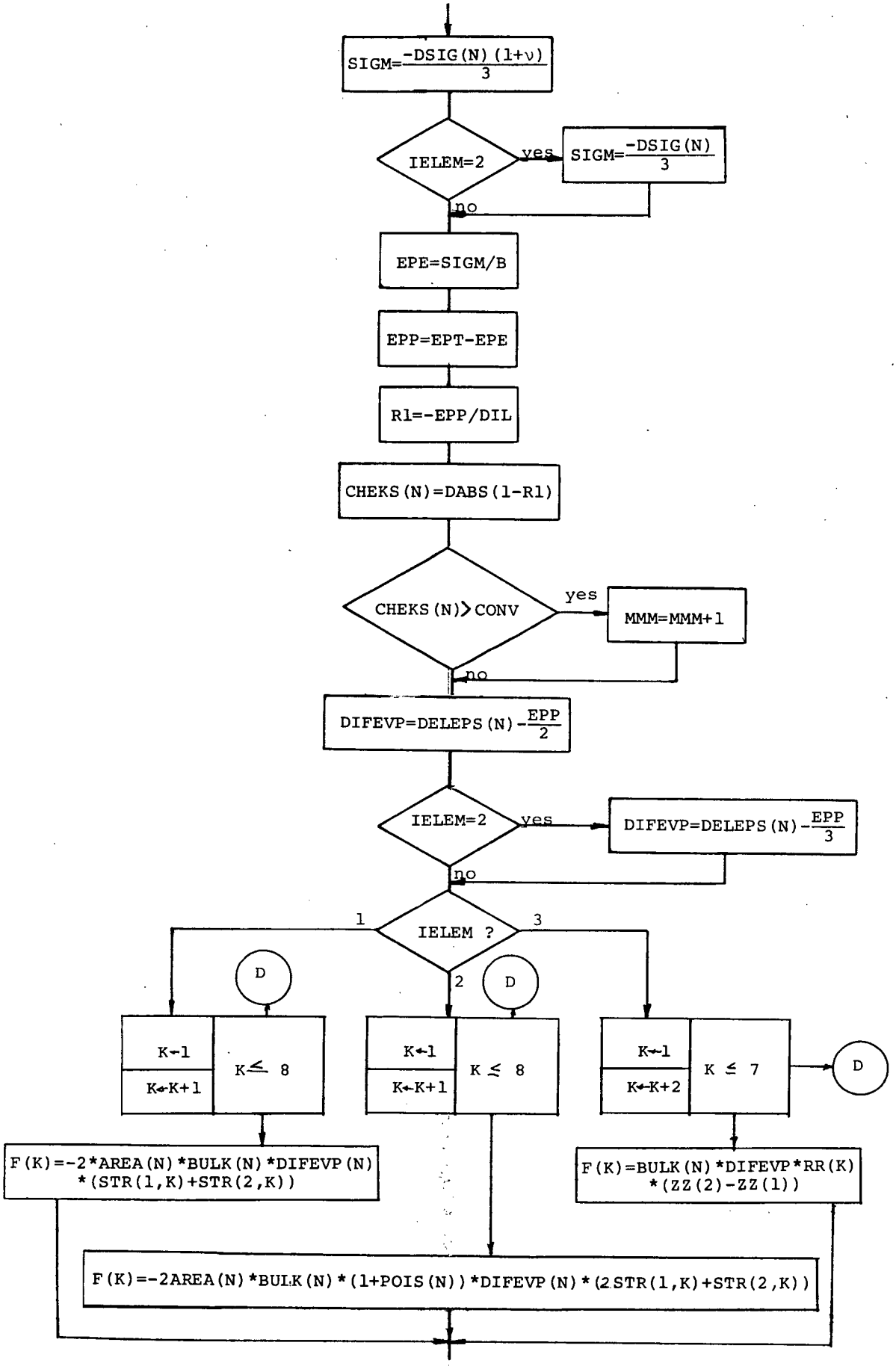
SIGM=-DSIG(N)(1+ν)/3
IELEM=2
yes
SIGM=-DSIG(N)/3
no
EPE=SIGM/B
EPP=EPT-EPE
R1=-EPP/DIL
CHEKS(N)=DABS(1-R1)
CHEKS(N)>CONV
yes
MMM=MMM+1
no
DIFEVP=DELEPS(N)-EPP/2
IELEM=2
yes
DIFEVP=DELEPS(N)-EPP/3
no
IELEM ?
1
2
3
D
D
D
K←1
K←K+1
K≤ 8
K←1
K←K+1
K ≤ 8
K←1
K←K+2
K ≤ 7
F(K)=-2*AREA(N)*BULK(N)*DIFEVP(N)
*(STR(1,K)+STR(2,K))
F(K)=BULK(N)*DIFEVP*RR(K)
*(ZZ(2)-ZZ(1))
F(K)=-2AREA(N)*BULK(N)*(1+POIS(N))*DIFEVP(N)*(2STR(1,K)+STR(2,K))

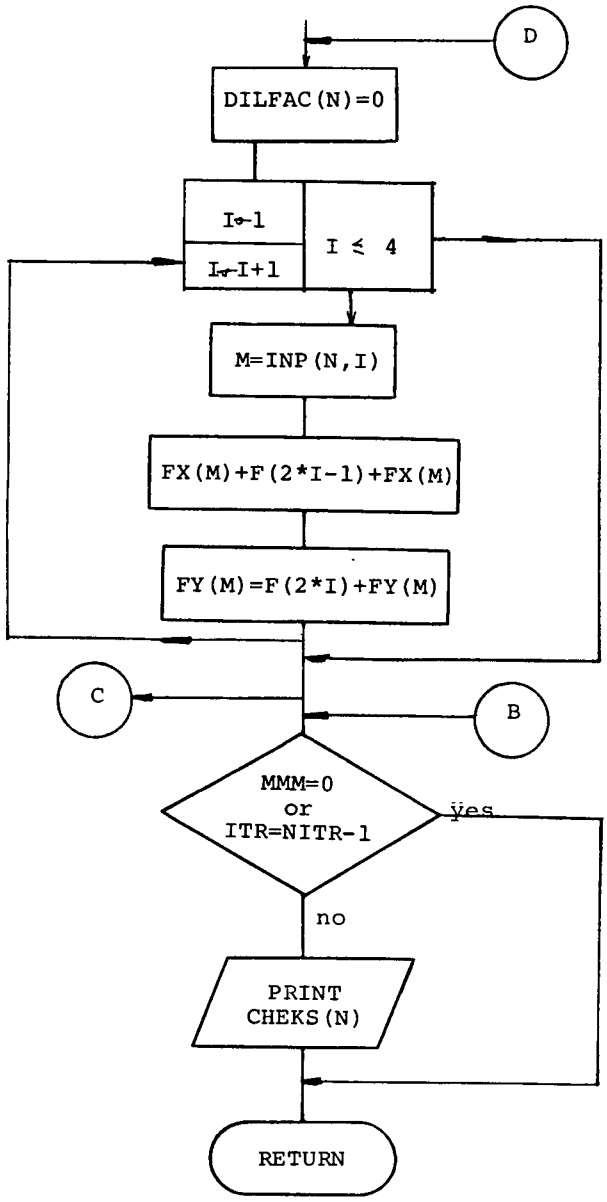
D
DILFAC(N)=0
I←1
I←I+1
I ≤ 4
M=INP(N,I)
FX(M)+F(2*I-1)+FX(M)
FY(M)=F(2*I)+FY(M)
C
B
MMM=0
or
ITR=NITR-1
yes
no
PRINT
CHEKS(N)
RETURN

or $\nu = 0$ for $R < K$

where: $R = \tan^2(45 + \frac{\phi_d}{2})$

$K = \tan^2(45 + \frac{\phi_{cv}}{2})$

The shear induced volume change is then calculated by:

$$d\varepsilon_{vs} = -d\gamma \sin\nu$$

Using the assumption of isotropic volume change and plane strain

$$d\varepsilon_{vs} = d\varepsilon_{1s} + d\varepsilon_{3s} = 2d\varepsilon_{1s} \qquad (4\text{-}4)$$

In the finite element formulation, the internal virtual work done by a set of virtual displacements is:

$$dW_i = \int_V \{\bar{\varepsilon}\}^T \{\sigma\}\, dV \qquad (4\text{-}5)$$

where: $\{\bar{\varepsilon}\}$ = virtual strain vector

$\{\sigma\}$ = stress vector

but:

$$\{\bar{\varepsilon}\} = (B)\{\bar{\delta}\} \qquad (4\text{-}6)$$

where: (B) = strain displacement matrix

$\{\bar{\delta}\}$ = virtual displacement vector

The internal virtual work is therefore:

$$dW_i = \int_V \{\bar{\delta}\}^T (B)^T \{\sigma\} dV \qquad (4\text{-}7)$$

The stress is determined from the strain:

$$\{\sigma\} = (D)\{\varepsilon\} \qquad (4\text{-}8)$$

where: (D) = stress-strain matrix

Upon substitution of 4-8 into 4-7, the internal virtual work is:

$$dW_i = \int_V \{\bar{\delta}\}^T (B)^T (D)\{\varepsilon\} dV \qquad (4\text{-}9)$$

The external virtual work done by the external forces undergoing these displacements is:

$$dW_e = \{\bar{\delta}\}^T \{f_s\} \qquad (4\text{-}10)$$

where: $\{f_s\}$ = nodal force vector

Equating the internal virtual work and the external work:

$$\{\bar{\delta}\}^T\{f_s\} = {}_V\int\{\bar{\delta}\}^T(B)^T(D)\{\varepsilon\}dV \qquad (4\text{-}11)$$

The vector of nodal displacements, $\{\bar{\delta}\}^T$, is constant over the volume of the element. Also, for an element of unit thickness, t:

$$dV = tdA \qquad (4\text{-}12)$$

Cancelling the virtual nodal displacements in 4-11 and substituting 4-12 into 4-11 gives an expression for the nodal forces:

$$\{f_s\} = {}_A\int(B)^T(D)\{\varepsilon\}tdA \qquad (4\text{-}13)$$

The strain vector for the polar coordinate element is:

$$\begin{Bmatrix} d\varepsilon_r \\ d\varepsilon_\theta \\ d\gamma_{r\theta} \end{Bmatrix} = \frac{1}{2}\begin{Bmatrix} d\varepsilon_{vs} \\ d\varepsilon_{vs} \\ 0 \end{Bmatrix} = \frac{d\varepsilon_{vs}}{2}\begin{Bmatrix} 1 \\ 1 \\ 0 \end{Bmatrix}$$

and the force vector will be:

$$\{f_s\} = {}_A\int(B)^T(D)\begin{Bmatrix} 1 \\ 1 \\ 0 \end{Bmatrix}\frac{d\varepsilon_{vs}}{2}tdA \qquad (4\text{-}14)$$

The stresses and strains are evaluated at the centre of the element. This is essentially one point Gauss quadrature. The force required to give the correct volumetric strain then becomes:

$$\{f_s\} = W(B)^T(D)\begin{Bmatrix} 1 \\ 1 \\ 0 \end{Bmatrix}\frac{d\varepsilon_{vs}}{2} \qquad (4\text{-}15)$$

The strain displacement matrix (B) and the stress-strain matrix (D) are evaluated at the midpoint of the element. The coefficient W is a weighting function from the Gauss quadrature.

It should be noted here that for the axisymmetric case, if the form of the shear induced volume change was not assumed to be isotropic, only the form of the required strain vector must be changed.

For the polar coordinate element in Figure 32, due to the boundary condition of no displacements in the circumferential direction, forces are applied only in the radial direction.

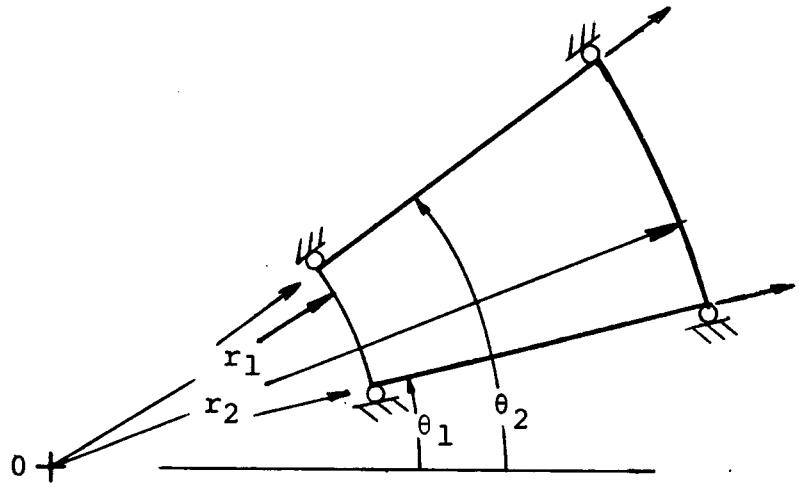

Figure 32. Four Node Polar Coordinate Finite Element

Only four forces need be calculated, forces 1, 3, 5 and 7 in the figure. These forces are given by equation 4-15.

The above formulation is used on the first iter ation in a load step. On the second and subsequent iterations, if the volume change is not correct, a force vector is calculated on the basis of the additional volume change required to achieve the correct shear volume coupling in the element. This force vector is added into the total load vector for the element.

When calculating the stresses in the element, the additional strains introduced in the element due to shear volume coupling must be taken into account. Basically:

$$\{\Delta\sigma\} = (D)\{\Delta\varepsilon - \Delta\varepsilon_s\} \qquad (4\text{-}16)$$

where: $\{\Delta\sigma\}$ = stresses due to applied loads

$\{\Delta\varepsilon\}$ = strains calculated from solution of finite element problem

$\{\Delta\varepsilon_s\}$ = strain due to the forces calculated for shear volume coupling if the element were completely free to move

$$\{\Delta\varepsilon_s\} = \begin{Bmatrix} 1 \\ 1 \\ 0 \end{Bmatrix} \frac{\Delta\varepsilon_{vs}}{2}$$

Equation 4-16 is used in the form:

$$\{\Delta\sigma\} = (D)(B)^T\{\delta\} - (D)\begin{Bmatrix} 1 \\ 1 \\ 0 \end{Bmatrix}\frac{\Delta\varepsilon_{vs}}{2} \qquad (4\text{-}17)$$

where: $\{\delta\}$ = nodal displacements from solution of finite element problem with external loads and forces for shear volume coupling.

The two other element types are handled in exactly the same manner. The only differences are that the stress-strain matrix, (D), is different and the stresses and strains are for the x, y coordinate system. The forces must be applied in both the x and y directions at each node, since for the general case the element will not be fixed in one of these directions. In the triaxial element, the slip strain in any one direction will be one-third the total volumetric slip strain, while in the plane strain element, the slip strain in the x or y direction will be one-half of the total volumetric slip strain.

Figure 33 shows the results of a σ_3 = constant triaxial test on medium dense sand. The total volume change has been divided into the components due to hydrostatic stress change and due to shear volume coupling. The curve for the shear induced volume change was used for the dilatant parameter, D_t. Figure 34 shows the comparison between the program results and test results. This comparison does not validate the theory of separating the volume changes into the hydrostatic and shear induced components, but it does show that this numerical technique can be used to replicate test results. This comparison is a check on the logic of the solution technique.

The shear volume coupling technique was also checked against the closed form linear dilatant model developed in Chapter 2. Figures 35, 36 and 37 show the comparison of the closed form solution and the finite element calculation. Agreement is excellent.

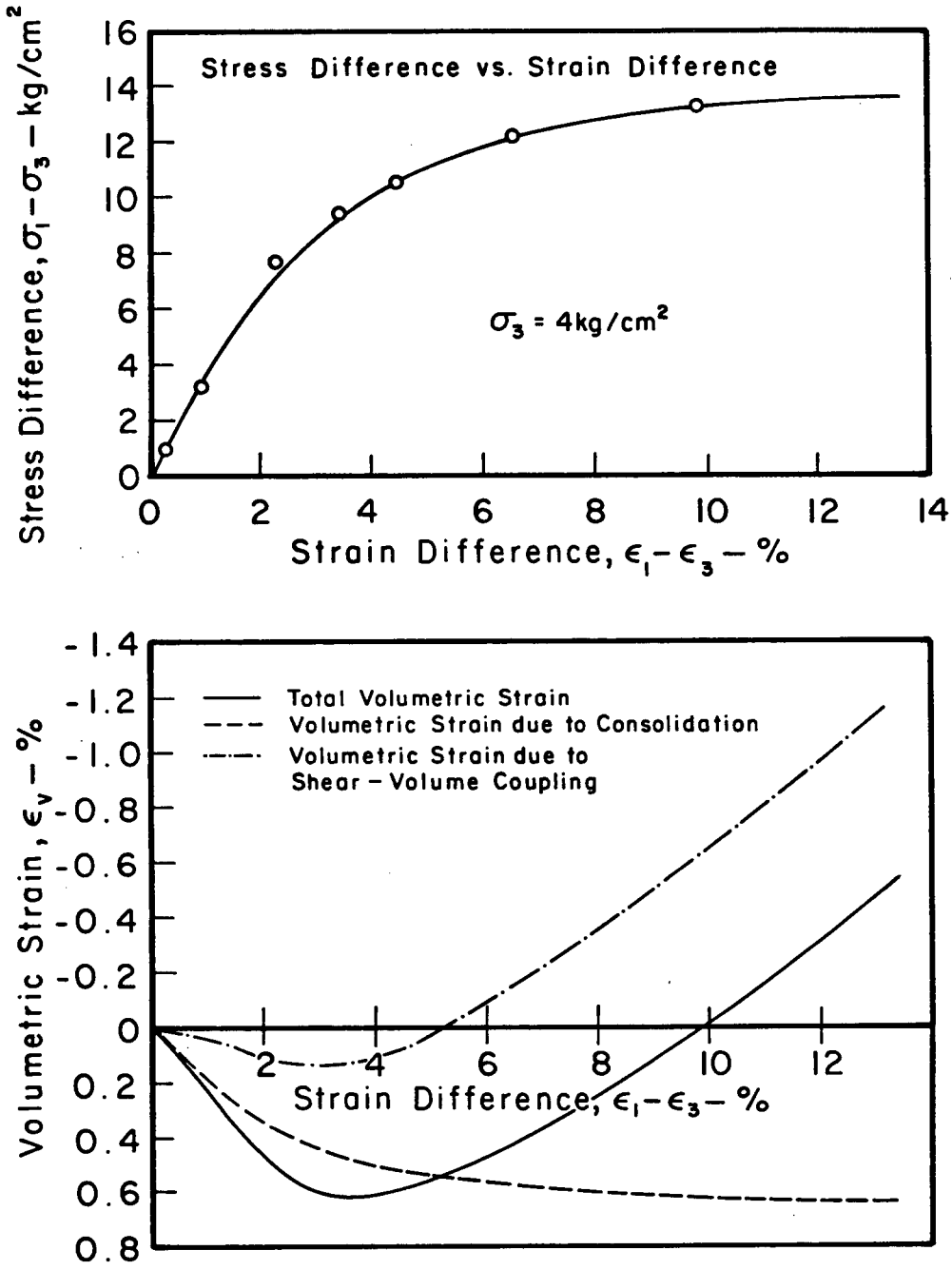

Figure 33: Constant σ_3 Triaxial Test on Medium Dense Sand. (After Varadarajan and Mishra, 1980).

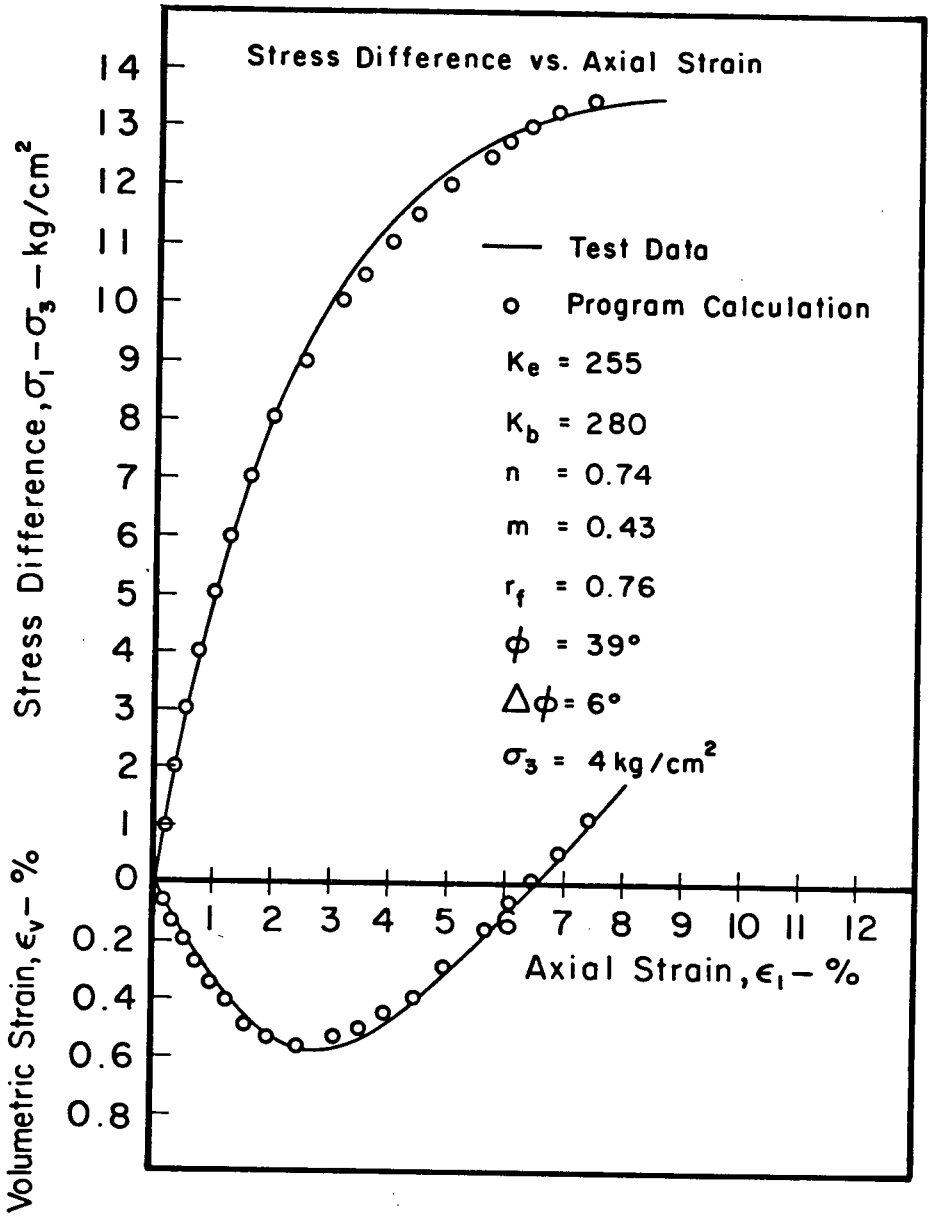

Figure 34 Finite Element Analysis of σ_3 constant Triaxial Test.

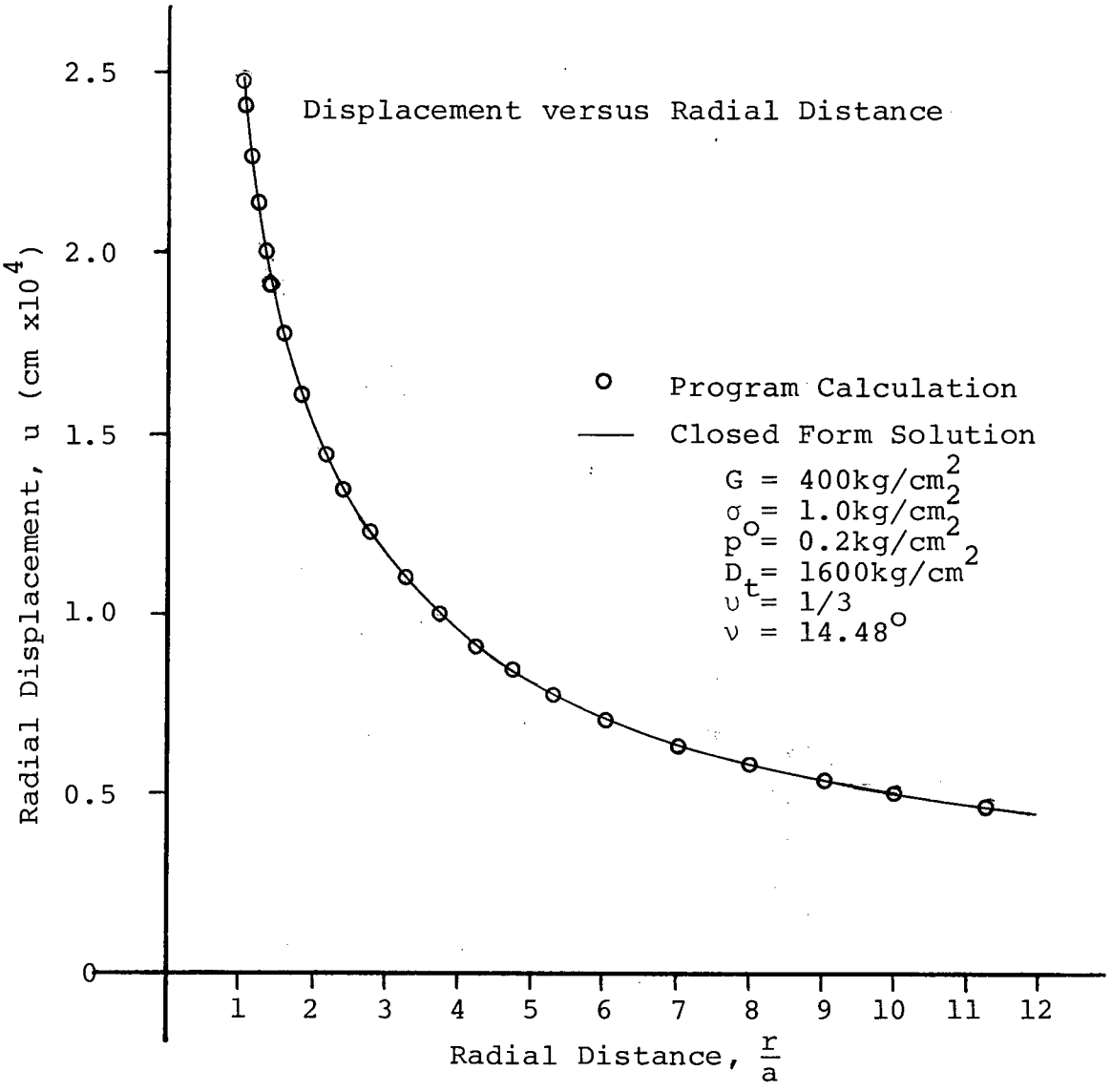

Figure 35. Comparison of Displacements in Linear Dilatant Material from Closed Form Solution and Finite Element Calculation

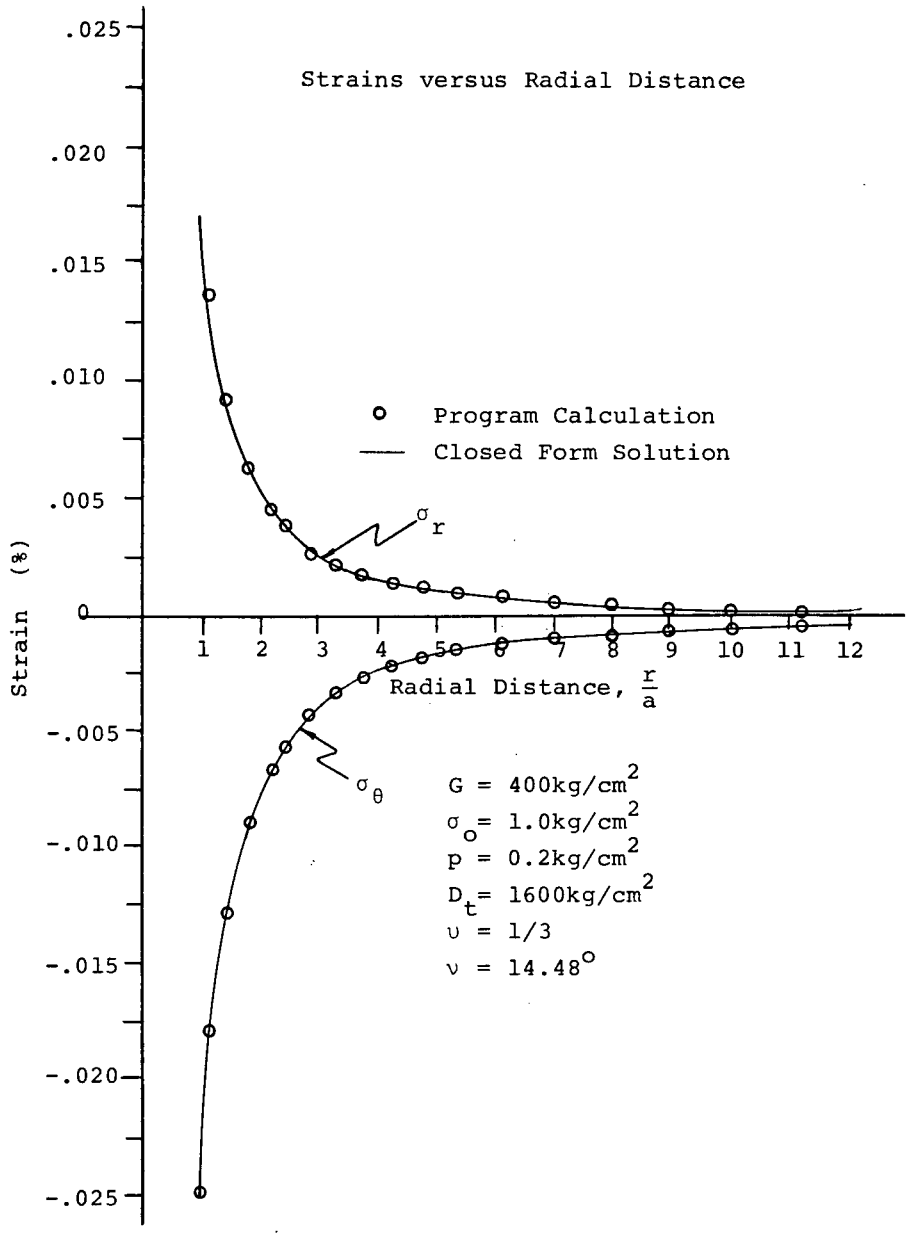

Figure 36. Comparison of Strains in Linear Dilatant Material From Closed Form Solution and Finite Element Calculation

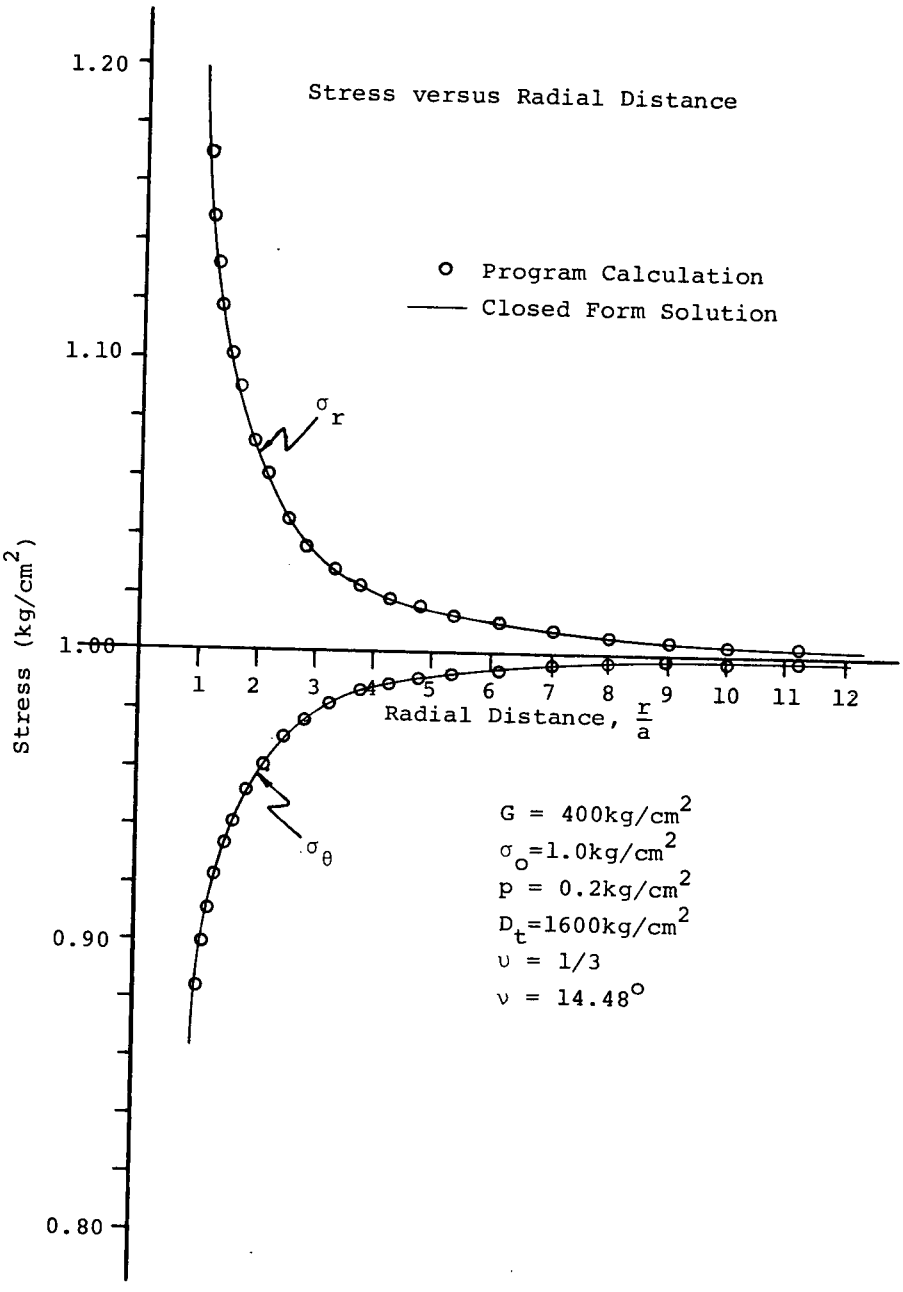

Figure 37. Comparison of Stresses in Linear Dilatant Material from Closed Form Solution and Finite Element Program Calculation

4.4 Stress Redistribution

For loading type problems, stress redistribution presents no difficulty when working with principal planes, as in the axisymmetric case in polar coordinates. In loading problems, the need for stress redistribution occurs because the shear modulus cannot usually be set to zero without causing numerical instabilities. This means that elements that have failed, and should not pick up any more shear stress, will be forced to pick up shear stress and hence, will violate the failure criterion. Principal planes carry no shear stress, so within the solution technique, no equations must be solved that would have a zero diagonal if the shear modulus were set to zero. Therefore, for this special case, the shear modulus may be set to zero. Elements that fail will not pick up shear stress. Elements can be forced up the failure surface, following a zig-zag path, as shown in the p-q plot of Figure 38. This path can be made to closely approach the failure surface by using small load increments.

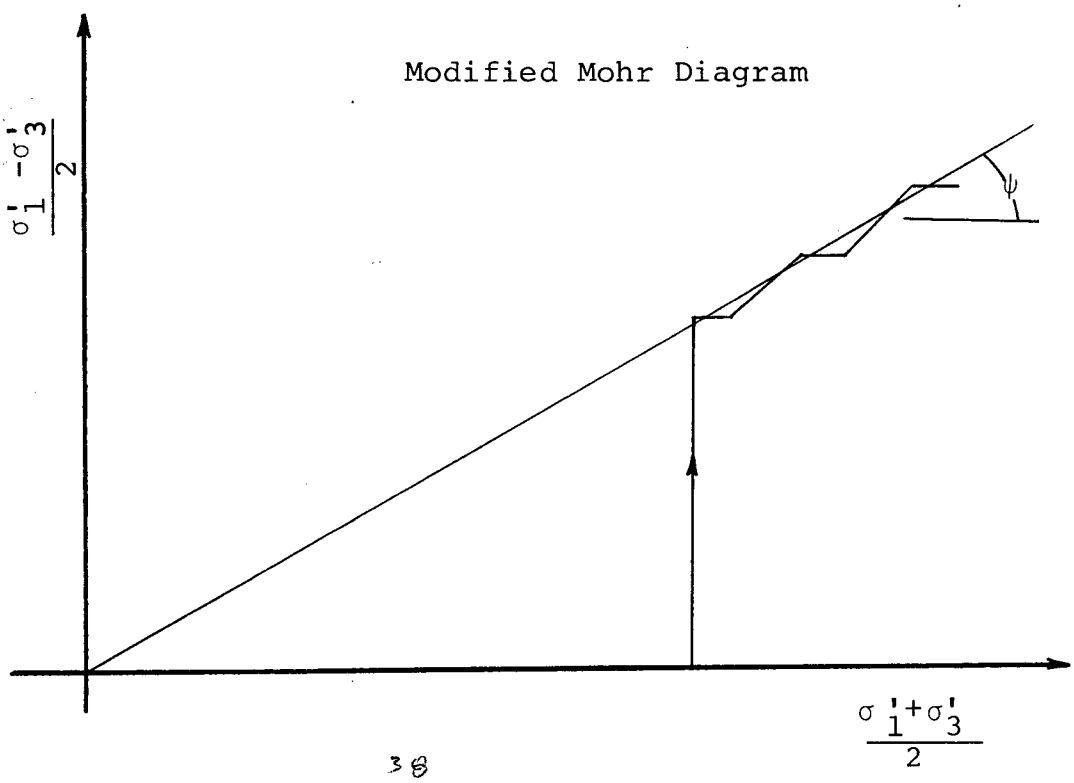

Figure 38. Stress Path for Failed Element

Chapter 5

Results of Finite Element Analysis

5.1 Finite Element Mesh

The response of sand to the expansion of a cylindrical cavity was investigated using the finite element mesh in Figure 39. The mesh was extended to fifty cylinder radii to ensure that the effect of the elastic springs, which extend the domain to infinity, was minimized. Soil properties used in the analysis are shown in Table II. Soil stiffness properties were chosen for a soil of about 70% relative density. However, by changing the value of ϕ_{cv}, the volumetric response of the soil can be changed from that of a dense sand to that of a loose sand. Four cases were looked at: no dilation (the standard incremental linear elastic model) and three different values of ϕ_{cv}. An initial horizontal stress of 1.0kg/cm^2 was used to investigate the effects of changing dilatancy. This corresponds to a test depth of about ten meters and a k_o = 1.0. The effect of confining stress was investigated using initial horizontal stresses of 1.0, 1.5 and 2.0kg/cm^2 and a $\phi_{cv} = 30^o$.

5.2 Pressure Expansion Curves

Pressure expansion curves for the various soil conditions are shown in Figure 40. The curves have the characteristic shape of field results. Figure 41 compares the finite element results with closed form elastic plastic results. The figure shows that the nonlinear elastic material is much softer than the elastic plastic material. In assessing the soil model, for the stress-strain relation used, the shape of the relation has a major effect on the soil response, while the addition of dilation has a smaller effect.

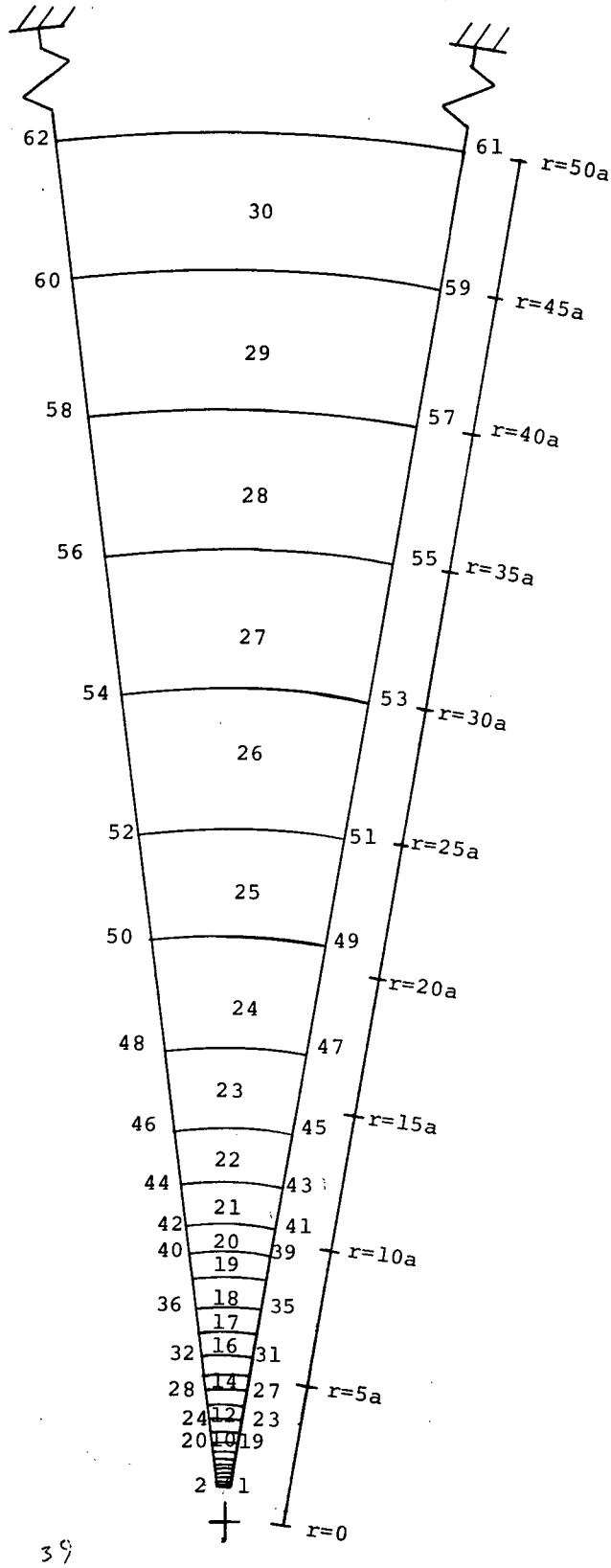

39

Figure 39. Finite Element Mesh

TABLE II

SOIL PROPERTIES

$k_E = 800.$
$n = 0.5$
$k_B = 800.$
$m = 0.5$
$r_f = 0.9$
$\phi_1 = 39.^{\circ}$
$\Delta\phi = 4.0^{\circ}$
$c = 0.0$

Volume Change Characteristic	Initial Horizontal Stress (kg/cm^2)
No dilation	1.0
$\phi_{cv} = 36^0$	1.0
$\phi_{cv} = 33^{\circ}$	1.0
$\phi_{cv} = 30^{\circ}$	1.0, 1.5, 2.0

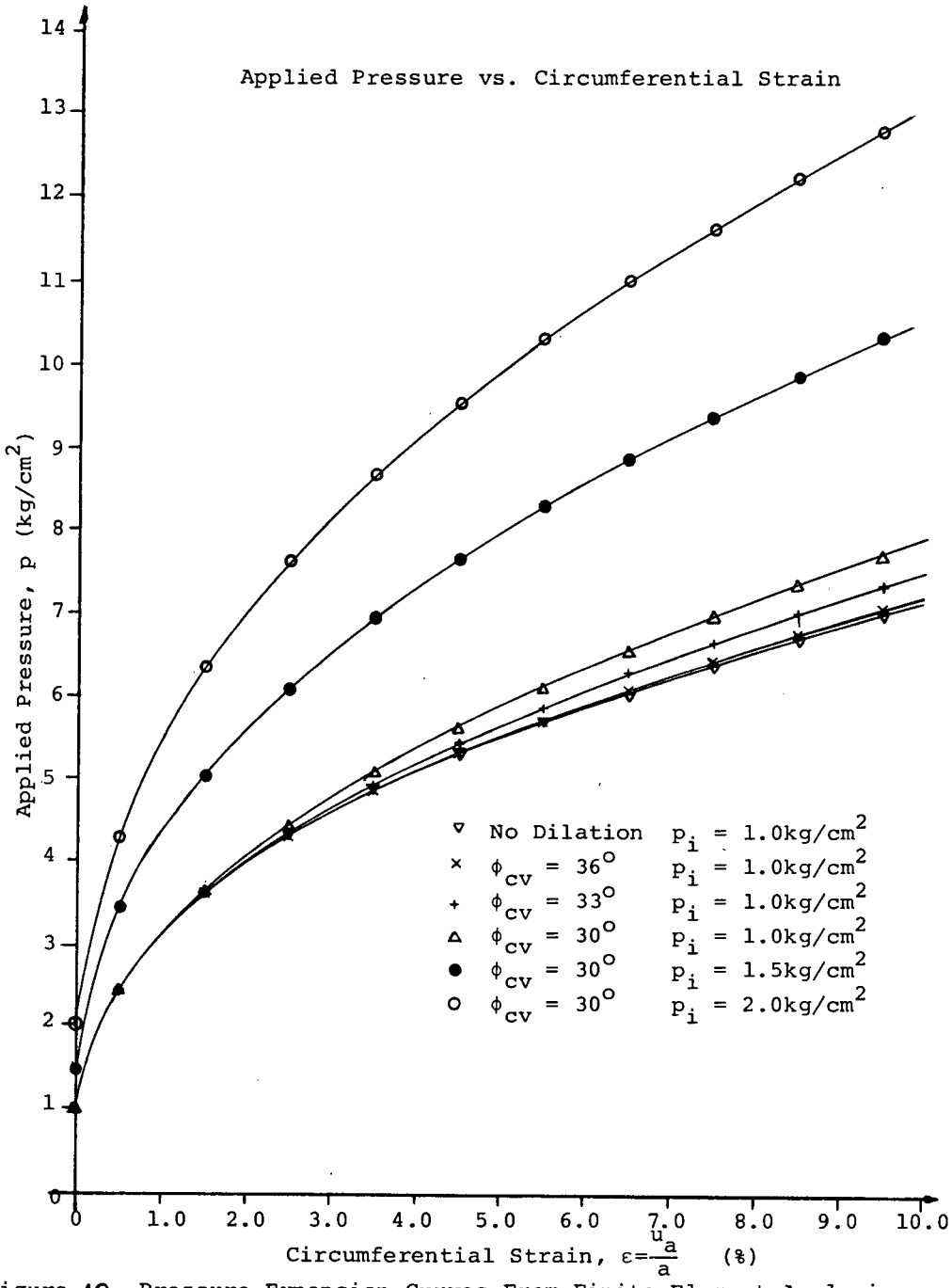

Figure 40. Pressure-Expansion Curves From Finite Element Analysis

40

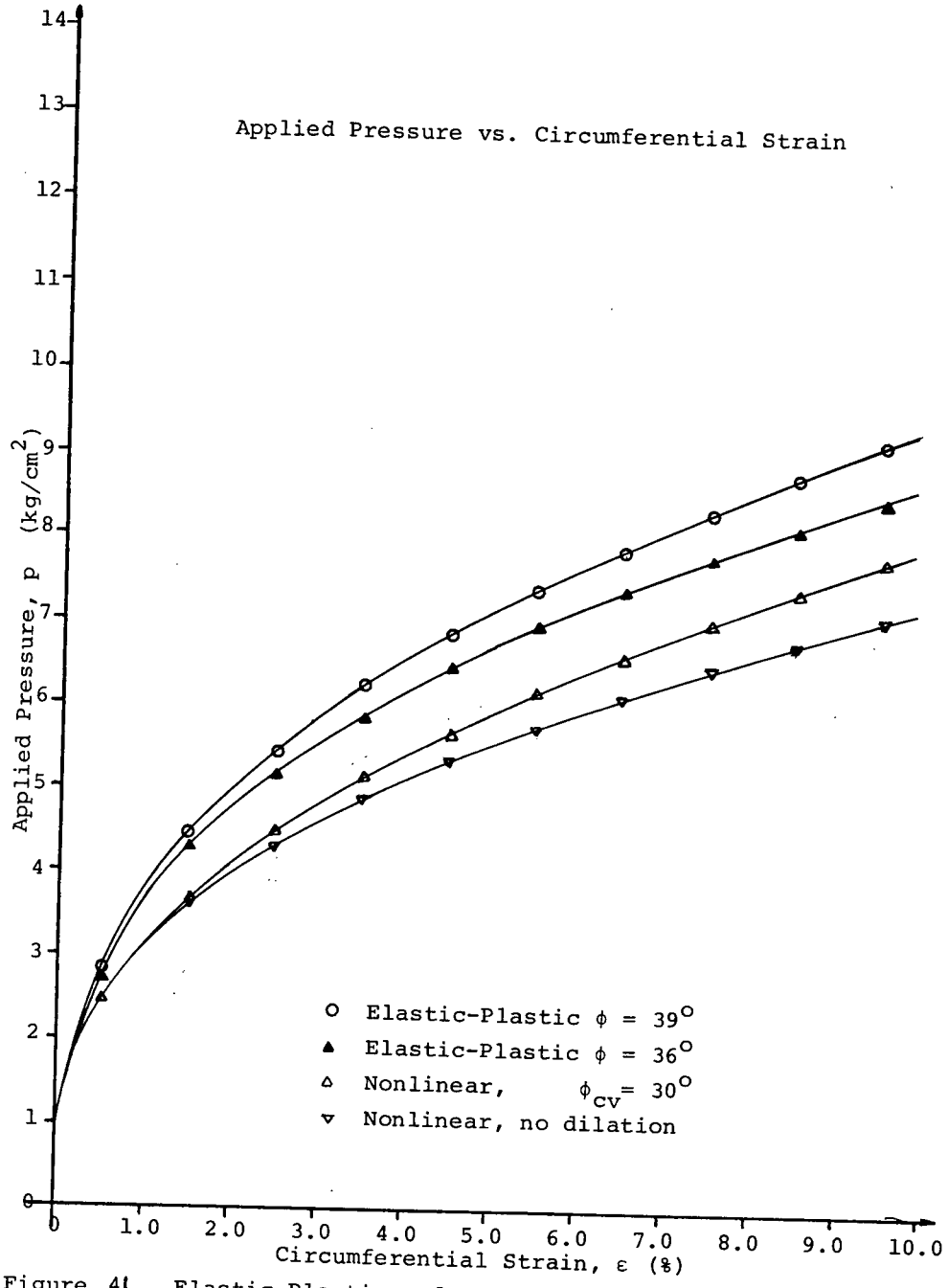

Figure 41. Elastic-Plastic and Nonlinear Soil P-ε Curves

41

5.3 Volumetric Response

Volumetric response of the soil is shown in Figure 42. The nonlinear soil with no dilation has only volume contraction. This is the response that all finite element programs without shear volume coupling produce. As shown in Figure 40, this produces the softest soil response and cannot possibly be used to estimate volume changes in dilatant materials. Volumetric response varied from what would be termed a loose sand, with expansion beginning only after large strains, to a medium dense sand with expansion beginning at low strains. The three tests on sand with the same constant volume friction angle but varying initial stress show the suppression of dilation with increasing stress level. Dilation angles, determined from the slopes of the near linear portion of the volumetric strain versus shear strain curves, vary from $\nu = -0.3^{\circ}$ for the case with no dilation to $\nu = 6.7^{\circ}$ for the soil with $\phi_{cv} = 30^{\circ}$ and an initial stress of $1.0 kg/cm^2$.

5.4 Stress Paths

The computed stress paths followed by the soil around the expanding cavity are shown in Figure 43. For a given initial stress, all soils follow the same stress path, regardless of volume change characteristics. Also, all elements within a soil follow the same stress path, although each element is at a different point on the stress path at any given instant. The elastic-plastic stress path is also shown. At low stress levels the elastic-plastic path varies considerably from the nonlinear soil stress path, but once yield occurs, all soils on the same failure surface follow the same stress path.

Once yield occurs, the stresses must obey the yield cri-

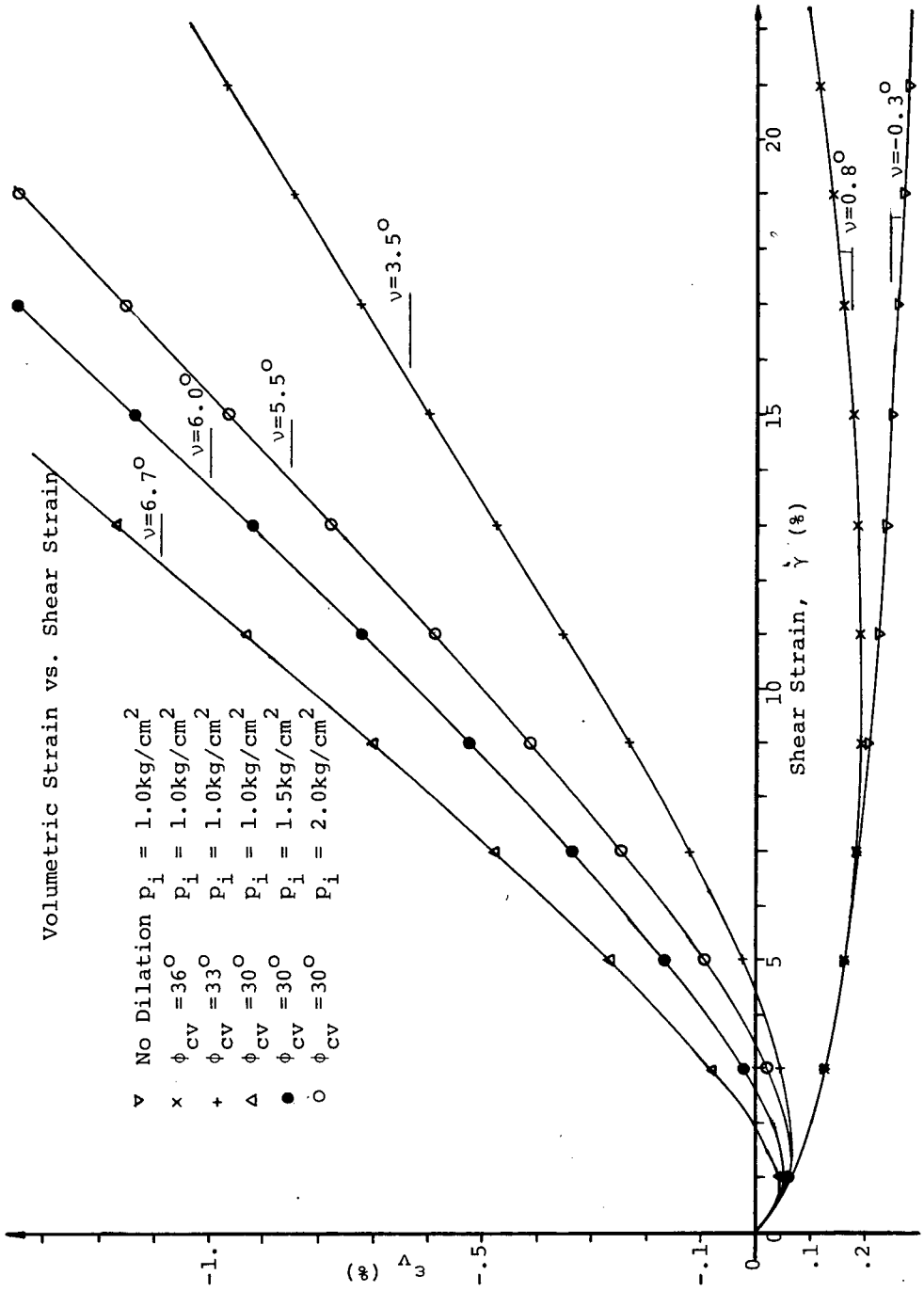

Figure 42. Volumetric Response of Soil from F.E. Analysis

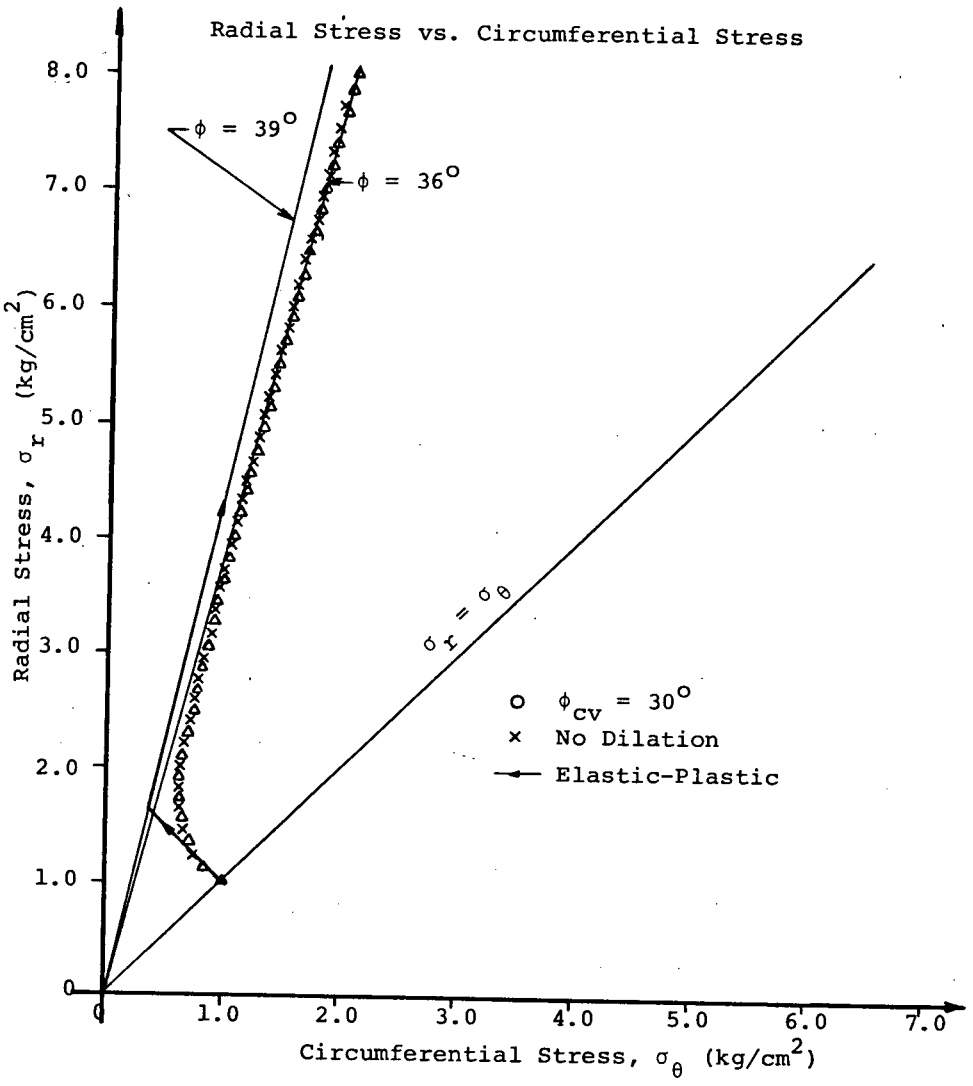

Figure 43. Stress Paths Followed by Soil Around Expanding Cylinder

terion. The equilibrium equation after yield produces a single differential equation that may be solved with the stress boundary condition. Soil properties, aside from the yield condition, are not required to determine the stress field. All soils with the same friction angle will follow the same stress path after failure, but the displacements and strain in the soils will depend on the soil stiffness properties.

5.5 Displacement Field, Strains and Stresses

Figure 44 shows a comparison of the displacement fields for a total cylinder pressure of 6.25kg/cm^2 and an initial stress of 1.0kg/cm^2. The nonlinear material with no dilation has the largest displacement at the cylinder face, but the displacements in the dilatant material propagate further into the material. The difference that dilation makes is marginal beyond about 3 cylinder radii. A purely elastic material has much smaller displacements, while the elastic-plastic material has displacements that are smaller but of the same order of magnitude as the nonlinear material displacements. Displacements decay approximately as $\frac{1}{r}$ in all cases. The nonlinear material with no dilation has displacements decaying as $\frac{1}{r^{1.03}}$, while the dilatant material has displacements decaying as $\frac{1}{r^{0.96}}$.

Figure 45 shows a comparison of the strains for the same cylinder pressure. As with the displacements, the nondilatant soil has the highest shear strain at the cylinder face, but the dilatant soil has higher shear strains further away from the cylinder. Again, beyond about 3 cylinder radii, dilation makes little difference. Soil nonlinearity is the major factor changing the soil response.

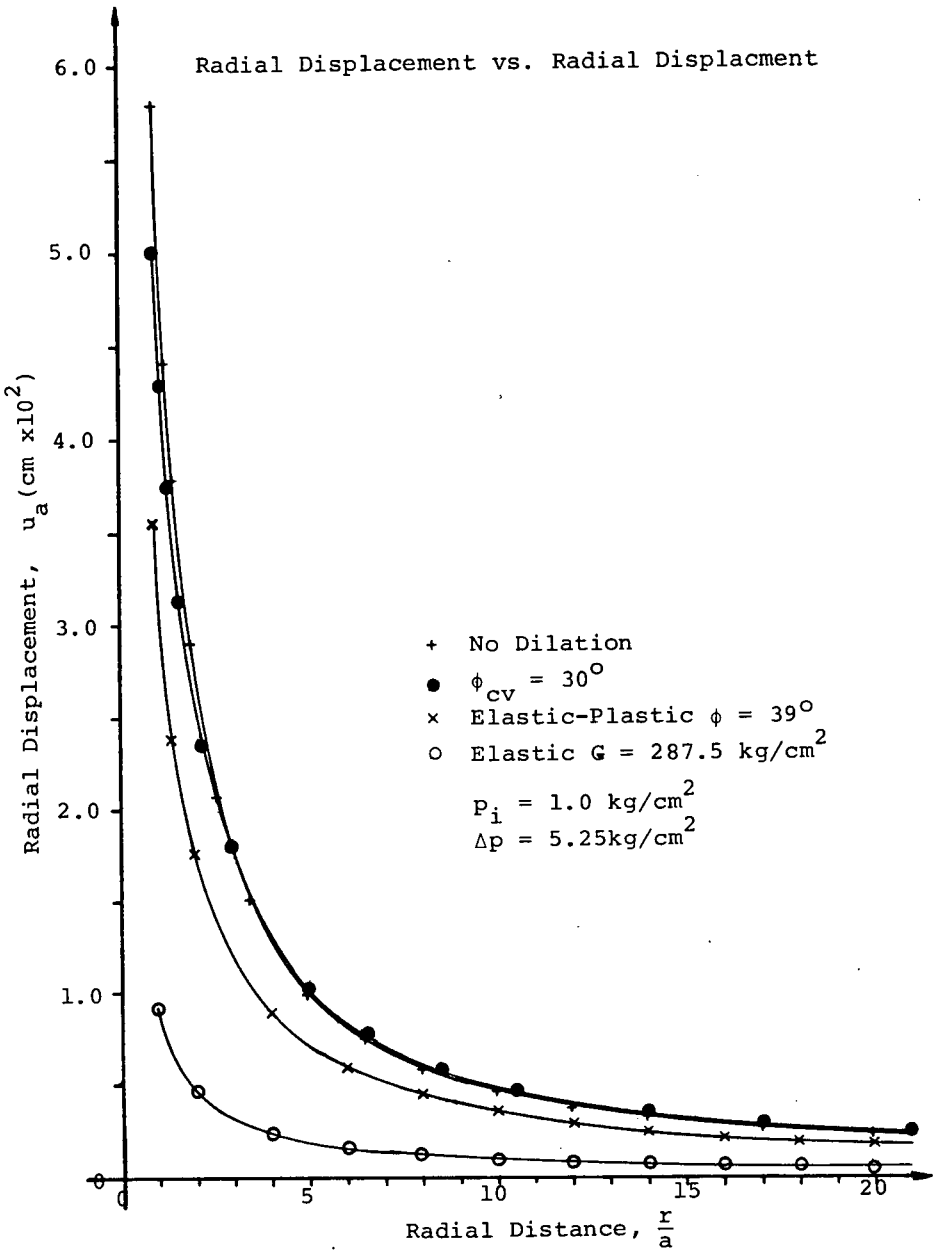

Figure 44. Comparison of Displacements Around Expanding Cylinder

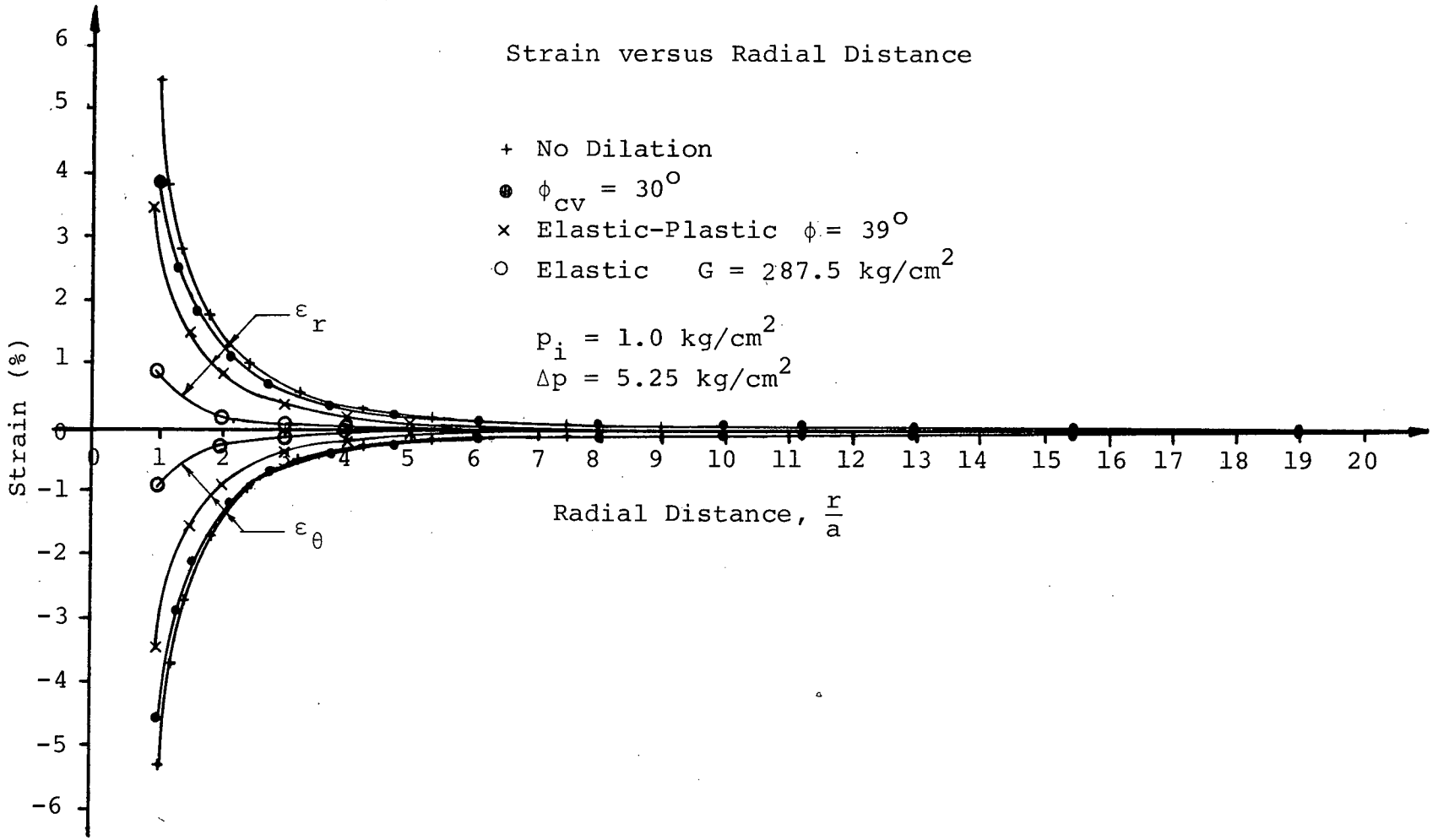

Figure 45. Comparison of Strains in Soil Around Expanding Cylinder

The stress field for this cylinder pressure is shown in Figure 46. As previously discussed, volume change makes no difference to the nonlinear soil stress field once yield has been reached. Stresses decay slower in the nonlinear soil than in the elastic material, so higher shear stresses exist further from the cylinder in the nonlinear soil. The stresses in the elastic-plastic material are slightly different from the nonlinear material because the friction angle does not change in the elastic-plastic material as it does in the nonlinear soil.

The mean normal stress increases significantly in the nonlinear soils and in the elastic-plastic material. The increase in mean normal stress significantly affects the soil response, as both the bulk modulus and the initial tangent shear modulus increase with stress level in the nonlinear material. As the test progresses the soil becomes stiffer for a given stress difference.

5.6 Distribution of Shear Modulus in Finite Element Domain

The distribution of shear modulus within the soil is shown in Figure 47. In the nonlinear soils volume change characteristics have little effect on the variation of shear modulus. This is as expected, as the stress distribution within the soils are the same. The elastic material has a constant shear modulus while the elastic-plastic material has zero shear modulus in the plastic zone and a constant shear modulus in the elastic region. The nonlinear material shear modulus increases slowly with radial distance towards the elastic value.

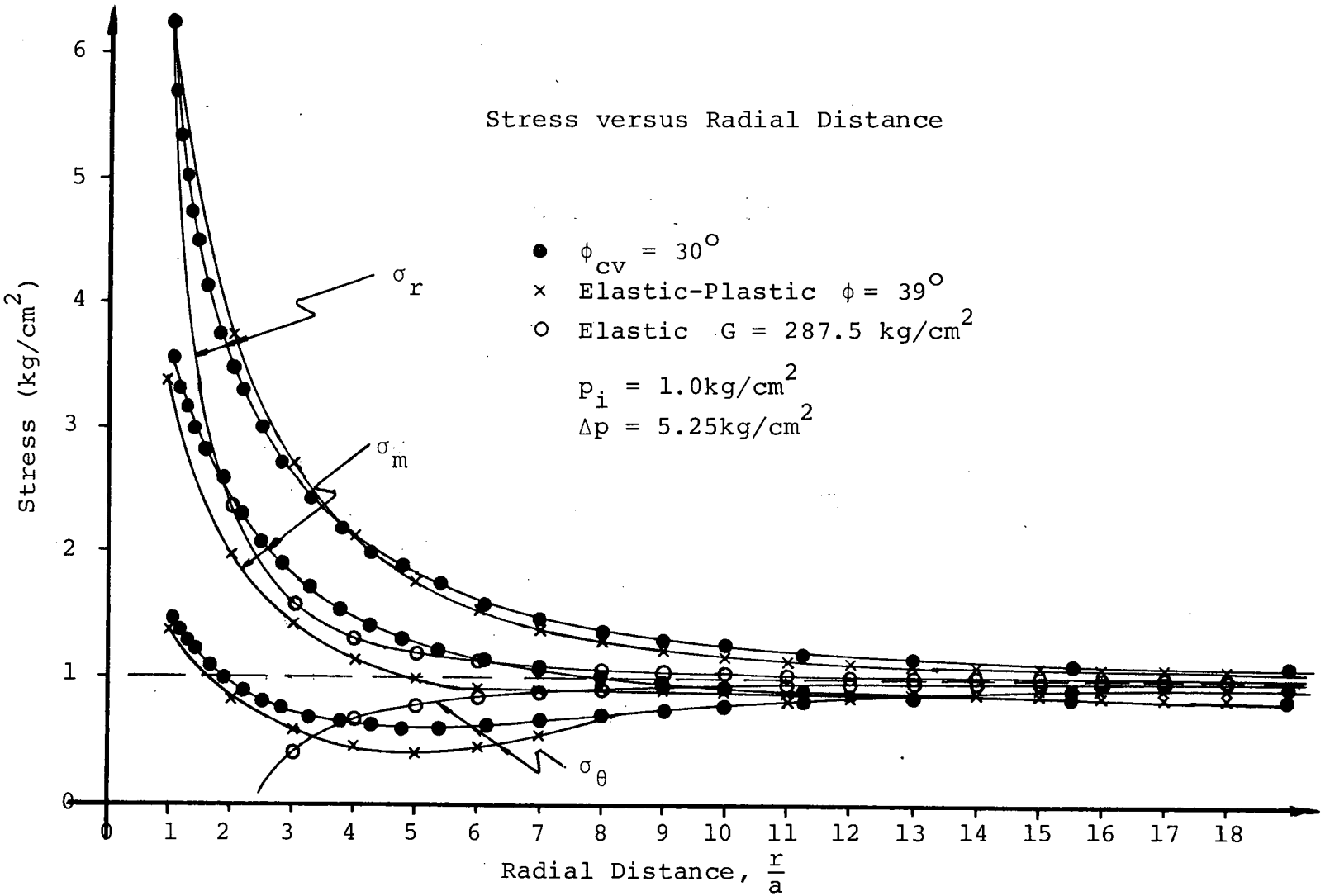

Figure 46. Comparison of Stresses in Soil Around Expanding Cylinder

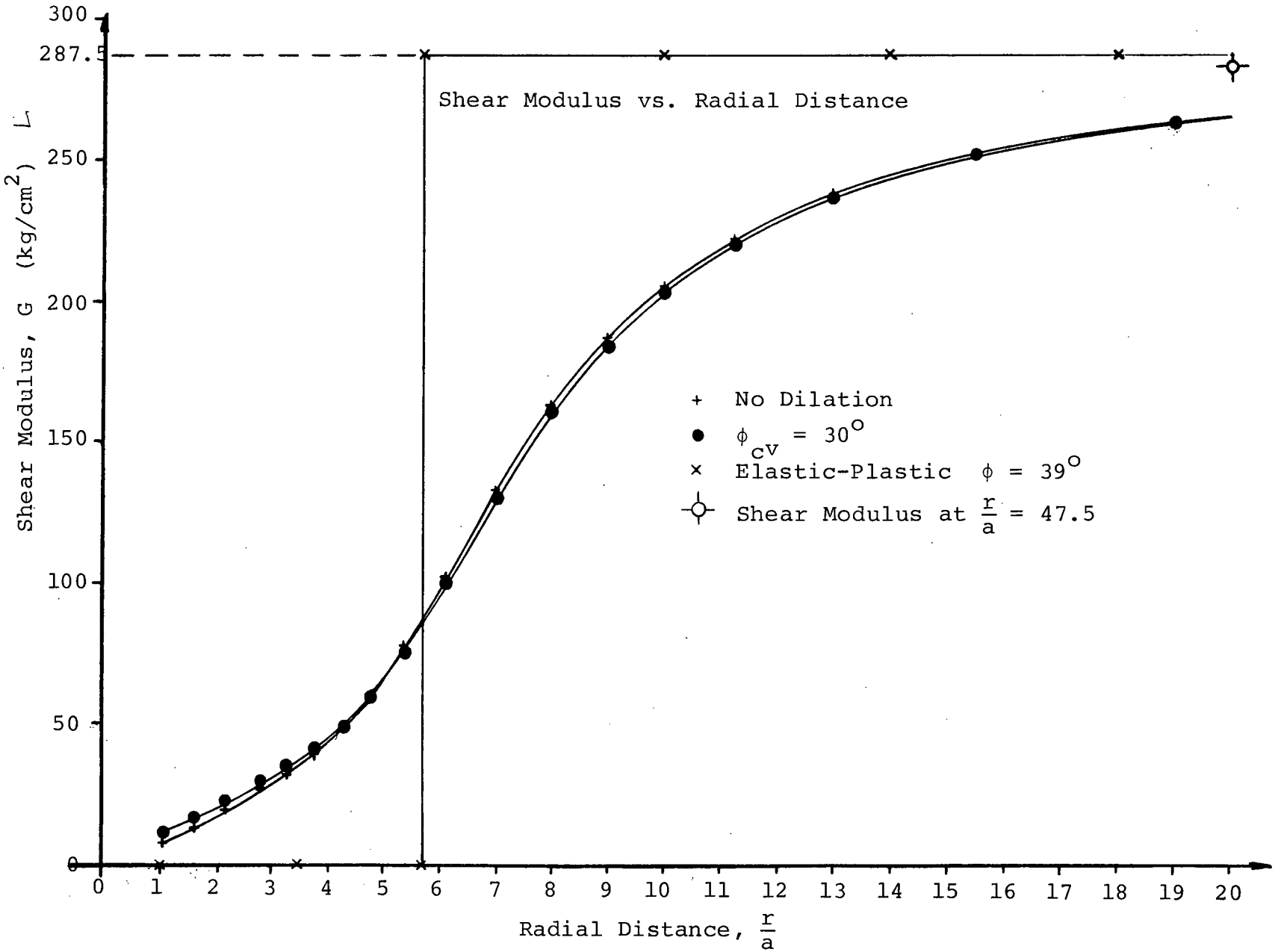

Figure 47. Shear Modulus in Soil Around Expanding Cylinder

5.7 Determination of Friction Angle and Dilation Angle

Computed log-log pressure expansion curves are shown in Figure 48. A summary of the values of friction angle and dilation angle calculated by Hughes' method is shown in Table III. The method gives good agreement with the results of the finite element analysis. The dilation determined from the finite element analysis was taken from the slope of the volumetric strain versus shear strain curves shown in Figure 42. The friction angles were determined from an average stress ratio near the end of the test. The soil does not have a unique friction angle, as the friction angle changes with stress level. The friction angle continually decreases as the test progresses, but the decrease in the angle is small at higher strains, when the mean normal stress does not change rapidly with strain.

The elastic-plastic material plots as a straight line at all strains on a log-log pressure expansion plot.

5.8 Stress-Strain Curves

Stress-strain curves can be developed from the pressure expansion curves. An example of the method is shown in Figure 49. The value of friction angle is determined by Hughes' method. Over most of the test the soil is at failure with $\sigma_\theta = \frac{1}{R}\sigma_r$, where R is calculated from the friction angle. The value of R changes as strains increase, but the error in using a constant value of the stress ratio is small. At low strain the soil may be approximated as an elastic material, in which case: $\Delta\sigma_\theta = \Delta\sigma_r$ This elastic response is shown in the figure. The soil is assumed to yield at the strain at which the elastic σ_θ curve intersects the σ_θ curve determined from the radial stress and

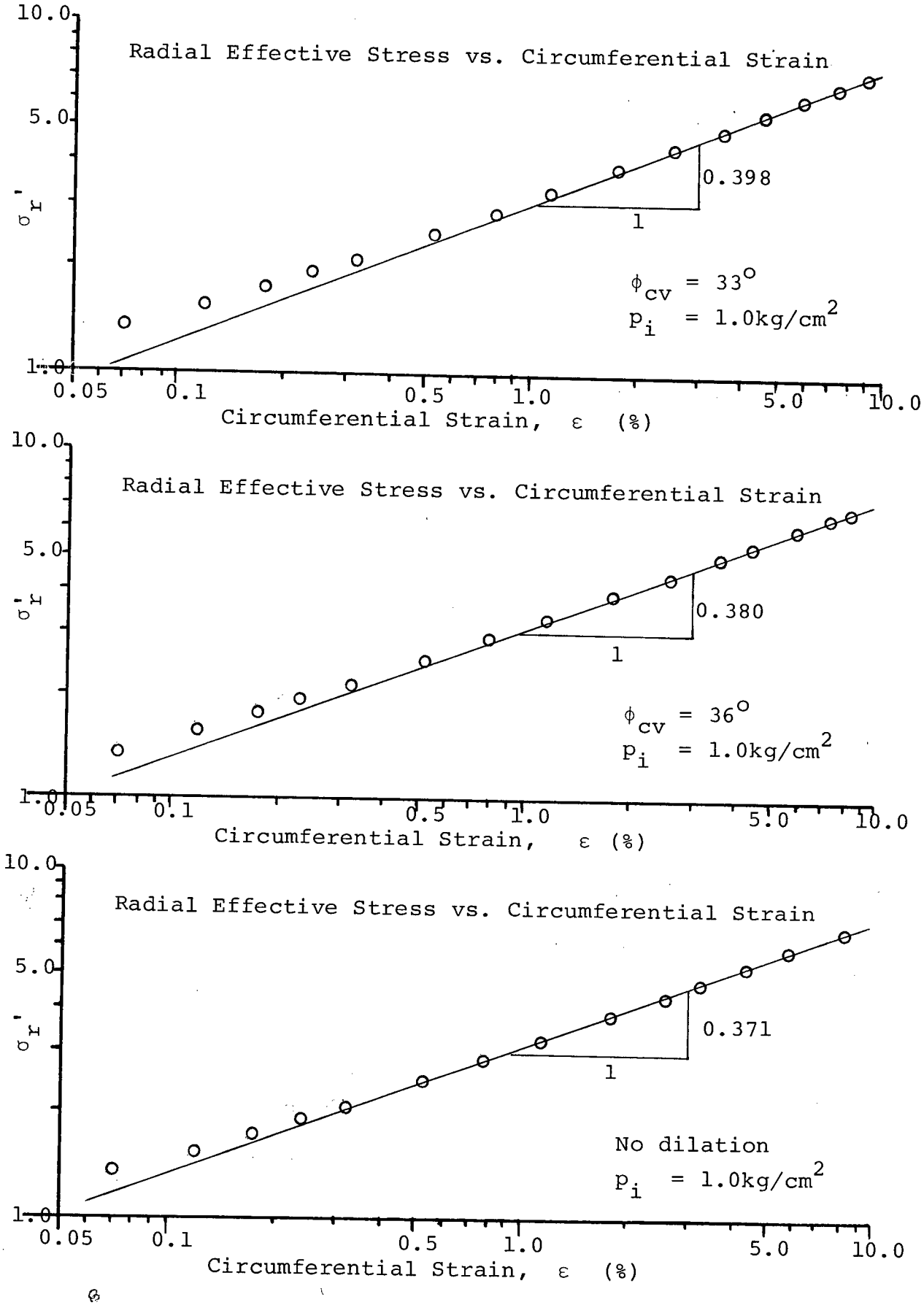

Figure 48. Log-Log Pressure Expansion Curves from F.E. Analysis

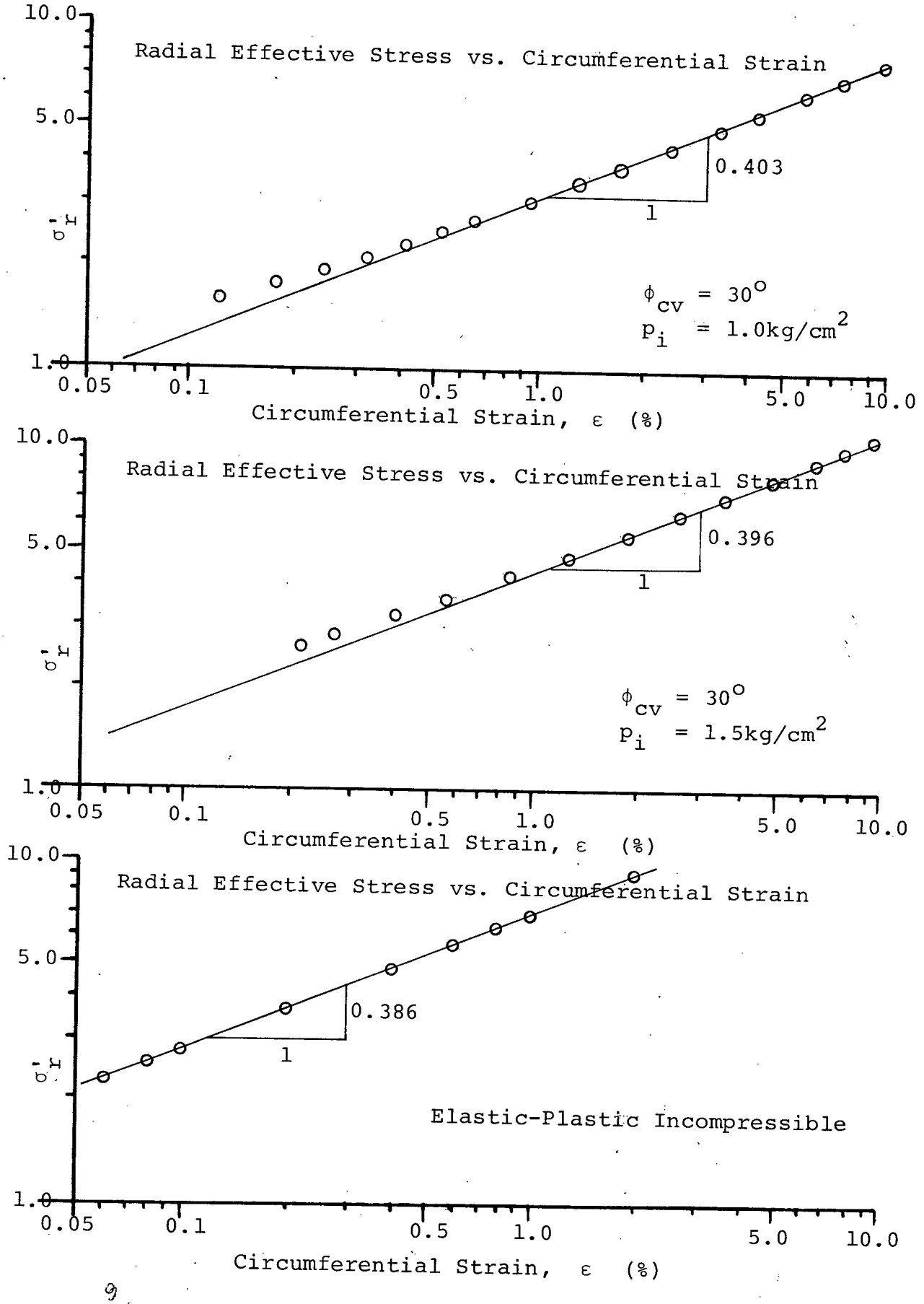

Figure 48 Log-Log Pressure Expansion Curves from F. E. Analysis

TABLE III

Comparison of Friction Angles and Dilation Angles

Volume Change	Hughes et al Method		Finite Element Results	
	ϕ	ϕ_{cv}	ϕ	ϕ_{cv}
No Dilation	36.4	-0.18	36.5	-0.3
ϕ_{cv} = 36.	36.7	0.90	36.5	0.8
ϕ_{cv} = 33.	36.3	4.0	36.3	3.5
ϕ_{cv} = 30.	35.1	6.0	36.1	6.7

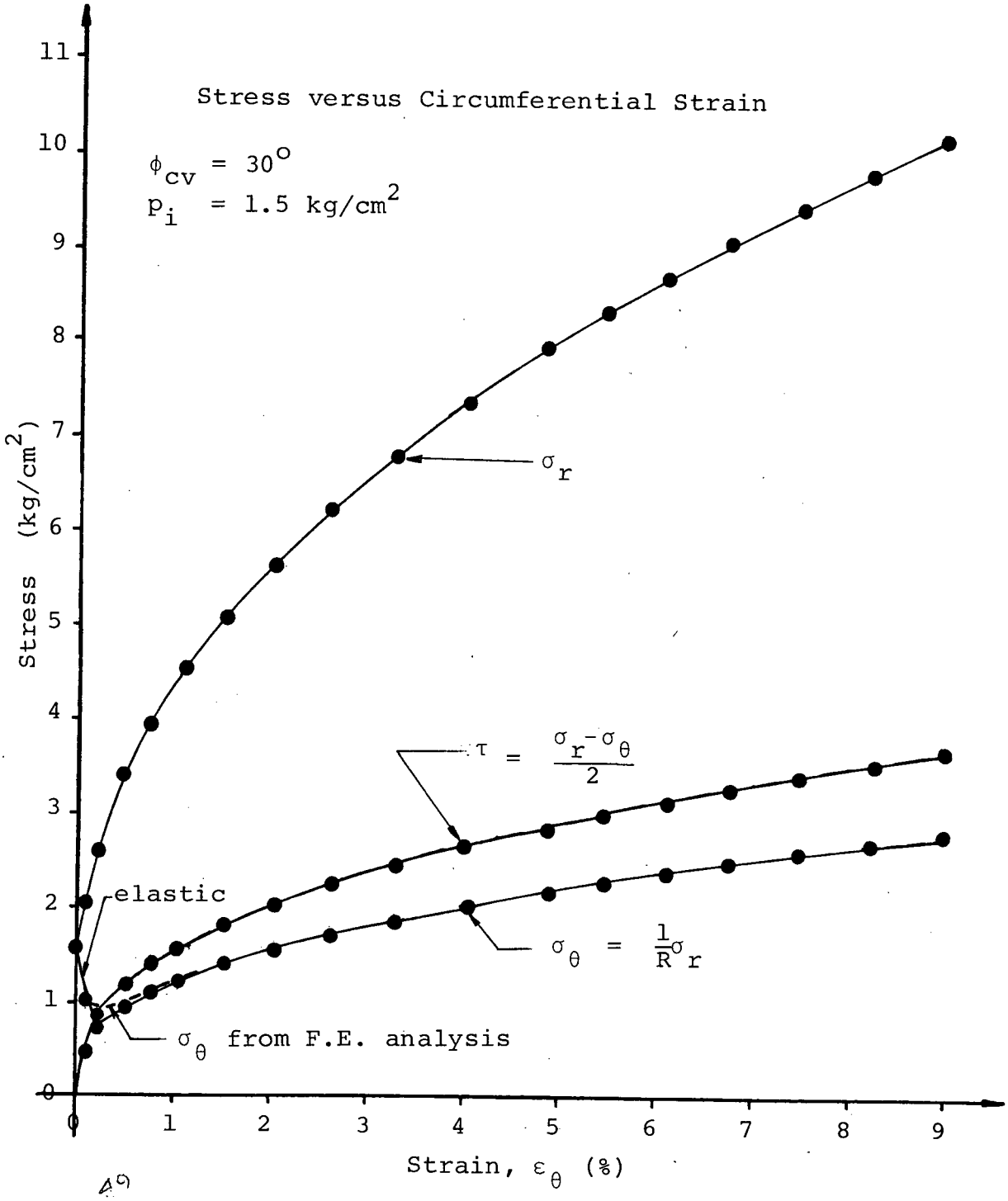

Figure 49. Calculation of Shear Stress From Pressure-Expansion Curve

assuming the soil was at a constant stress ratio. The variation of σ_θ with strain follows the elastic curve to the intersection, then follows the $\frac{1}{R}\sigma_r$ to the end of the test. The variation of σ_θ with strain as determined from the finite element analysis is shown in the figure for comparison. There is some error near the yield strain, but overall agreement is good. The shear stress determined as $\tau_{max} = (\sigma_r - \sigma_\theta)/2$ is also shown in the figure.

The curve so far developed has τ_{max} versus ε_θ. The stress strain curve of τ_{max} versus γ_{max} is desired. An approximation of the shear strain can be made from the circumferential strain by assuming that all the volume change is shear induced, in which case:

$$d\varepsilon_v = d\varepsilon_r + d\varepsilon_\theta$$

and,

$$d\gamma = d\varepsilon_r - d\varepsilon_\theta$$

but,

$$d\varepsilon_v = -d\gamma \sin\nu$$

Therefore:

$$d\gamma = -2\varepsilon_\theta/(1 + \sin\nu) \qquad (5\text{-}1)$$

The relation between γ and $2\varepsilon_\theta/(1 + \sin\nu)$ determined from the finite element analysis is shown in Figure 50. As can be seen, a small error is introduced by neglecting the volumetric strain due to increasing mean normal stress. Also plotted on the figure is a comparison of γ and $2\varepsilon_2$. Greater error would be introduced by assuming $\gamma = 2\varepsilon_\theta$, as in the elastic case.

Shear stress-shear strain relations calculated by the above method are shown in Figure 51. The curves determined from the finite element analysis are shown for comparison. Agreement is very good. The error would not be significant in practice.

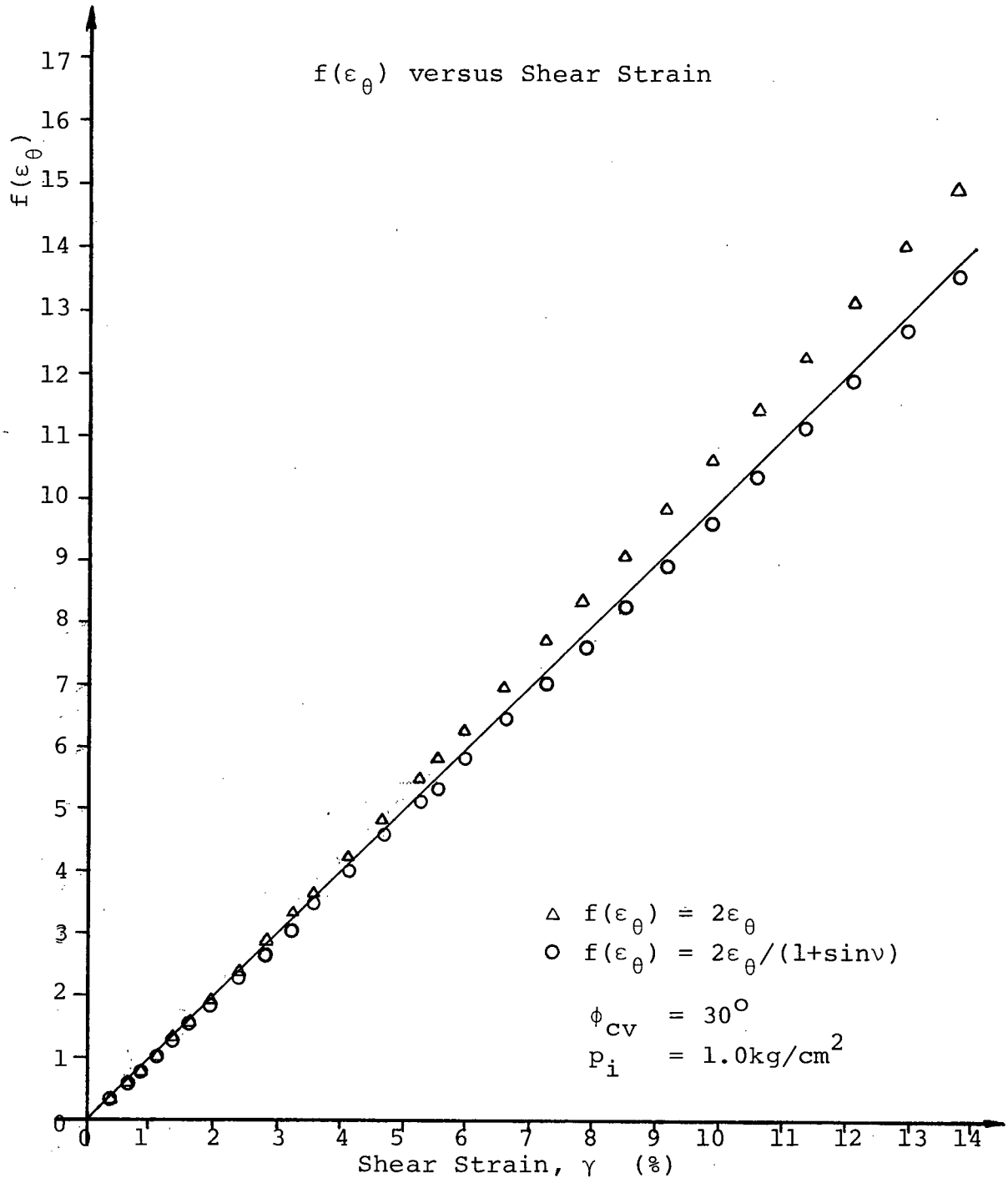

Figure 50. Determination of Shear Strain from Circumferential Strain

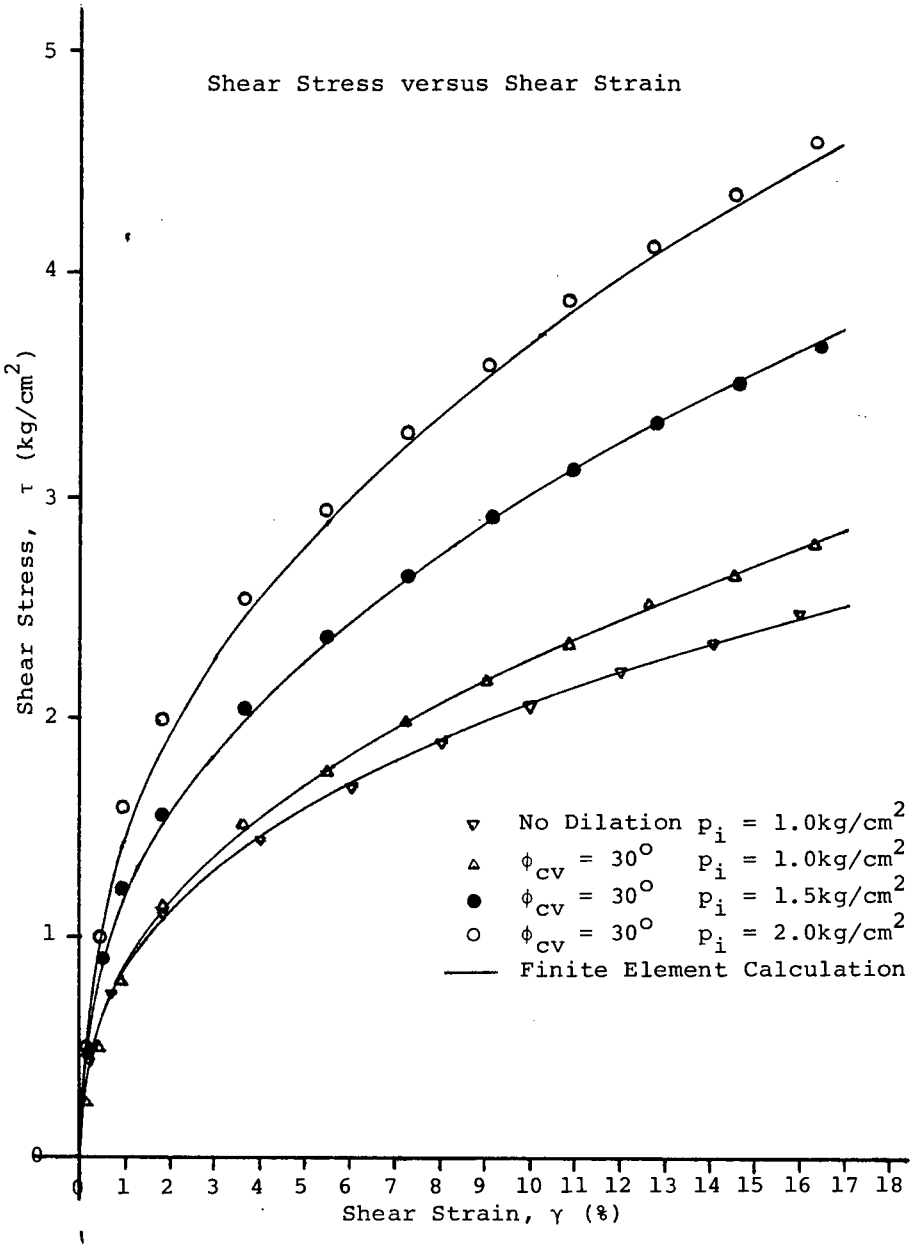

Figure 51. Stress-Strain Curves Developed From Pressure-Expansion Curves

5.9 Hyperbolic Stress-Strain Parameters

Hyperbolic parameters are usually determined using a transformed plot of γ/τ versus γ. An approximately linear curve results, and the initial tangent shear modulus and maximum shear stress are determined from the intercept and slope of the curve. This transformed plot was made for the three highly dilatant sands, Figure 52. The resulting curves are highly nonlinear. A straight line fit to the upper portion of the curves produces unrealistically low estimates of the initial tangent shear modulus.

It is thought that the reason for the nonlinear behaviour is the increase in mean normal stress during the test. The variation of the mean normal stress with strain is shown in Figure 53. For a given test all soil elements lie on the curve, though each is at a different point at any time. The increase in mean normal stress increases both the bulk modulus and the initial tangent shear modulus, Figure 54 and 55. The soil responds to a pressure increase by moving across a set of shear stress versus shear strain curves, each with a higher initial modulus. Determining the variation of the initial modulus with mean normal stress only from the pressure expansion curve is not possible for this complicated stress path.

5.10 Determining Initial Stress and Shear Modulus

An alternate method of determining the initial tangent shear modulus, G_i, was developed. In an elastic material the slope of the pressure expansion curve is 2G. At low strains soil may be approximated as an elastic material. By plotting $\frac{p-p_i}{2}$ against ε_θ, the intercept is G_i. The curve is nonlinear at

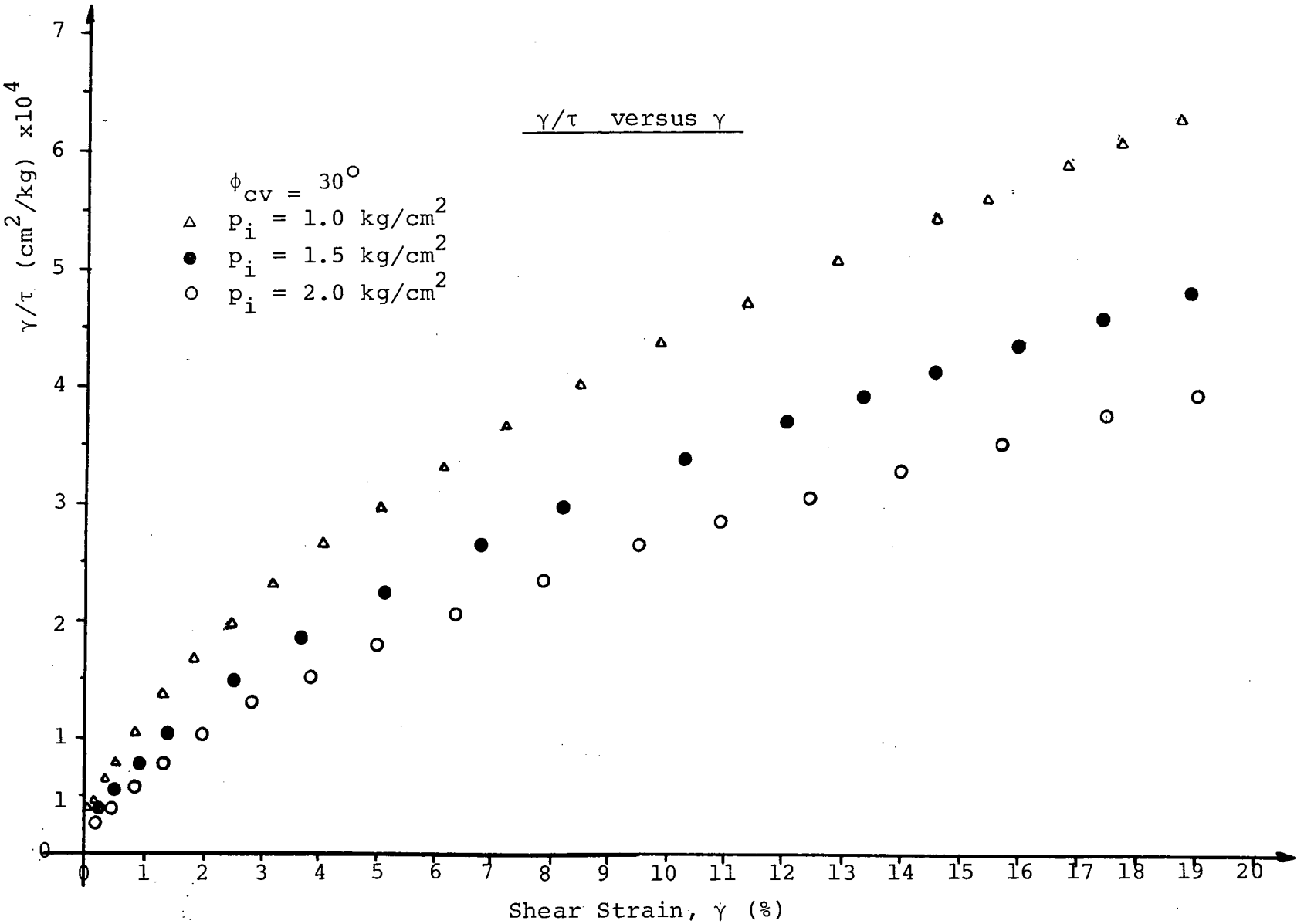

Figure 52. Transformed Plot to Determine Hyperbolic Parameters

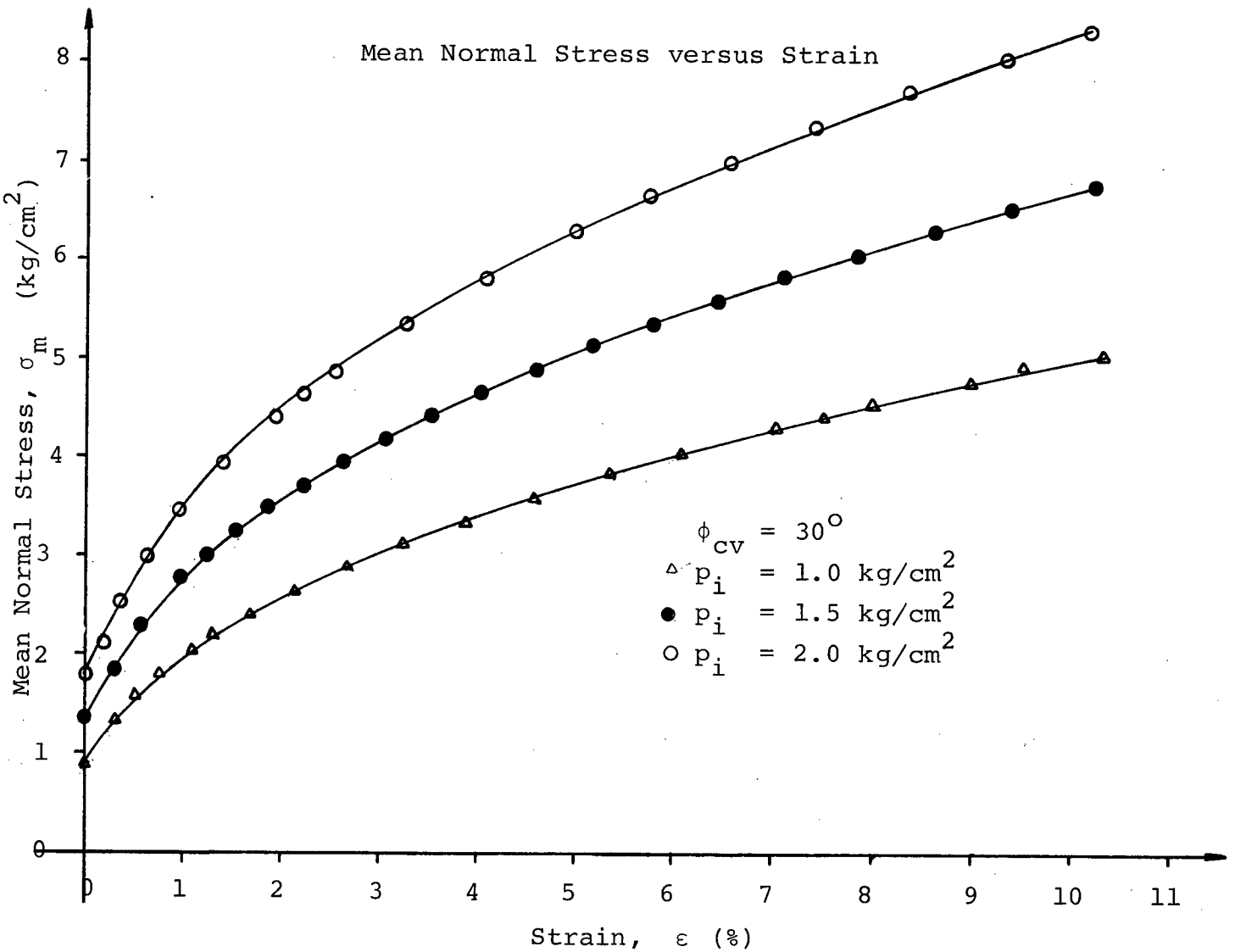

Figure 53. Variation of Mean Normal Stress with Strain

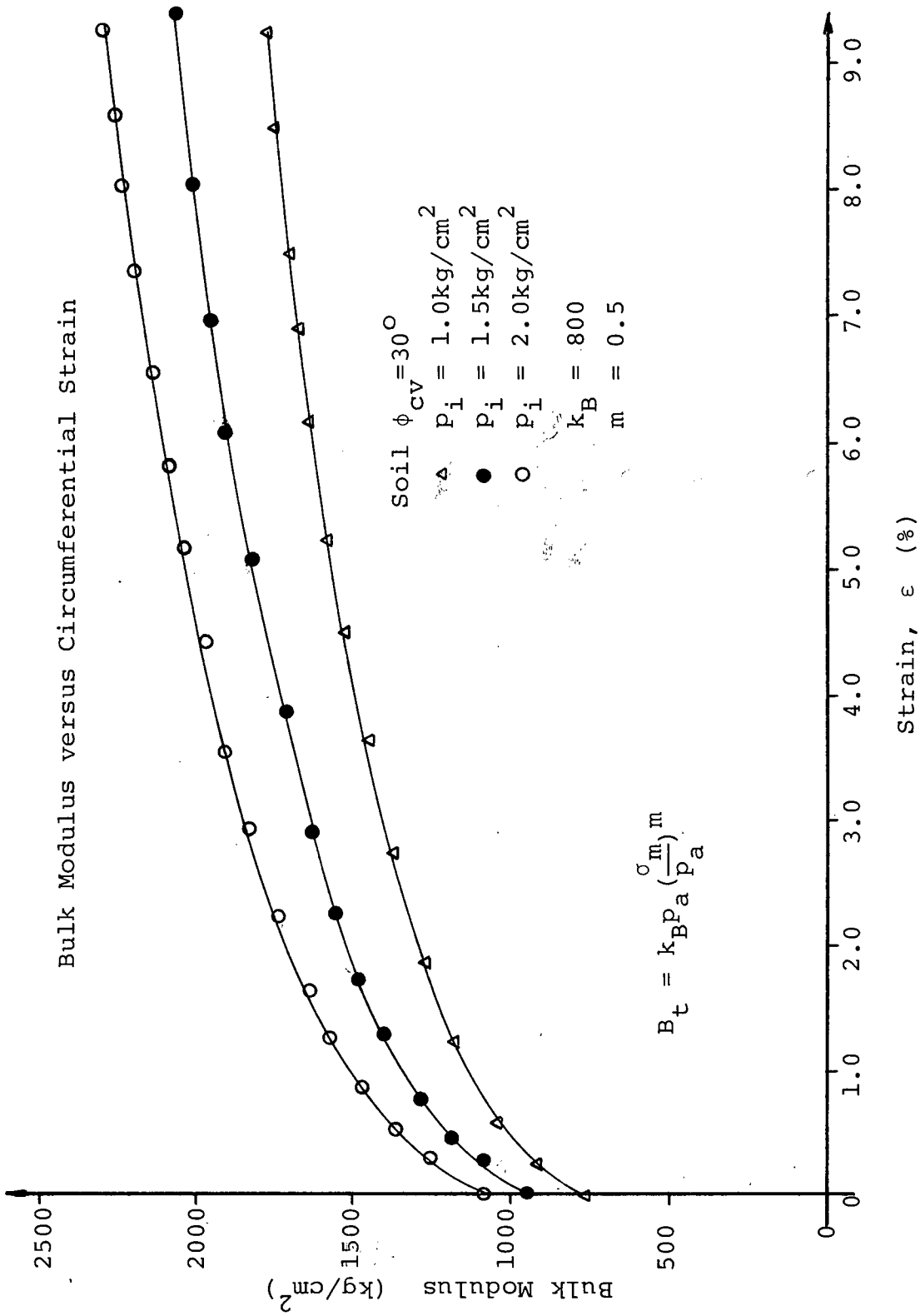

Figure 54. Variation of Bulk Modulus with Strain Level

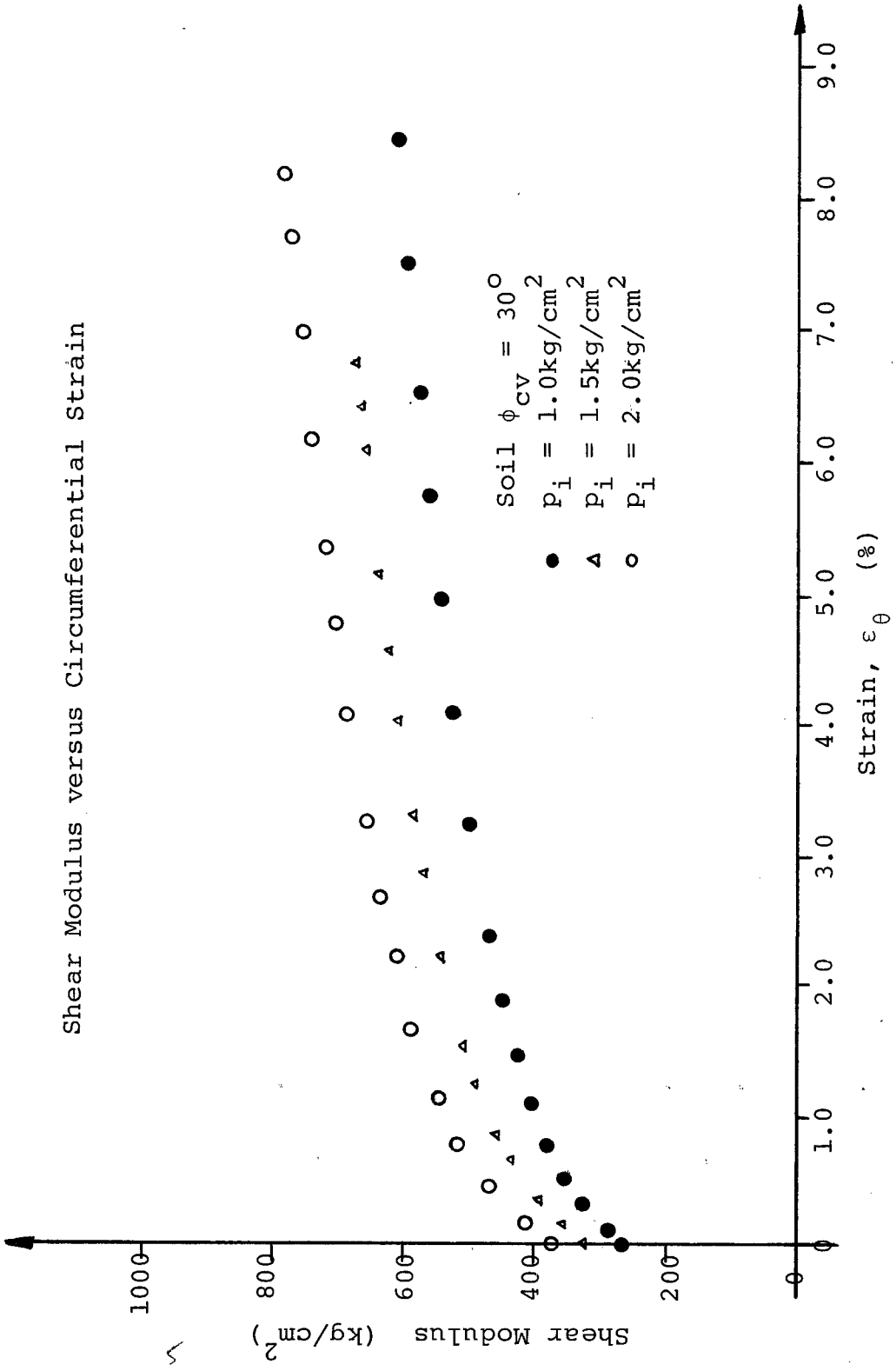

Figure 55. Variation of Shear Modulus with Strain Level

high strains, but at strains less than 1%, it is approximately linear. Three cases are plotted in Figure 56. The calculated values of G_i are in good agreement with the input values.

Plotting $\frac{p-p_i}{2\varepsilon_\theta}$ against ε_θ is not an attempt to produce hyperbolic parameters. Instead it is a method to determine the initial tangent shear modulus. The value $\frac{p-p_i}{2\varepsilon_\theta}$ is an equivalent elastic shear modulus that continually decreases with strain. To determine the shear modulus, the curve specifying the variation of the equivalent elastic modulus with strain is projected to the intercept with the zero strain axis. This method could be used with other variables being substituted for the circumferential strain, for example, the equivalent elastic shear modulus could be plotted against cylinder pressure since the modulus decreases as the pressure increases.

This is a difficult method to use with field data. Usually very few readings are taken at low strains. Missing the low strain readings can cause the initial modulus to be underestimated. A comparison of shear moduli from five tests at MacDonald's test site on Sea Island is shown in Table IV. Also shown are the moduli calculated from the initial slope of the pressure expansion curves and the modulus calculated from the rebound portion of the curve. The predicted modulus should agree with the modulus from the initial slope of the pressure expansion curve, but agreement is variable.

Another problem is the determination of the initial horizonatal stress, p_i. The calculation of G_i is sensitive to the chosen value of p_i. Choosing a value of p_i too small will cause G_i to be overpredicted, as shown in Figure 57. Choosing

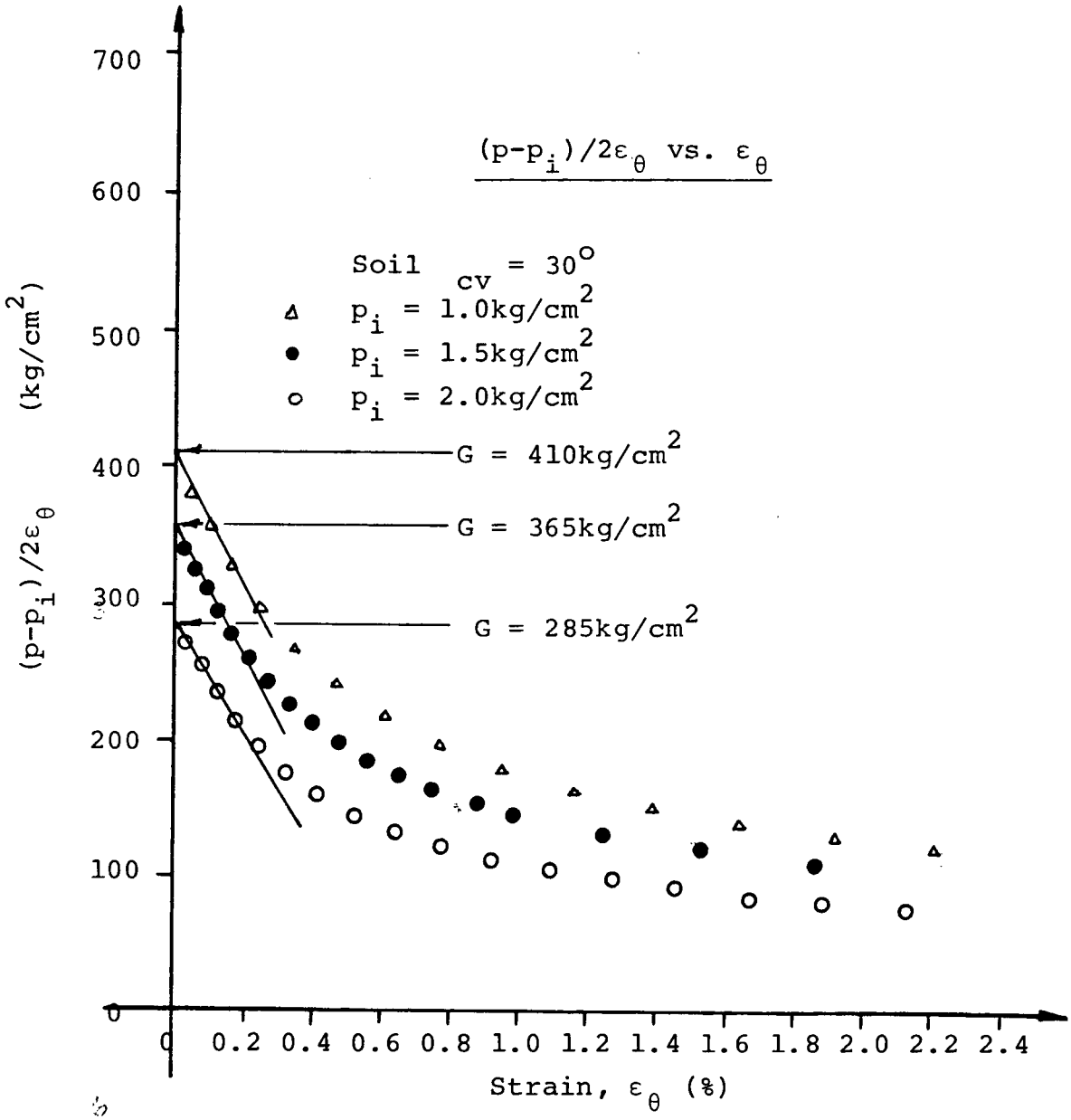

Figure 56. Calculation of Initial Shear Modulus From Pressure-meter Data

TABLE IV

Comparison of Calculated Initial Shear Modulus Values

Pressuremeter Tests at Sea Island Test Site

Test Number	Depth (m)	Initial Shear Modulus, G_i		
		Initial Slope of p-ε Curve. (kg/cm^2)	Unload Portion of Curve (kg/cm^2)	New Method (kg/cm^2)
1	3.0	110	130	110
2	3.8	75	260	130
3	4.6	400	170	60
4	5.3	70	280	130
5	6.3	50	300	280

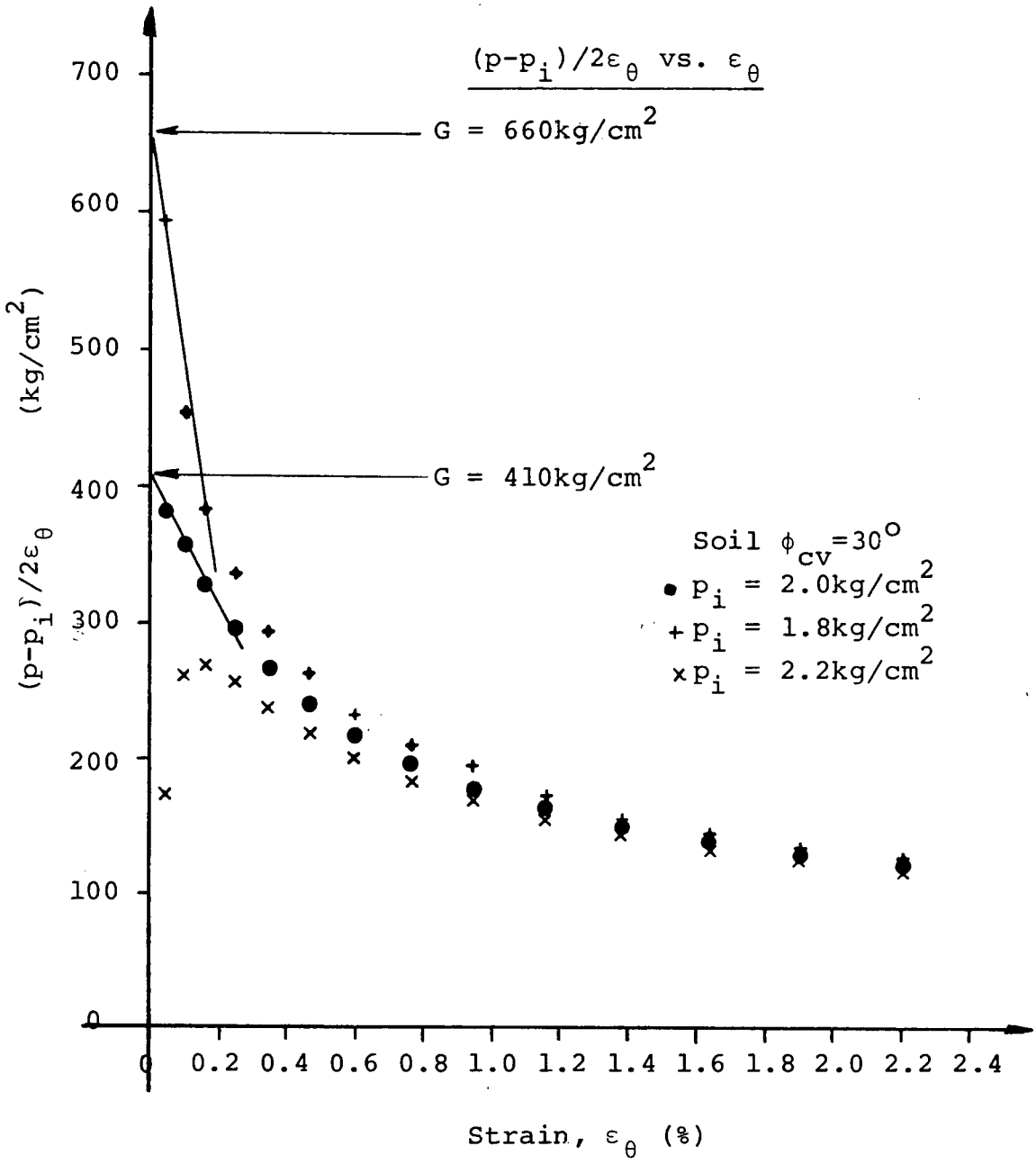

Figure 57 Sensitivity of Calculated Shear Modulus to Initial Estimate of Horizontal Soil Stress

a value of p_i too large causes the equivalent elastic shear modulus to first increase then decrease. This behaviour can be used to estimate p_i, since p_i will be no larger than the value that causes the equivalent elastic shear modulus to increase with strain. A comparison of p_i from the above method with the initial stress predicted by Hughes is shown in Table V. Agreement is fairly good.

A better estimate of both the shear modulus and the initial horizontal stress could be made if more data was taken at low strains. However, this would be pressing the limit of sensitivity of measurement of the cylinder displacement and possibly would not produce reliable and reproducable results.

TABLE V

Comparison of Initial Horizontal Stresses

Test Number	Initial Horizontal Stress	
	Intercept of p-ε curve (kg/cm^2)	New Method (kg/cm^2)
1	0.45	0.62
2	0.87	0.76
3	0.40	0.05
4	2.22	2.16
5	2.13	1.96

5.11 Determination of Hyperbolic Soil Model Parameters

Shear modulus parameters, k_G and n, can be determined if test data is available from a minimum of three depths within a soil horizon. Parameters are determined by plotting the non-dimensional initial shear modulus values versus the in-situ stress on a log-log plot. The parameter k_G is the intercept of the line at $Pi/Pa = 1.0$, and the parameter n is the slope of the line. Figure 58 shows the plot for the results from the finite element analysis. The calculated values of k_G and n agree with the input values.

Estimates of the Young's modulus parameter k_E can be made from k_G. The Poisson's ratio for soil usually is in the range 0.0 to 0.5, which implies:

$$2k_G \leq k_E \leq 3k_G$$

The bulk modulus parameter, k_B, will be approximately equal to k_E, and the parameter 'm' is usually assumed to be equal to 'n'.

These estimates of the soil properties would be adequate for preliminary analyses and parametric studies of soil response. However, critical structures should have additional testing of the soils to determine the properties more accurately.

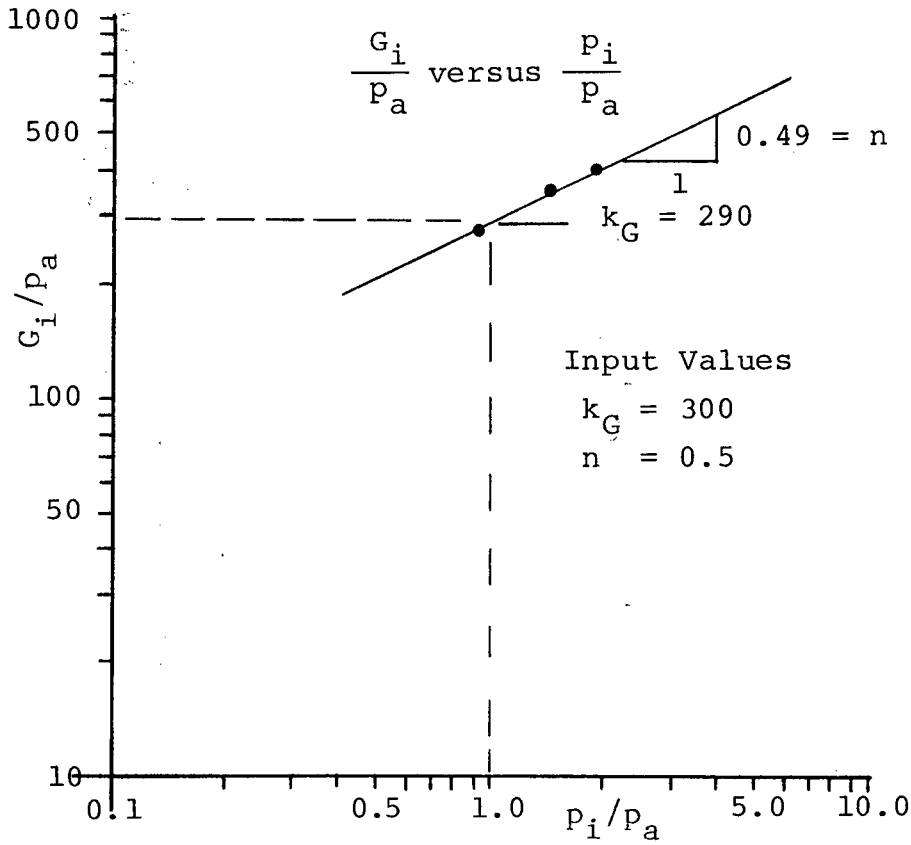

Figure 58. Determination of Soil Stiffness Parameters For Hyperbolic Stress-Strain Relation

Chapter 6

Summary and Conclusion

A finite element analysis of the response of soil to the expansion of a cylindrical cavity was performed. A plane strain finite element in polar coordinates was developed to allow efficient solution of the axisymmetric problem. The polar coordinate element gives excellent agreement with closed form elastic solutions.

The volumetric response of a soil subjected to a shear stress is one of the predominant differences between soil and other materials. The volumetric response can be adequately modelled with a modified form of Rowe's stress-dilatancy equation. The shear-volume coupling model uses Rowe's theory above a developed friction angle equal to ϕ_{cv}. At developed friction angles below ϕ_{cv} no shear induced volume change is assumed to occur. A new triaxial finite element incorporating this shear-volume coupling model gives good agreement with triaxial test data.

The finite element analysis shows that the nonlinearity of the soil stress-strain relation significantly affects the soil response to the pressuremeter. A nonlinear incremental elastic soil is much softer than an equivalent elastic-plastic material. Dilation tends to stiffen the soil, but even a highly dilatant soil is not as stiff as the elastic-plastic material. The volumetric response of the soil does not affect the stresses once yield has occurred. All soils with the same friction angle will have the same stress distribution. However, the volumetric response does affect the strain distribution around the pressuremeter.

The method of determining friction angles and dilation angles proposed by Hughes et al gives good agreement with finite element results. However, in practice, unless ϕ_{cv} is determined in laboratory tests, the accuracy of the calculated values of ϕ and ν will depend on the accuracy of the estimate of ϕ_{cv}.

The initial shear modulus can be estimated from pressuremeter results. A method of determining the shear modulus was proposed. This method of plotting an equivalent elastic shear modulus against the strain gives good agreement with finite element results. The method is difficult to use in practice. It requires an estimate of the initial horizontal stress and several pressure readings at strains less than one percent.

The proposed method can be used to estimate the initial horizontal soil stress. In most cases estimates of the initial stress made by this method are in fair agreement with the lift off pressure corrected for the static water pressure. Using the estimate of the initial stress, an initial shear modulus was calculated. Comparing this value of shear modulus with the shear modulus calculated from the initial slope of the pressure expansion curve to with the rebound portion of the pressure expansion curve does not show good agreement. However, agreement is better with the rebound modulus than with the initial modulus.

In theory the pressuremeter is an attractive method of determining strength and deformation characteristics of soil.

However, soil is extremely complex and present analysis of the pressuremeter cannot account entirely for this complexity. Even if soil response could be completely quantified, the pressuremeter could not give all the soil properties. There are too many soil variables to uniquely determine from the limited amount of data obtained in the pressuremeter test. Either other tests must be performed or some empirical correlation must be used to analyze pressuremeter data.

REFERENCES

Baguelin, F., Jézéquel, J.F., and Shields, D.H., "The Pressuremeter and Foundation Engineering", Series on Rock and Soil Mechanics, Trans Tech Publications, Germany, 1978

Barden, L., and Khayatt, A.J., "Incremental Strain Rate Ratios and Strength of Sand in the Triaxial Test", Geotechnique, Vol. 19, No 4, 1966, pp. 338-357

Byrne, P.M., and Grigg, R.F., "Oilstress: A Computer Program for Nonlinear Analysis of Stresses and Deformations in Oilsands", Soil Mechanics Series No. 42, Dept. of Civil Engineering, U.B.C., July, 1980

Byrne, P.M., and Duncan, J.M., "NLSSIP: A Computer Program for Nonlinear Analysis of Soil-Structure Interaction Problems", Soil Mechanics Series No. 41, Dept. of Civil Engineering, U.B.C., 1979

Boyce, W.E., and DiPrima, R.C., "Elementary Differential Equations and Boundary Value Problems", John Wiley and Sons, New York, Third Edition, 1977

Cook, R.D., "Concepts and Applications of Finite Element Analysis", John Wiley and Sons, New York, First Edition, 1974

Cole, E.R.L., "The Behaviour of Soils in Simple Shear Apparatus" Ph.D. Thesis, Cambridge University, England, 1967

Duncan, J.M., Byrne, P.M., Wong, K.S., and Mabry, P., "Strength, Stress-Strain and Bulk Modulus Parameters for Finite Element Analyses of Stresses and Movements in Soil Masses", Report No. WCB/GT/78-02 to National Science Foundation, April, 1978

Duncan, J.M., and Chang, C-Y, "Nonlinear Analysis of Stress and Strain in Soils", Journal of the Soil Mechanics and Foundations Division, ASCE, Wol. 96, No SM5, Sept., 1970, pp. 1629-1651.

El-Sohby, M.A., and Andrawes, K.Z., "Deformation Characteristics of Granular Materials Under Hydrostatic Compression", Canadian Geotechnical Journal, Vol. 9, 1972, pp. 338-350

Frydman, S., and Zeitlen, J.G., "Some Pseudo-Elastic Properties of Granular Soil", Proceedings, 7th International Conference on Soil Mechanics and Foundation Engineering,

Mexico, Vol 1, 1969, pp/ 135-141

Gibson, R.E., and Anderson, W.F., "In-situ Measurement of Soil Properties with the Pressuremeter", Civil Engineering, Vol. 56, May, 1961, pp. 615-620

Gunaratne, M, "A Nonlinear Incremental Finite Element Program for the Analysis of Shafts and Tunnels in Oilsands", M.A.Sc. Thesis, U.B.C., 1981

Hansen, B., "Line Ruptures Regarded as Narrow Rupture Zones, Basic Equation Based on Kinematic Considerations", Proceedings, Brussels Conference on Earth Pressure Problems, Brussels, Vol. 1, 1958, pp. 39-48

Horne, M.R., "The Behaviour of An Assembly of Rotund, Rigid, Cohesionless Particles, I&II, Proceedings of the Royal Society, London, Vol. 286, A, 1964, pp.62-96

Hughes, J.M.O., Wroth, C.P., and Windle, D., "Pressuremeter Tests in Sand", Geotechnique, Wol. 27, No. 4, Dec. 1977, pp. 455-477

Hughes, J.M.O., "Pressuremeter Testing", Class Notes for C.E. 577, U.B.C., Nov., 1979

Kitamura, R., "Mechanical Properties of Particulate Material Under General Stress Conditions", Soils and Foundations, Vol. 21, No. 3, Sept., 1981, pp. 67-82

Kokusho, T., "Nonlinear Analysis of a Soil with Arbitrary Dilatancy by Finite Element Method", Soils and Foundations Vol. 18, No. 1, Mar., 1978, pp. 73-89

Ko., H-Y., and Scott, R.F., "Deformation of Sand at Failure", Journal of the Soil Mechanics and Foundations Division, ASCE, Vol. 94, No. SM4, July, 1968, pp. 883-898

Kondner, R.L., "Hyperbolic Stress-Strain Response: Cohesive Soils", Journal of the Soil Mechanics and Foundations Division, ASCE, Vol. 89, No. SM1, 1963, pp. 115-143

Kondner, R.L., and Zelasko, J.S., "A Hyperbolic Stress-Strain Formulation for Sands", Proceedings, 2nd Pan-American Conference on Soil Mechanics and Foundations Engineering, Brazil, Vol. 1, 1963, pp289-324

Krishnamurthy, M., Nagaraj, T.S., and Sridharan, A., "Stress Path Effects on the Dilatant Behaviour of Sand", Geotechnical Engineering, Vol. 12, 1981, pp. 41-51

Lade, P.V., and Duncan, J.M., "Elastoplastic Stress-Strain Theory for Cohesionless Soil", Journal of the Geotechnical Engineering Division, ASCE, Vol. 101, No. GT10, Oct., 1975, pp. 1037-1053

Lindenberg, J., and Koning, H.L., "Critical Density of Sand", Geotechnique, Vol. 31, No. 2, 1981, pp. 231-245

Marsland, A., and Randolph, M.F., "Comparison of the Results From Pressuremeter Tests and Large In-Situ Plate Tests in London Clay", Geotechnique, Vol. 27, No. 2, June, 1977, pp. 217-243

Oda, M., "The Mechanism of Fabric Changes During Compressional Deformation of Sand", Soils and Foundations, Vol. 12, No, 2, June, 1972, pp. 1-18

Palmer, A.C., "Undrained Plane-Strain Expansion of a Cylindrical Cavity in Clay: A Simple Interpretation of the Pressuremeter Test", Geotechnique, Vol. 22, No. 4, Sept. 1972, pp. 451-457

Rowe, P.W., "The Stress-Dilatancy Relation for Static Equilibrium of an Assembly of Particles in Contact", Proceedings of the Royal Society, London, Vol. 269, A, 1962, pp. 500-529

Rowe, P.W., "Theoretical Meaning and Observed Values of Deformation Parameters in Soil", Stress-Strain Behaviour of Soil, Roscoe Memorial Symposium, Cambridge, G.T. Foulis, Henley-on-Thames, 1971, pp. 143-194

Tatsuoka, F., "Stress-Strain Behaviour of an Idealized Anisotropic Granular Material", Soils and Foundations, Vol. 20, No. 3, Sept., 1980, pp. 75-90

Stroud, M.A., "The Behaviour of Sand at Low Stress Levels in the Simple Shear Apparatus", Ph.D. thesis, Cambridge, England, 1967

Timoshenko, S.P., and Goodier, J.N., "Theory of Elasticity", McGraw-Hill Book Company, New York, Third Edition, 1970

Tobita, Y., and Yanagisawa, E., "Stress-Strain Relationship of Sand and its Application to FEM Analysis", International Symposium of Soils under Cyclic and Transient Loading, Swansea, January, 1980, pp. 653-664

Vaid, Y.P., Byrne, P.M., and Hughes, J.M.O., "Dilation Rate as a Measure of Liquefaction Resistance of Saturated Granular Materials", Soil Mechanics Series, No. 43, Dept. of Civil Engineering, U.B.C., Nov., 1980

Varadarajan, A., and Mishra, S.S., "Stress-path Dependent Stress Strain-Volume Change Behaviour", International Symposium on Soils under Cyclic and Transient Loading, Swansea, Jan., 1980, pp. 109-119

Vesic, A.S., "Expansion of Cavities in Infinite Soil Mass", Journal of the Soil Mechanics and Foundations Division,

ASCE, Vol. 98, No. SM3, March, 1972, pp. 265-290

Vesic. A.S., and Clough, G.W., "Behaviour of Granular Material under High Stresses", Journal of the Soil Mechanics and Foundations Division, ASCE, Vol. 94, No. SM3. May, 1968, pp. 661-688

Wroth, C.P., and Hughes, J.M.O., "An Instrument for the In-Situ Measurement of the Properties of Soft Clay," 8th International Conference on Soil Mechanics and Foundation Engineering, Moscow, 1973, Vol. 1.2, pp. 487-494

Wroth, C.P., and Windle, D., "Analysis of the Pressuremeter Test Allowing for Volume Change", Geotechnique, Vol. 25, No. 3, 1975, pp. 598-604

APPENDIX A

Four Node Polar Coordinate Finite Element

Appendix A

Formulation of Four Node Polar Coordinate Finite Element

The four node isoparametric element cannot model curved boundaries. In order to accurately model the curved boundary of the pressuremeter, a fine mesh would be required. This would require large amounts of computer time to solve. An eight node isoparametric element could be used, but this models quadratic boundaries. To reduce the mesh size and to accurately model the circular boundary of the pressuremeter a four node plane strain polar coordinate element was developed. This element has two degrees of freedom per node. A higher order element can be developed by also specifying derivatives at the nodes.

The four node element has the numbering scheme shown in Figure 59. The displacements at the nodes are u and v, the displacement in the radial and circumferential directions respectively. The element has a linear displacement field:

$$u = a_1+a_2r+a_3\theta+a_4r\theta$$
$$v = b_1+b_2r+b_3\theta+b_4r\theta$$

The nodal displacements are then given by:

$$\begin{Bmatrix} u_1 \\ u_2 \\ u_3 \\ u_4 \\ v_1 \\ v_2 \\ v_3 \\ v_4 \end{Bmatrix} = \begin{bmatrix} 1 & r_1 & \theta_2 & r_1\theta_2 & 0 & 0 & 0 & 0 \\ 1 & r_1 & \theta_1 & r_1\theta_1 & 0 & 0 & 0 & 0 \\ 1 & r_2 & \theta_1 & r_2\theta_1 & 0 & 0 & 0 & 0 \\ 1 & r_2 & \theta_2 & r_2\theta_2 & 0 & 0 & 0 & 0 \\ 0 & 0 & 0 & 0 & 1 & r_1 & \theta_2 & r_1\theta_2 \\ 0 & 0 & 0 & 0 & 1 & r_1 & \theta_1 & r_1\theta_1 \\ 0 & 0 & 0 & 0 & 1 & r_2 & \theta_1 & r_2\theta_1 \\ 0 & 0 & 0 & 0 & 1 & r_2 & \theta_2 & r_2\theta_2 \end{bmatrix} \begin{Bmatrix} a_1 \\ a_2 \\ a_3 \\ a_4 \\ b_1 \\ b_2 \\ b_3 \\ b_4 \end{Bmatrix}$$

Which in matrix notation is:

$$\{\delta\} = (A)\{\alpha\}$$

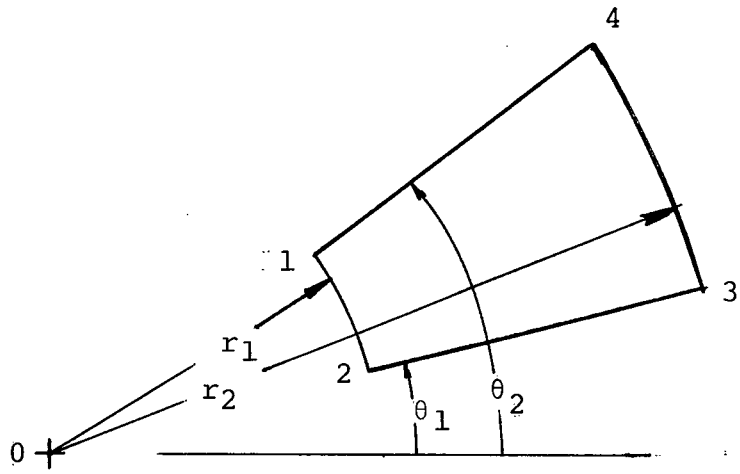

59

Figure 59. Four Node Polar Coordinate Finite Element

This is inverted to give:

$$\{\alpha\} = (A)^{-1}\{\delta\}$$

Where:

$$(A)^{-1} = \frac{1}{(r_1-r_2)(\theta_1-\theta_2)}\begin{bmatrix} -r_2\theta_1 & r_2\theta_2 & -r_1\theta_2 & r_1\theta_1 & 0 & 0 & 0 & 0 \\ \theta_1 & -\theta_2 & \theta_2 & -\theta_1 & 0 & 0 & 0 & 0 \\ r_2 & -r_2 & r_1 & -r_1 & 0 & 0 & 0 & 0 \\ -1 & 1 & -1 & 1 & 0 & 0 & 0 & 0 \\ 0 & 0 & 0 & 0 & -r_2\theta_1 & r_2\theta_2 & -r_1\theta_2 & r_1\theta_1 \\ 0 & 0 & 0 & 0 & \theta_1 & -\theta_2 & \theta_2 & -\theta_1 \\ 0 & 0 & 0 & 0 & r_2 & -r_2 & r_1 & -r_1 \\ 0 & 0 & 0 & 0 & -1 & 1 & 1 & 1 \end{bmatrix}$$

The strains are obtained from the displacement field:

$$\varepsilon_r = -(\frac{\partial u}{\partial r})$$
$$\varepsilon_\theta = -(\frac{u}{r} + \frac{1\partial v}{r\partial\theta})$$
$$\gamma_{r\theta} = -(\frac{1\partial u}{r\partial\theta} + \frac{\partial v}{\partial r} - \frac{v}{r})$$

Compressive strains are positive.

For the present case, from the symmetry of the problem, there is no variation of u or v with theta, and there is no displacement in the theta direction. This would simplify the derivation of the element stiffness matrix, but in order to keep the element as general as possible, the complete expressions for strain will be used.

The displacement field may be specified as:

$$\begin{Bmatrix} u \\ v \end{Bmatrix} = \begin{bmatrix} 1 & r & \theta & r\theta & 0 & 0 & 0 & 0 \\ 0 & 0 & 0 & 0 & 1 & r & \theta & r\theta \end{bmatrix}\{\alpha\}$$

The vector $\{\alpha\}$ is the vector of the coordinates of the element nodes and contains only constants. This vector is given by:

$$\{\alpha\} = (A)^{-1}\{\delta\}$$

On differentiation of the strain field, the strain vector is determined:

$$\{\varepsilon\} = -\begin{bmatrix} 0 & 1 & 0 & \theta & 0 & 0 & 0 & 0 \\ \frac{1}{r} & 1 & \frac{\theta}{r} & \theta & 0 & 0 & \frac{1}{r} & 1 \\ 0 & 0 & \frac{1}{r} & 1 & -\frac{1}{r} & 0 & -\frac{\theta}{r} & 0 \end{bmatrix} (A)^{-1}\{\delta\}$$

or:

$$\{\varepsilon\} = -(C)(A)^{-1}\{\delta\}$$

Therefore the strain displacement matrix (B) is:

$$(B) = -(C)(A)^{-1}$$

Upon performing the matrix multiplication:

$$(B)^T = \frac{-1}{(r_1-r_2)(\theta_1-\theta_2)} \begin{bmatrix} \theta_1-\theta & (\frac{r}{r}2-1)(\theta-\theta_1) & \frac{r}{r}2-1 \\ -\theta_2+\theta & (\frac{r}{r}2-1)(\theta_2-\theta) & -\frac{r}{r}2+1 \\ \theta_2-\theta & (\frac{r}{r}1-1)(\theta-\theta_2) & \frac{r}{r}1-1 \\ -\theta_1+\theta & (\frac{r}{r}1-1)(\theta_1-\theta) & -\frac{r}{r}1+1 \\ 0 & \frac{r}{r}2-1 & (\frac{r}{r}2)(\theta_1-\theta)-\theta \\ 0 & -\frac{r}{r}2+1 & (\frac{r}{r}2)(\theta-\theta_2)+\theta \\ 0 & \frac{r}{r}1-1 & (\frac{r}{r}1)(\theta_2-\theta)-\theta \\ 0 & -\frac{r}{r}1+1 & (\frac{r}{r}1)(\theta-\theta_1)+\theta \end{bmatrix}$$

The element stiffness matrix is then given by:

$$(K) = \int_V (B)^T (D)(B)\,dV$$

or: $$(K) = \int_A (B)^T (D)(B)\,dA \quad \text{for a unit thickness}$$

The stress-strain matrix (D) is the standard matrix for plane strain problems:

$$(D) = \frac{E}{(1+\upsilon)(1-2\upsilon)} \begin{bmatrix} 1-\upsilon & \upsilon & 0 \\ \upsilon & 1-\upsilon & 0 \\ 0 & 0 & \frac{1-2\upsilon}{2} \end{bmatrix}$$

where: υ = Poisson's ratio

E = Young's modulus

This integral could be evaluated, however since the matrix (B) contains both r and θ terms, it would be long and tedious.

Instead, the integral is evaluated numerically. Four point Gauss quadrature is used. Within the program, the boundary conditions for the axisymmetric problem have been incorporated. These are:

$$v = 0 \text{ at all points}$$

$$\text{and } \frac{\delta(\ )}{\delta\theta} = 0$$

In addition, forces can only be applied in the radial direction.

Elastic springs have been incorporated in the polar coordinate mesh. The springs are attached at the outer most nodes. They model the effect of an infinite elastic medium. Spring stiffness is determined by looking at the expansion of a cylinder in an infinite elastic medium. For a cylinder of radius, a, the pressure required to give a unit displacement of the cylinder boundary is:

$$p = \frac{2G}{a}$$

where: G = material shear modulus

The total force applied to a unit length of the cylinder is:

$$f = pA = p(2\pi a) = \frac{2G}{a}(2\pi a)$$

or: $f = 4\pi G$ independent of radius

Therefore, by analogy to $F = K\Delta$ the spring stiffness is:

$$k = 4\pi G$$

This is the stiffness for the complete cylinder. When analyzing a sector, with two springs, the individual spring stiffness becomes:

$$k = \tfrac{1}{2}(4\pi G)\left(\frac{\theta}{2\pi}\right) = G\theta$$

where: θ = sector angle, in radians

$\tfrac{1}{2}$ accounts for two springs for the sector

The polar coordinate element was checked against closed form elastic solutions using the mesh shown in Figure 60. Results are in very close agreement when the mesh size is small in regions of large stress and strain gradients. Strains versus radial distance are shown in Figure 61, stresses versus radial distance are shown in Figure 62 and displacement versus radial distance is shown in Figure 63. The stress path followed by element 1 is shown in Figure 64.

Of special interest in the polar coordinate element is the limit on Poisson's ratio. In most numerical work Poisson's ratio must be limited to a value less than 0.5 to prevent numerical instabilities. However, in this case the radial and circumferential directions define principal planes. No shear stress or shear strain occurs on these planes, so by introducing the boundary conditions that $v=0$ and $\delta u/\delta\theta=0$ in the solution routine, equations with a possible divide by zero error are eliminated. This means that Poisson's ratio may be set to 0.5 without numerical instability. This also allows stress paths along the failure surface to be followed without using a stress redistribution routine. Those elements on or above the failure surface have the shear modulus, $G=0$. These elements pick up no additional shear stress on continued loading, so will move back onto the failure surface as the mean normal stress increases. Figure 65 shows the stress path of a failed element on a Modified Mohr diagram. The use of small load steps allows accurate modelling of stress paths along the failure envelope.

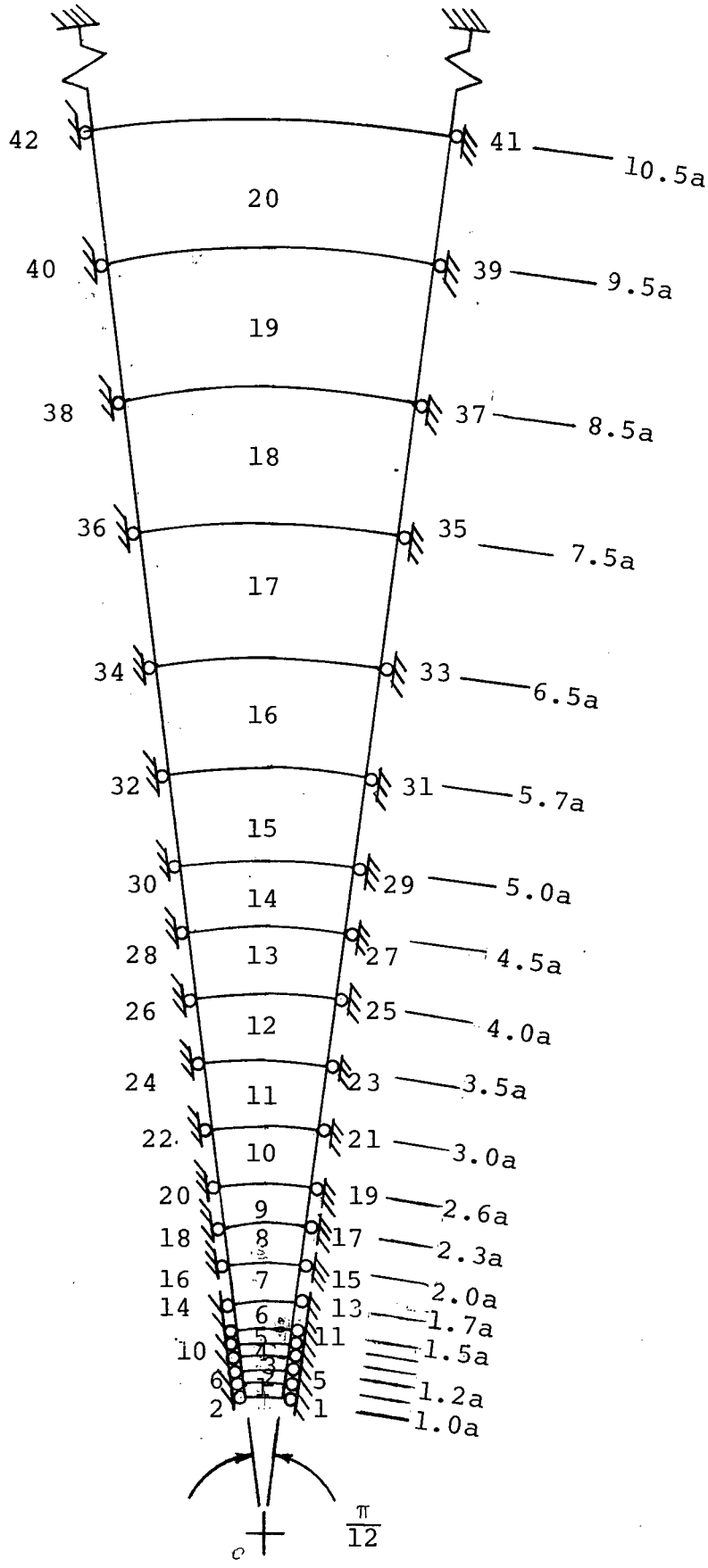

Figure 60. Finite Element Mesh

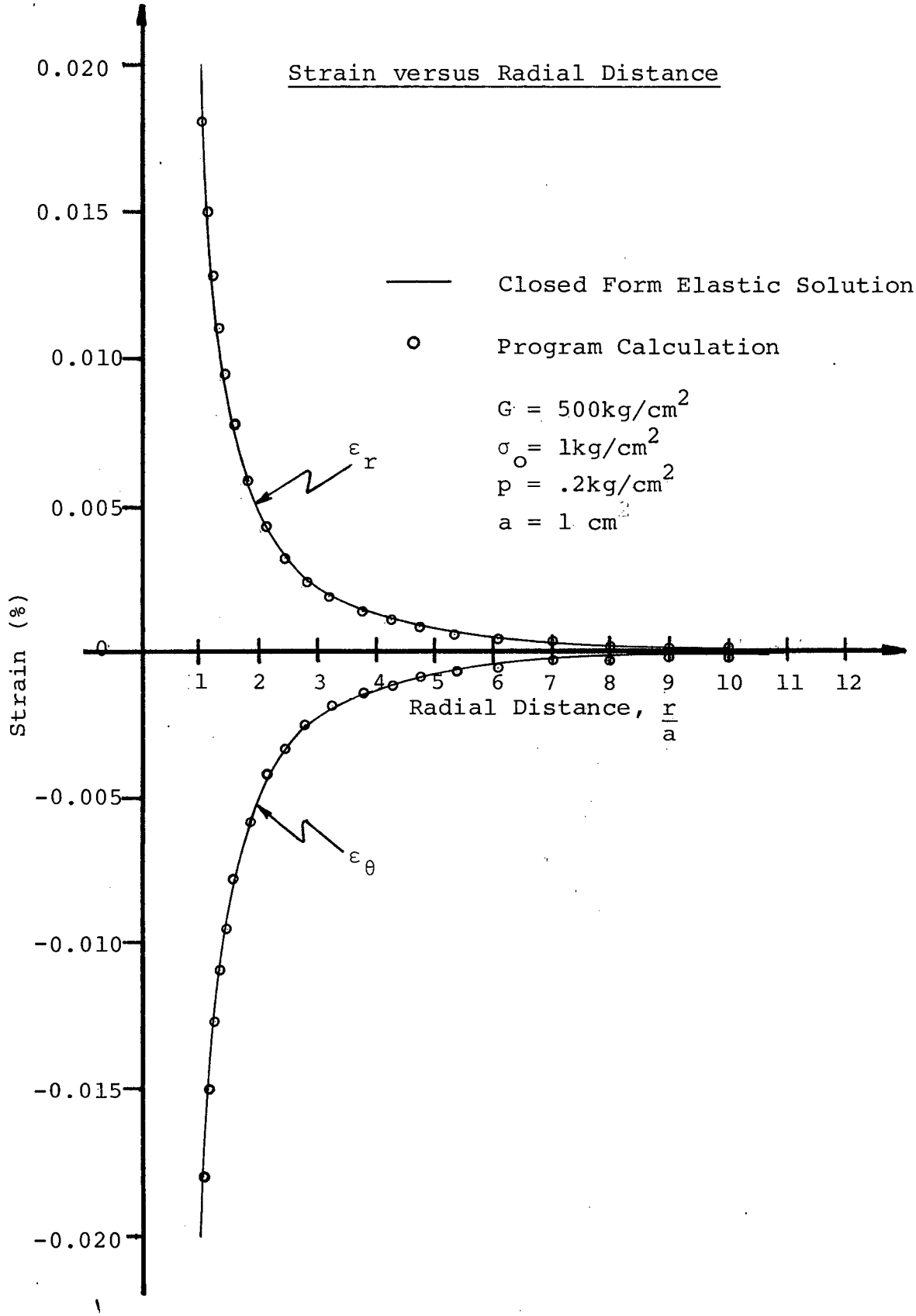

Figure 61. Expansion of Cylinder in Infinite Elastic Medium

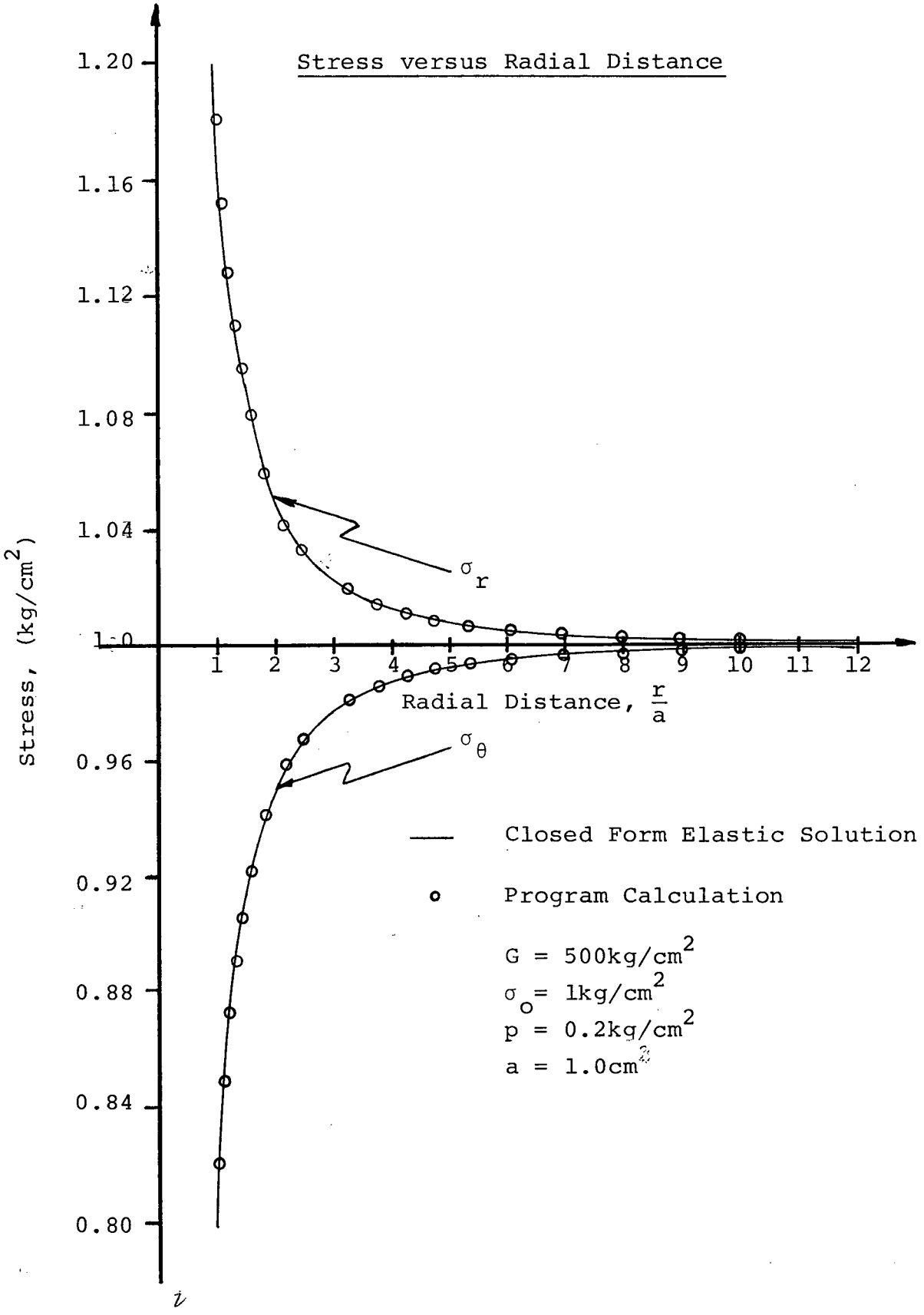

Figure 62. Expansion of Cylinder in Infinite Elastic Medium

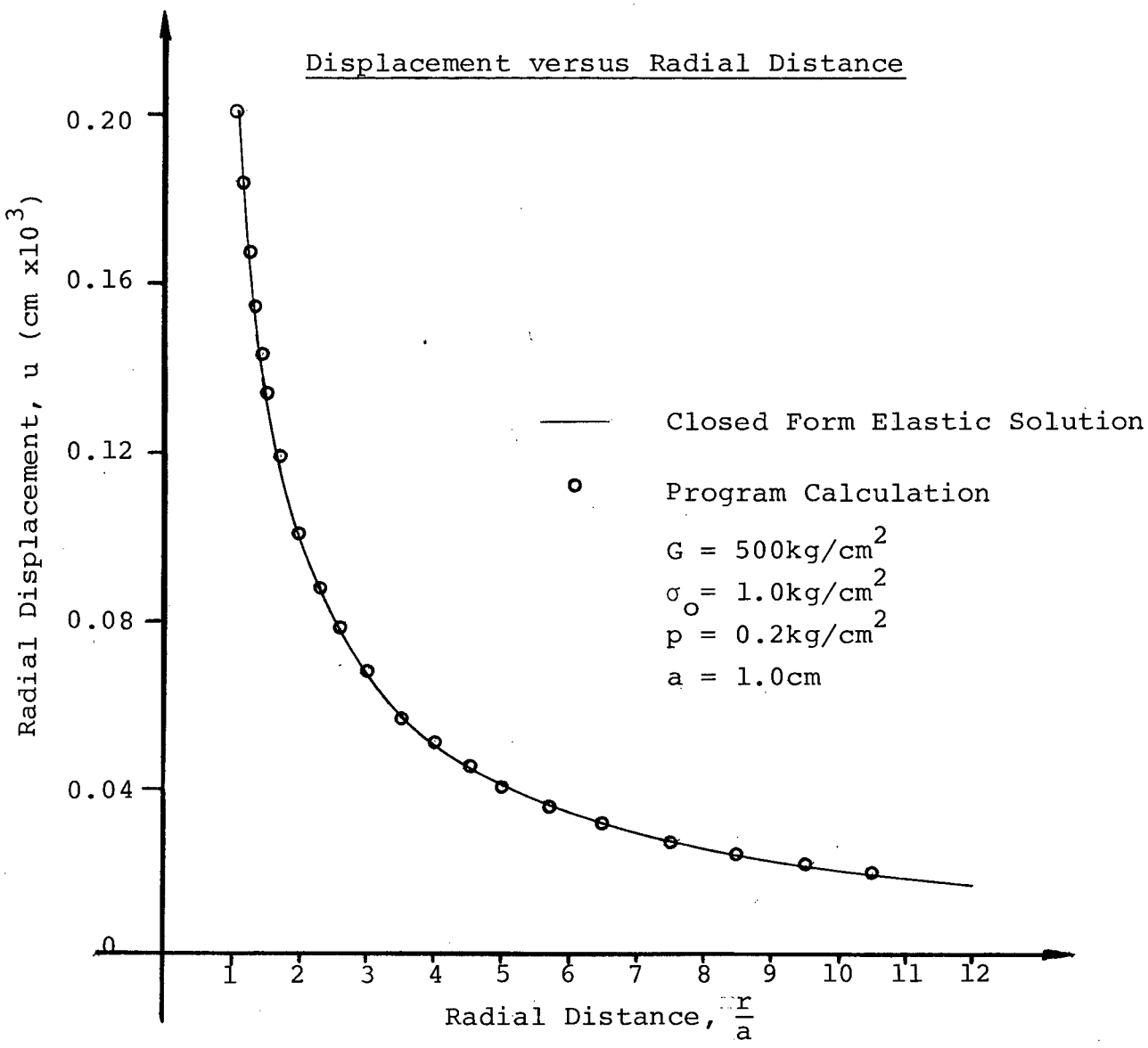

Figure 63. Expansion of Cylinder in Infinite Elastic Medium

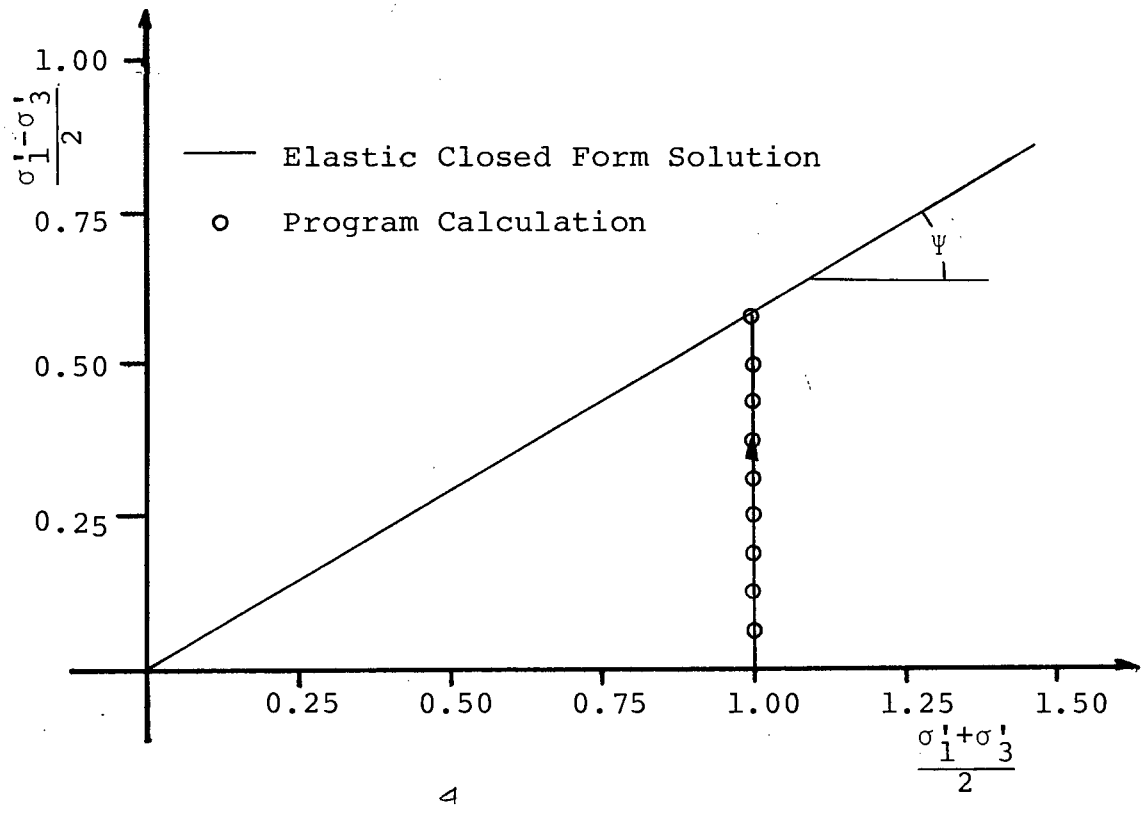

Figure 64. Stress Path for Elastic Element

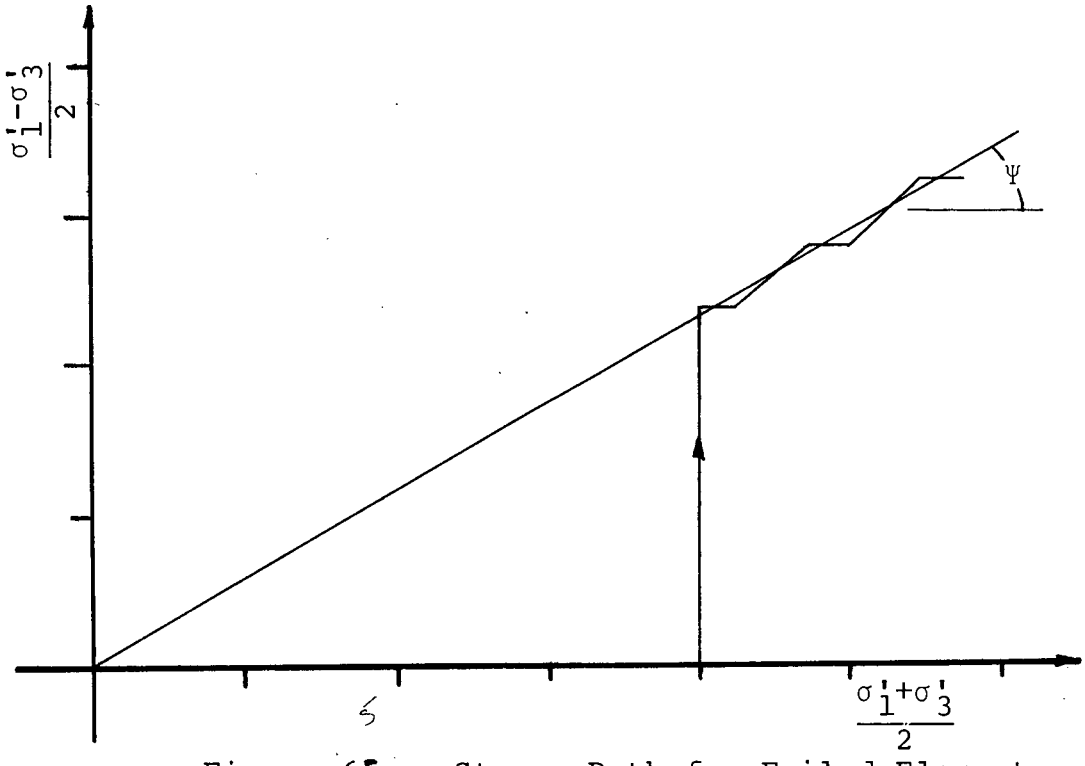

Figure 65. Stress Path for Failed Element

APPENDIX B

Stress-Strain Matrix for Triaxial Finite Element

Appendix B

Stress-Strain Matrix for Triaxial Finite Element

The plane strain four node isoparametric element used in the NLSSIP can be easily modified so that it can model the triaxial test. The isoparametric formulation is retained. Only the stress-strain matrix must be changed from the plane strain element. The new element is not cylindrical. It is a brick element of unit thickness with four nodes specifying the element.

In the isoparametric element formulation, the stiffness matrix is given by an integral over the volume of the element:

$$(K) = \int_V (B)^T (D)(B)\,dV$$

where: (K) = element stiffness matrix

(B) = element strain-displacement matrix

(D) = element stress-strain matrix

For the plane strain element (D) is:

$$(D) = \frac{E}{(1+\upsilon)(1-2\upsilon)} \begin{bmatrix} 1-\upsilon & \upsilon & 0 \\ \upsilon & 1-\upsilon & 0 \\ 0 & 0 & \frac{1-2\upsilon}{2} \end{bmatrix}$$

Under triaxial conditions the relations between strain and stress are:

$$\varepsilon_x = \frac{1}{E}(\sigma_x - \upsilon(\sigma_y + \sigma_z))$$
$$\varepsilon_y = \frac{1}{E}(\sigma_y - \upsilon(\sigma_x + \sigma_z))$$
$$\varepsilon_z = \frac{1}{E}(\sigma_z - \upsilon(\sigma_x + \sigma_y))$$
$$\gamma_{xy} = \frac{1}{G}\tau_{xy}$$
$$\gamma_{yz} = \frac{1}{G}\tau_{yz}$$
$$\gamma_{zx} = \frac{1}{G}\tau_{zx}$$

The triaxial element is oriented such that the y axis is along the long axis of the element, Figure 66.

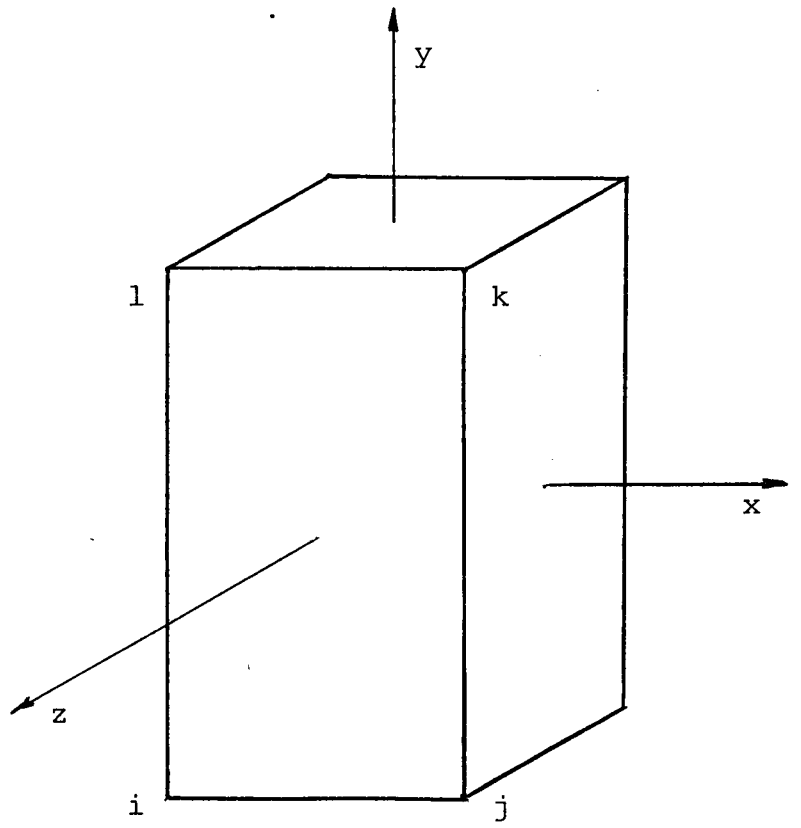

Figure 66. Triaxial Model Finite Element

For this geometry the coordinate planes define principal planes:

$$\varepsilon_x = \varepsilon_z$$

$$\gamma_{xy} = \gamma_{zx} = \gamma_{zy} = 0$$

$$\sigma_x = \sigma_z$$

$$\tau_{xy} = \tau_{zx} = \tau_{zy} = 0$$

and:

$$\begin{Bmatrix} \varepsilon_x \\ \varepsilon_y \\ \gamma_{xy} \end{Bmatrix} = \begin{bmatrix} \frac{1-\upsilon}{E} & \frac{-\upsilon}{E} & 0 \\ \frac{-2\upsilon}{E} & \frac{1}{E} & 0 \\ 0 & 0 & \frac{1}{G} \end{bmatrix} \begin{Bmatrix} \sigma_x \\ \sigma_y \\ \tau_{xy} \end{Bmatrix}$$

Inverting this matrix gives the stress-strain matrix:

$$(D) = \frac{E}{(1+\upsilon)(1-2\upsilon)} \begin{bmatrix} 1 & \upsilon & 0 \\ 2\upsilon & 1-\upsilon & 0 \\ 0 & 0 & \frac{1-2\upsilon}{2} \end{bmatrix}$$

This may be simplified by using the parameters B' and G,

where: $B' = \frac{3B}{2(1+\upsilon)}$ and $B = \frac{E}{3(1-2\upsilon)}$

$$G = \frac{E}{2(1+\upsilon)}$$

Resulting in:

$$(D) = \begin{bmatrix} 2B' & B'-G & 0 \\ 2(B'-G) & B'+G & 0 \\ 0 & 0 & G \end{bmatrix}$$

The variable B' is a modified bulk modulus used only for programming convenience.

The stress-strain matrix developed above is correct when forces are applied in the y-direction or the x-direction, but is not correct for those cases when forces are applied in both the x-direction and the z-direction, as is the usual case in the triaxial test. The principal of virtual work can be used to produce the correct stress-strain matrix. In the principal

of virtual work, the work done by the internal stresses undergoing a virtual displacement is equated to the work done by the external forces undergoing the virtual displacement. The internal virtual work is given by:

$$W_{int} = \int_V \{\bar{\varepsilon}\}^t \{\sigma\} dV$$

where: $\{\bar{\varepsilon}\}^T$ = virtual strains in the element

$\{\sigma\}$ = internal stresses in element

Expanding the vectors gives:

$$W_{int} = \int_V \{\varepsilon_x \ \varepsilon_y \ \varepsilon_z \ \gamma_{xy} \ \gamma_{yz} \ \gamma_{zx}\} \begin{Bmatrix} \sigma_x \\ \sigma_y \\ \sigma_z \\ \tau_{xy} \\ \tau_{yz} \\ \tau_{zx} \end{Bmatrix} dV$$

Using the strain and stress boundary conditions outlined above gives:

$$W_{int} = \int_V \{\bar{\varepsilon}_x \ \bar{\varepsilon}_y \ \bar{\gamma}_{xy}\} \begin{Bmatrix} 2\sigma_x \\ \sigma_y \\ \tau_{xy} \end{Bmatrix} dV$$

but, $\{\sigma\} = (D)\{\varepsilon\}$

Therefore:

$$\begin{Bmatrix} 2\sigma_x \\ \sigma_y \\ \sigma_{xy} \end{Bmatrix} = \begin{bmatrix} 4B' & 2(B'-G) & 0 \\ 2(B'-G) & B'+G & 0 \\ 0 & 0 & G \end{bmatrix} \begin{Bmatrix} \varepsilon_x \\ \varepsilon_y \\ \gamma_{xy} \end{Bmatrix}$$

$$= (\bar{D})\{\varepsilon\}$$

The strains are determined from the nodal displacements:

$$\{\varepsilon\} = (B)\{\delta\}$$

where: $\{\delta\}$ = vector of nodal displacements

Therefore the internal virtual work becomes:

$$W_{int} = \int_V \{\bar{\delta}\}^T (B)^T (\bar{D}) (B) \{\delta\} dV$$

The external virtual work is:

$$W_{ext} = \{\bar{u}_1\ \bar{v}_1\ \bar{w}_1\ \bar{u}_2\ \bar{v}_2\ \bar{w}_2\ \bar{u}_3\ \bar{v}_3\ \bar{w}_3\ \bar{u}_4\ \bar{v}_4\ \bar{w}_4\} \begin{Bmatrix} f_{1x} \\ f_{1y} \\ f_{1z} \\ \vdots \\ f_{4x} \\ f_{4y} \\ f_{4z} \end{Bmatrix}$$

where: $\bar{u}_1$ = virtual displacement of node 1 in x direction

$\bar{v}_1$ = virtual displacement of node 1 in y direction

$\bar{w}_1$ = virtual displacement of node 1 in z direction

f_{1x}= force at node 1 in x direction

f_{2x}= force at node 1 in y direction

f_{3x}= force at node 1 in z direction

For the triaxial case:

$$\bar{u}_1 = \bar{w}_1, \quad \bar{u}_2 = \bar{w}_2, \quad \bar{u}_3 = \bar{w}_3, \quad \bar{u}_4 = \bar{w}_4$$

and: $f_{1x}=f_{1z}, \quad f_{2x}=f_{2z}, \quad f_{3x}=f_{3z}, \quad f_{4x}=f_{4z}$

Which gives the external virtual work:

$$W_{ext} = \{\bar{u}_1\ \bar{v}_1\ \bar{u}_2\ \bar{v}_2\ \bar{u}_3\ \bar{v}_3\ \bar{u}_4\ \bar{v}_4\} \begin{Bmatrix} 2f_{1x} \\ f_{1y} \\ 2f_{2x} \\ f_{2y} \\ 2f_{3x} \\ f_{3y} \\ 2f_{4x} \\ f_{4y} \end{Bmatrix}$$

$$W_{ext} = \{\hat{\bar{\delta}}\}^T\{f\}$$

The external and internal virtual work are equated, giving:

$$\{\bar{\delta}\}^T\{f\} = \int_V \{\bar{\delta}\}^T(B)^T(\bar{D})(B)\{\delta\}dV$$

Or:
$$\{f\} = \int_V (B)^T (\bar{D}) (B) dV \{\delta\}$$

The stiffness matrix is then:

$$(K) = \int_V (B)^T (\bar{D}) (B) dV$$

The stress-strain matrix $(\bar{D})$ is used when forming the stiffness matrix. It has been modified to account for forces being applied in both the x and z directions. This matrix is used in the program subroutine ISQUAD, which assembles the element stiffness matrix.

Once the nodal displacements have been determined, the strains are determined by:

$$\{\varepsilon\} = (B)\{\delta\}$$

The stresses are determined by:

$$\{\sigma\} = (D)(B)\{\delta\}$$

When calculating the stresses, the unmodified matrix (D) is used.

In the above formulation the force vector is of the form:

$$\{f\} = \begin{Bmatrix} f_{1x}+f_{1z} \\ f_{1y} \\ \vdots \\ f_{4x}+f_{4z} \\ f_{4y} \end{Bmatrix}$$

This required modification of the stress-strain matrix. An alternate approach could be used, in which case the force vector would be of the form:

$$\{f\} = \begin{Bmatrix} f_{1x} \\ f_{1y} \\ \vdots \\ f_{4x} \\ f_{4y} \end{Bmatrix}$$

The stress-strain matrix requires no modification in this case. While giving the correct stresses and strains, this approach

does not give the correct internal and external virtual work done during a load step.

APPENDIX C

Pressuremeter Test Data,

MacDonald's Farm, Sea Island

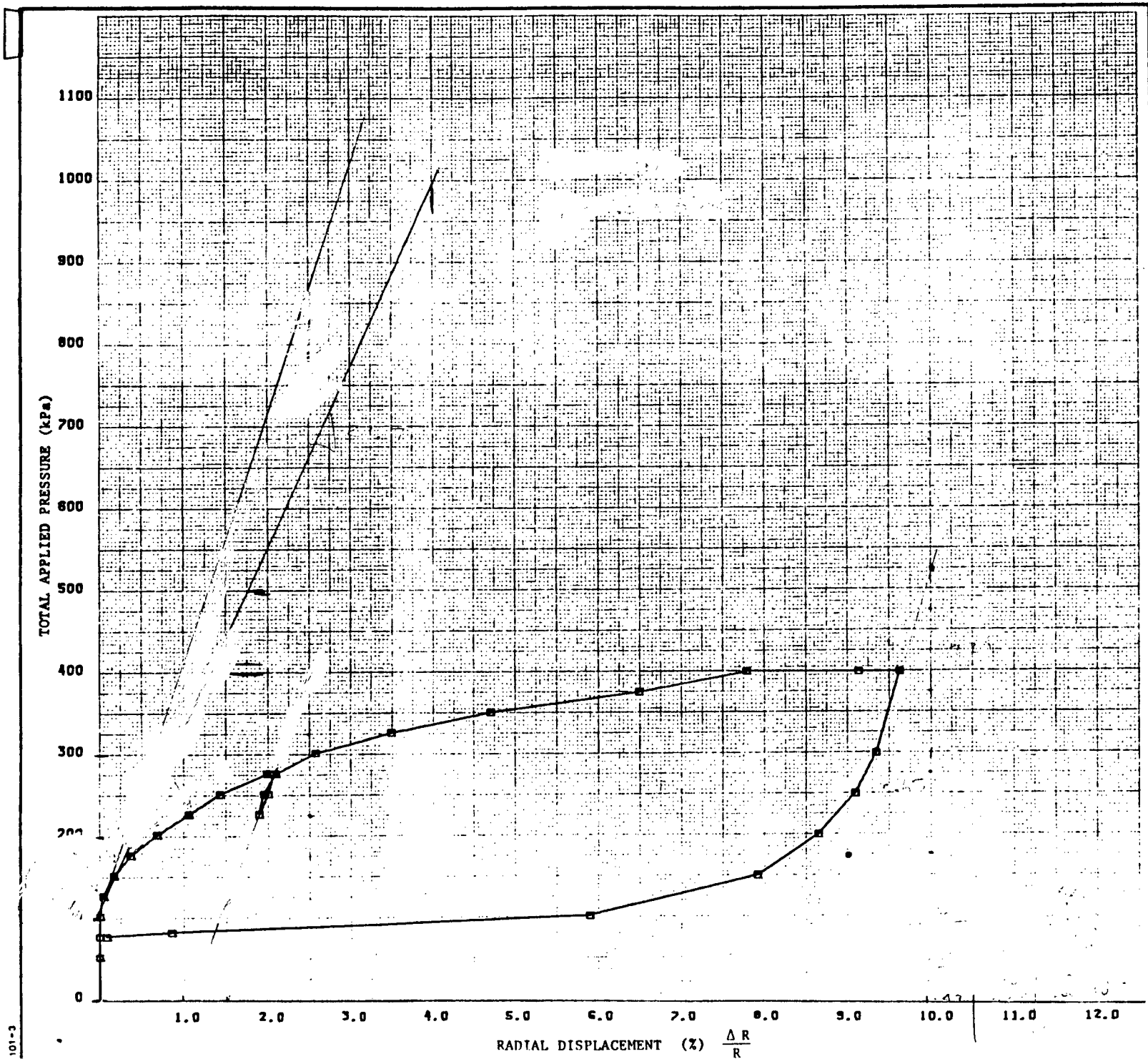

NOTES

VERT SCALE: 100KPA= 2CM

HOR SCALE: 1% TO 2CM

BORE HOLE No. SBPTI	TEST No. 1
DEPTH EL 10 FT	TEST DATE 03 DEC 1981
ARM (3.09 m)	

MATERIAL TESTED

FINE SAND

SITU TECHNOLOGY INC.
Vancouver, B.C. Seattle, Wa.

UNIVERSITY OF B.C.

H.S.B PRESSUREMETER

PLOT OF APPLIED PRESSURE
V.S.
RADIAL DISPLACEMENT

U.B.C. DEMO

JOB NO. 40-81N063

154

101-3

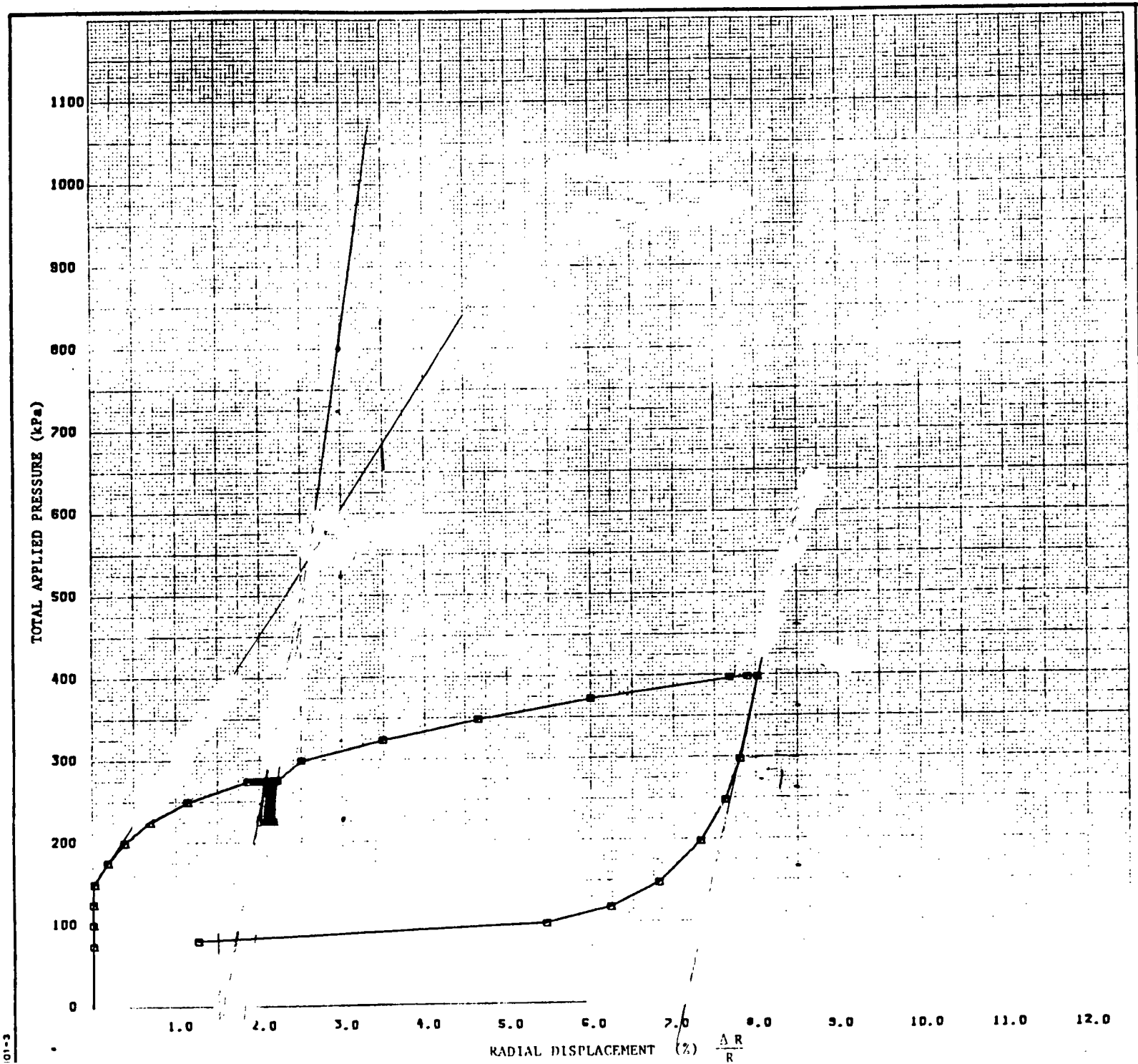

NOTES

VERT SCALE: 100KPA= 2CM

HOR SCALE: 1% TO 2CM

BORE HOLE No. SBPTI	TEST No. 2
DEPTH EL 12.5 FT	TEST DATE 03 DEC 1981
ARM (3.81)	

MATERIAL TESTED

FINE SAND

SITU TECHNOLOGY INC.
Vancouver, B.C. Seattle, Wa.

UNIVERSITY OF B.C.

H.S.B PRESSUREMETER

PLOT OF APPLIED PRESSURE
V.S.
RADIAL DISPLACEMENT

U.B.C. DEMO

JOB NO. 40-81N053

155

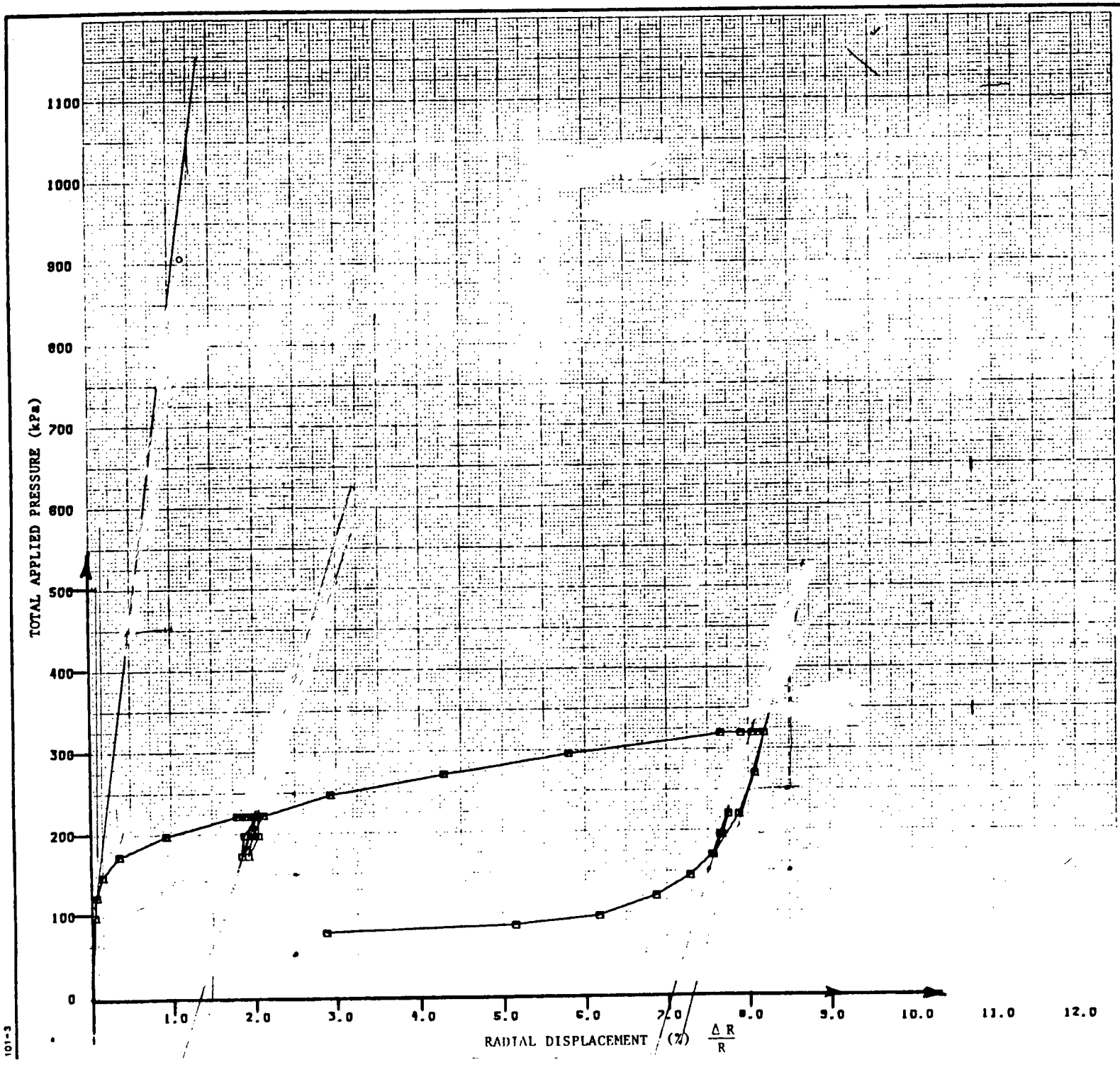

NOTES

VERT SCALE: 100KPA = 2CM

HOR SCALE: 1% TO 2CM

BORE HOLE No. SBPTI	TEST No. 3
DEPTH EL 15 FT	TEST DATE 03 DEC 1981
ARM (4.57)	

MATERIAL TESTED

FINE SAND

SITU TECHNOLOGY INC.
Vancouver, B.C. Seattle, Wa.

UNIVERSITY OF B.C.

H.S.B PRESSUREMETER

PLOT OF APPLIED PRESSURE
V.S.
RADIAL DISPLACEMENT

U.B.C. DEMO

JOB NO. 40-81N063

101-3

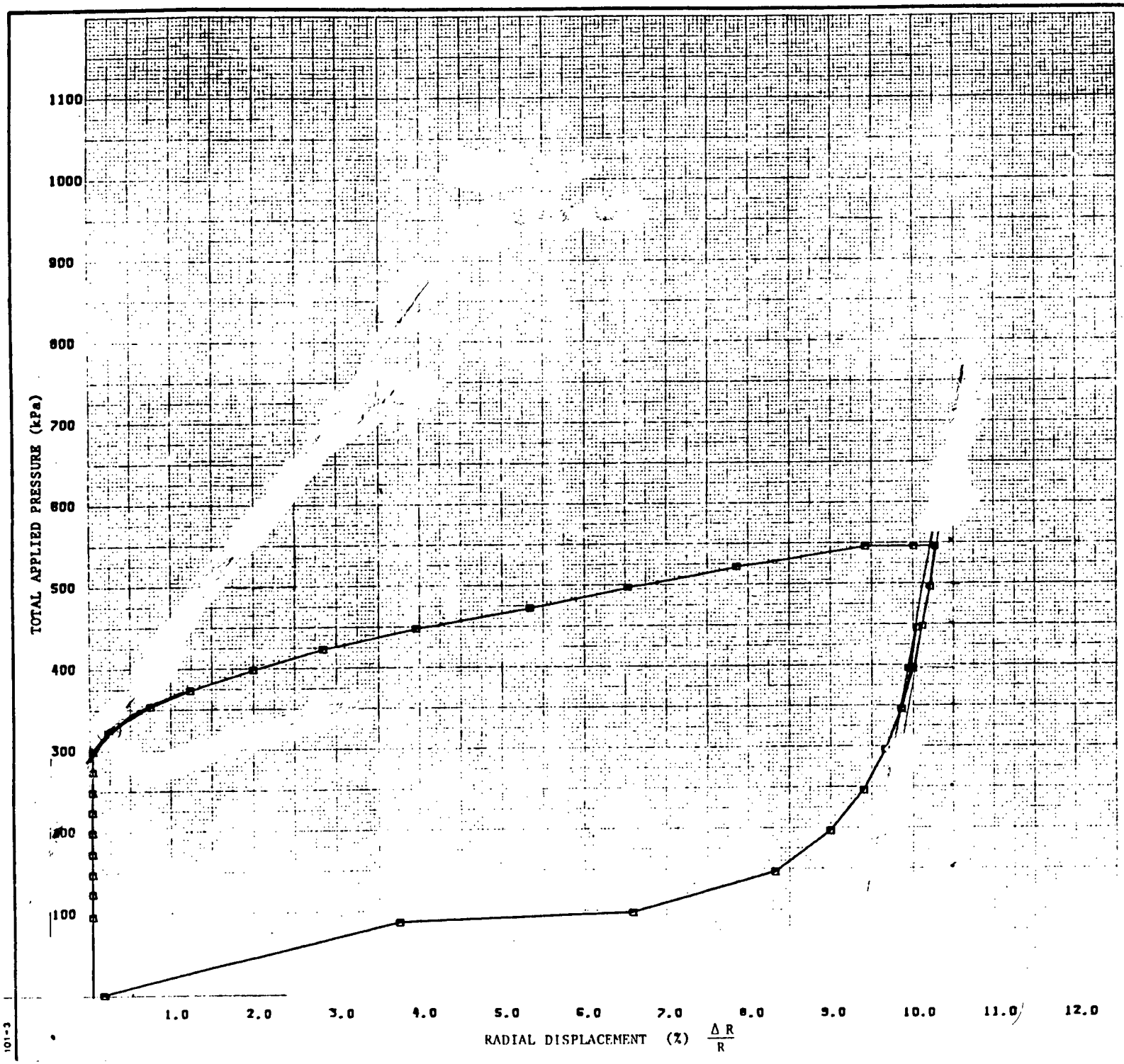

NOTES

VERT SCALE: 100KPA= 2CM

HOR SCALE: 1% TO 2CM

BORE HOLE No.	TEST No.
SBPTI	4
DEPTH EL 17.5 FT	TEST DATE 03 DEC 1981
ARM (5.33)	

MATERIAL TESTED

FINE MEDIUM SAND

SITU TECHNOLOGY INC.
Vancouver, B.C. Seattle, Wa.

UNIVERSITY OF B.C.

H.S.B PRESSUREMETER

PLOT OF APPLIED PRESSURE
V.S.
RADIAL DISPLACEMENT

U.B.C. DEMO

JOB NO. 40-81N053

157

101-3

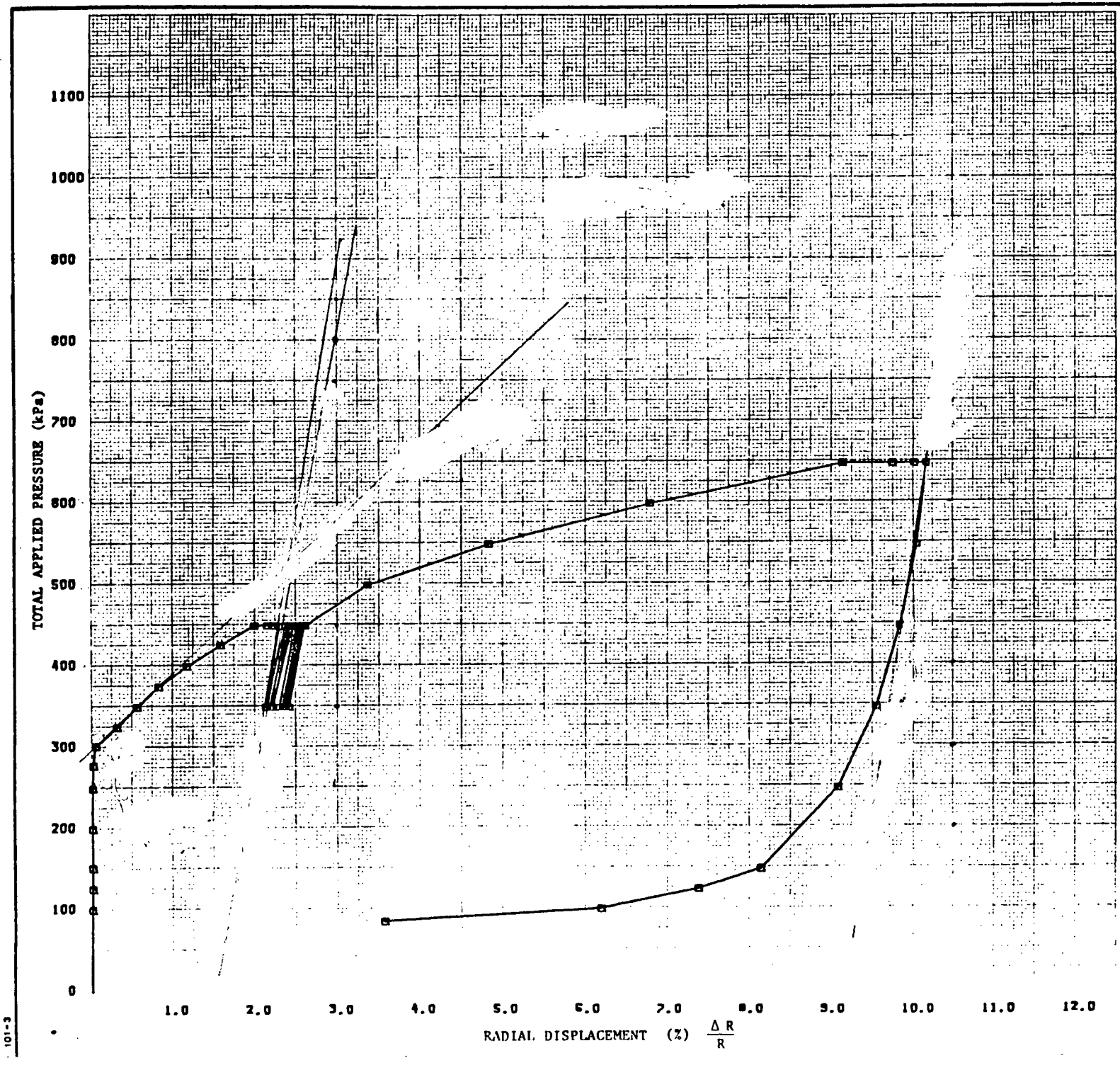

NOTES

VERT SCALE: 100KPA = 2CM

HOR SCALE: 1% TO 2CM

BORE HOLE No. SBPTI	TEST No. 5
DEPTH EL 20.5 FT	TEST DATE 03 DEC 1981
ARM (6.25 m)	

MATERIAL TESTED

FINE SAND

SITU TECHNOLOGY INC.
Vancouver, B.C. Seattle, Wa.

UNIVERSITY OF B.C.

H.S.B PRESSUREMETER

PLOT OF APPLIED PRESSURE
V.S.
RADIAL DISPLACEMENT

U.B.C. DEMO

JOB NO. 40-81N063

101-3